Martin Krus

Fraunhofer-Institut für Bauphysik
(Director: Prof. Dr.-Ing. habil. Dr. h.c. Dr. E.h. mult. Karl Gertis)

Moisture Transport and Storage Coefficients of Porous Mineral Building Materials

Theoretical Principles and New Test Methods

Fraunhofer IRB Verlag

Kontaktadresse:
Fraunhofer-Institut für
Bauphysik IBP
Institutsteil Holzkirchen
Miesbacher Straße 10, D-83626 Valley
Postfach 1152, D-83601 Holzkirchen
Telefon (08024) 643-0
Telefax (08024) 643-66

Satz und Druck: Satz- und Druckcenter des Fraunhofer-Informationszentrums Raum und Bau IRB, Stuttgart

Für den Druck des Buches wurde chlor- und säurefreies Papier verwendet.

 ISBN 3-8167-4535-0
Fraunhofer-Informationszentrum Raum und Bau IRB
Postfach 80 04 69, D-70504 Stuttgart
Nobelstraße 12, D-70569 Stuttgart
Telefon (0711) 9 70-25 00
Telefax (0711) 9 70-25 08

The present report is based on my doctoral thesis which was written in the course of my activity as a scientific researcher at the Fraunhofer Institute for Building Physics in Holzkirchen. It has been supported by a grant from the German Federal Ministry for Scientific Research as part of a joint project for the protection of heritage buildings. Scientific exchange among 14 countries during the IEA-Annex 24 project provided valuable input to this study.

I wish to thank Professor Karl Gertis for his guidance and generous assistance during the research work and in particular for the many practical suggestions in preparation of my thesis.

I would also like to thank Prof. H.W. Reinhardt for being my assistant thesis supervisor.

Special thanks are also due to Dr. H.M. Künzel and Dr. K. Kießl whose constant willingness to discuss the issues involved was of great assistance in developing new conceptual approaches. I would also like to express my sincere appreciation to Martha Westner for her careful and conscientious work in typing the manuscript and preparing the tables.

I would also like to express my appreciation to the entire staff of the Institute, and a special word of thanks to all undergraduates and those graduating whose work has assisted me over the years.

Last but not least I thank Mr. Kumaran and the NRC in Canada for the English translation of this report.

Contents

Nomenclature

Roman-letter notations

A [kg/m^2 √s]	water absorption coefficient
B [m/√s]	water penetration coefficient
B_0 [T]	external magnetic field
D_D [m^2/s]	water vapour diffusion coefficient in air
D_W [m^2/s]	liquid transport coefficient
D_{OD} [m^2/s]	surface diffusion coefficient
D_{wo} [m^2/s]	liquid transport coefficient in dry building material (exponential approximation)
D_{wf} [m^2/s]	liquid transport coefficient at capillary saturation (exponential approximation)
FID[V]	free induction decay (measuring signal)
FID_0 [V]	measuring signal immediately following pulse
g[kg/m^{2}s]	total mass flux density
g_E [kg/m^{2}s]	vapour effusion flux density
g_{OD} [kg/m^{2}s]	surface diffusion flux density
g_v [kg/m^{2}s]	vapour diffusion flux density
g_w [kg/m^{2}s]	liquid transport flux density
K_n [-]	Knudsen coefficient
L [m]	mean free path
M [kg/mol]	molecular weight
m_w [kg/m^2]	absorbed amount of water
M_z [T]	macroscopic nuclear magnetization in Z direction
M_{z0} [T]	macroscopic nuclear magnetization prior to pulse
N_L [mol^{-1}]	Loschmidt number
n [-]	number of measurements
P_k [Pa]	capillary pressure, suction pressure
P_L [Pa]	ambient atmospheric pressure
$P_ü$ [bar]	applied over pressure
P_0 [Pa]	standard pressure
p [Pa]	partial pressure of water vapour

p_s [Pa]	saturation vapour pressure
R [J/mol K]	universal gas constant
R_D [J/kgK]	gas constant for water vapour
r [m]	pore radius, radius of curvature
S/R [-]	signal-to-noise ratio
s [m]	depth of water penetration
T [K]	absolute temperature
T_1 [s]	longitudinal relaxation time
T_2 [s]	transverse relaxation time
t [s]	time
w [kg/m^3]	water content
w_f [kg/m^3]	capillary saturation
w_{max} [kg/m^3]	maximum water saturation
x [m]	spatial coordinates

Greek-letter notations

α [W/m^{2}K]	total heat transfer coefficient
β_p [kg/m^{2}sPa]	water vapour transfer coefficient
δ [kg/msPa]	water vapour permeability of stagnant air
δ^* [kg/msPa]	fictitious water vapour permeability
ϑ [°C]	temperature
λ [m/$\sqrt{s}$]	Boltzmann variable
μ [-]	water vapour diffusion resistance factor of dry building material
μ^* [-]	fictitious water vapour diffusion resistance factor of moist building material
ρ_w [kg/m^3]	density of water
σ [N/m]	surface tension of water
$\sigma_{L,W}$ [m]	average gas-kinetic impact diameter
φ [-]	relative humidity
ω [1/s]	angular frequency

1. Objectives in terms of building physics

It has become evident in recent years, both from research work and from practical and economic activity, that increasing attention is being paid to computer-based determination of moisture behaviour in building products and components. Present challenges such as the preservation of historic structures or the repair or insulation of exterior elements on existing buildings are closely linked with the issues of moisture conditions and changes in moisture behaviour as a result of protection measures. Considering the expenditures in time and money involved in experimentally checking moisture behaviour of building materials at full scale it is not difficult to appreciate the reason for studies aimed at developing computer-based analysis.

There already exist a number of computer models for combined moisture and heat transport. Some of these, such as Kießl's model [56] have been shown to yield reliable data. Requisite for computerized application of the models is accurate information on all necessary material properties. Whereas in the area of heat transport and of heat storage the basic principles of physics and the measuring method needed to determine material properties have long been generally known, there is still a need in many areas for research to explain the processes involved in the transport of moisture. A major problem of existing computer models is that they employ moisture transport and storage functions which are sometimes extremely complex, not very intuitive, and questionable in their physics. With the measuring technology presently available, determination of these functions would demand very high expenditure for an unacceptable level of accuracy. It is for this reason that broad application of computer analysis for moisture transport going beyond vapour diffusion analyses like those of the Glaser method [40] in DIN 4108 [25] for example has to date only been somewhat tentative in the area of physics relating to building and construction.

It is therefore the aim of this research effort to develop more suitable functions for water storage and transport coefficients on the basis of the physics involved in building and construction. This will make it possible to

describe the natural processes of moisture movement in porous mineral building materials in a more accurate way without involving an excessively large expenditure of measurement technology. New measuring methods are developed to validate the models on which these coefficients are based and to determine the coefficients. The new measuring methods make it possible to determine the characteristic functions in a highly meaningful way, with greater accuracy, and to some extent at higher speed. Furthermore, some of the transport functions may be derived from traditional material properties or estimated with acceptable accuracy.

In addition to the moisture storage function, this study investigates only liquid transport (capillary conductivity and "surface diffusion") and vapour diffusion. Other transport phenomena such as hydraulic seepage flow, osmosis, electrokinesis or thermodiffusion are excluded as they are of lesser significance in the physics pertaining in building and construction or because their mode of operation is as yet not understood (cf. Section 2.1.2).

This new information is also incorporated into development of a new computer process for unidimensional and two dimensional calculation of combined heat and moisture transport in building components [88]. A computer program makes it possible to check the correctness of the material properties used by comparing the computed results with actual test results. The validation involves the use of two examples to show that the material properties are valid not only under simplified test conditions. The conclusions resulting from the findings of the investigations into the moisture storage and transport processes of porous mineral building materials and concerning the use of the material properties are discussed at the end.

2. Review of existing literature and new approaches

Review of the literature is carried out separately in two chapters, beginning with discussion of the theoretical basics. In the second chapter experimental methods used to show the accuracy of the theoretical basics and to determine

storage and transport coefficients are presented and their applicability for the aims of the investigation is evaluated.

2.1 The general basics of moisture storage and transport

A very comprehensive literature review (650 works) on moisture transport in building materials was published by Kießl in 1980 [55]. Consequently mention will only be made here of the basics of significance for the present work as well as literature, mostly recent, not included in Kießl's survey.

The moisture balance of porous mineral building materials is determined by the moisture storage characteristics and the moisture transport phenomena taking place in the material in liquid and gaseous phases. Because the storage and transport of moisture in mineral building materials take place within the pores, scanning electron microscope photographs of aerated concrete and two sandstones are used to give an idea of the pore systems. Fig. 1 [39] shows aerated concrete at two different magnifications. In the left image, 22 x magnification clearly shows the 0.1 to 1 mm diameter macropores typical of aerated concrete. Further magnification to 11,000 x reveals the needle-like arrangement of the solid-matter structure. Fig. 2 shows the pore-space structure for Baumberger sandstone (left, 850 x magnification) and Sander sandstone (right, 450 x magnification) which are quite different in their structure despite the similar genesis of the two kinds of natural sandstone [41]. The Baumberger sandstone consists of a conglomerate of fine crystals a few micrometers in diameter which surround the pores. The Sander sandstone shows considerably larger crystals several tenths of a millimeter in diameter. The walls of the pore spaces are covered with fine flakes in some places.

These photos show how difficult it must be to find a simple mathematically treatable pore model capable of reproducing even approximately actual pore space geometry vis-a-vis its complex influences on moisture storage and moisture transport. In addition, as the examples show, there is the fact that the same pore model is applicable only to a small range of similar building

materials. Consequently, a number of different pore models have to be developed to describe the commonly used mineral building materials. It is for this reason that Brunauer [12] attempts to describe pore space by using hydraulic radius without a pore model.

In this study pore models are only used to better illustrate the discussions and data so as to assure comparability with test data obtained using different methods. The most widespread and simplest is the model of non-branching capillary tubes of differing radii (cylindrical pore model). Of course use of this simple pore model creates systematic errors which have to be taken into account in interpreting the results (cf. also [32] [112] [125]).

2.1.1 Storage of moisture

Three regions may be differentiated in porous mineral building materials: the region of sorption moisture, the capillary water region and the region of supersaturation. Following is a more detailed discussion of these three regions.

The sorption moisture region

The sorption moisture region is characterized by the accumulation of water referred to as sorption from the surrounding moist air until a state of equilibrium is reached. Under isothermic conditions, the relationship between the volume of the accumulated water and relative humidity is characterized by the sorption isotherm (see Fig. 3). For hygroscopic porous building materials sorption isotherms have a typical S-shaped profile ([55] [39] [61]) and often show a hysteresis effect between moisture absorption and release (adsorption and desorption). This hysteresis effect is widely viewed as the result of differing wetting characteristics for adsorption and desorption or other phenomena created by pore space geometry ([18] [45] [111]). However, measurements by Künzel [82] show that for most building materials the hysteresis effect is so slight that the adsorption isotherm is adequate to characterize the sorption moisture region. In the case of somewhat more pronounced hysteresis, investigations by Rode [115], who compared results

computed with and without taking the hysteresis into account, showed that sufficiently accurate calculation of moisture behaviour of such materials is possible by averaging of adsorption and desorption isotherms. The influence of temperature is indicated schematically in Fig. 3, bottom. Krischer [68] reports an approximately linear relationship in which equilibrium moisture content changes by a factor in the order of magnitude of 10^{-3} to 10^{-2} K^{-1} depending on relative humidity. The typical characteristics of a sorption isotherm for hygroscopic materials are shown in Fig. 3 (top). The lower area up to about 15% relative humidity is marked by monomolecular coating of the solid surface, followed by transition into an area of multimolecular coating which rises in linear fashion, ending at about 50 % relative humidity. From this curve it is possible to determine the inner surface using the BET theory [11]. The subsequent progressively rising area is attributed to capillary condensation. This involves the appearance of condensation phenomena in the micropore area with radii between roughly 2×10^{-9} and 10^{-7} m. According to Kelvin's law these are attributable to a lowering of saturation vapour pressure over concave menisci ([39] [45] [61]). The assumption of a spherical menisci in a cylindrical capillary yields, as derived in [55], the often-used formula of the Kelvin equation. It shows the relationship between relative humidity and that capillary radius up to which the cylinder pores are filled with capillary condensation:

$$\varphi = \exp\left[-\frac{2\sigma\cos\theta}{r\rho_w R_D T}\right] \qquad (1)$$

φ [-]	relative humidity
σ [N/m]	surface tension of water
θ [dgr]	wetting angle
r [m]	capillary radius
R_D [J/kgK]	gas constant for water vapour
T [K]	absolute temperature
ρ_w [kg/m^3]	density of water

Fig. 4 shows the curve for equation (1) assuming complete wetting.

Capillary moisture region

At relative humidities above 95% the sorption isotherm rises very sharply. However it is for this very region that there is no known method of measurement to determine relative humidity with high accuracy. It is therefore not possible to definitively apportion moisture content to relative humidity. It is here that the capillary moisture region, frequently also called the superhygroscopic region, begins. This region is marked by the ability of capillary-porous hygroscopic materials to take up water until capillary saturation is reached. Capillary saturation is defined as the material moisture content which can be attained through natural absorption under normal pressure without the influence of exterior forces. For capillary-porous building materials, capillary saturation is always below the water content possible from open pore space and is an important coefficient of the material. The reason that not all pore space is filled is the presence of entrapped air bubbles. The absorption capability results from the surface tension of liquids and the wettability of solid bodies in contact with the liquid. In [68] [127] [125] [39], [99] and [93] there is a full description of the capillary phenomena which can most clearly be depicted by the simple model of a cylindrical capillary (Fig. 5). In a partially filled capillary, a concave or convex bending of the surface (meniscus) develops due to the surface tension of the liquid and the interfacial tension between liquid and wall, which may be positive or negative. The curved surface of the liquid creates a pressure directed toward the centre of the curve which for a cylindrical capillary can be described by the following formula:

$$p_K = \frac{2\sigma\cos\theta}{r} \qquad (2)$$

p_K [Pa]	capillary pressure
σ [N/m]	surface tension of water
θ [grd]	wetting angle
r [m]	radius of curvature

Depending on the wetting angle this pressure is responsible for the rise (capillary ascension) or drop (capillary depression) of the meniscus in a capillary and can, as shown in Fig. 5, take on extreme values with decreasing radius. If capillaries of differing radii are connected with one another, the smaller ones will continue to draw moisture out of the larger capillaries until they themselves are saturated and thus cease to exert tension, that is until their meniscus has the same radius of curvature or until the larger capillary is emptied (see Fig. 5, middle, above).

In a capillary-porous body having continous pore-size distribution, all of the smaller pores will therefore be filled with water up to a certain pore size as a function of moisture content. There thus exists a correlation between the moisture content of a capillary-porous material and its capillary pressure defined by the largest pores still filled. If a moist capillary-porous building material is placed in contact with another dry building material, the latter will continue to absorb water until a state of equilibrium exists. This equilibrium is marked by the existence of equal capillary pressure in the two materials. When the two materials do not have the same pore size distribution, different moisture contents will be established.

This capillary pressure (often also called suction pressure) can be recorded using a variety of measuring techniques. The capillary pressure curve (capillary pressure as a function of moisture content) hence yields the storage function for the capillary moisture region. The suction pressure curve usually shows a hysteresis between humidifying and dehumidifying. This phenomenon, which is readily explained from the cylindrical capillaries with diameter varying along the capillary shown in Fig. 5 (bottom left), is referred to by Lykow [93] as capillary hysteresis. Molenda, Crausse and Lemarchand [98] show via a calculation of moisture balance that the measured hysteresis of the capillary pressure curve of a sand fill has a noticeable effect on its moisture balance. By contrast hysteresis has only a slight effect on aerated concrete. The reason for this lies in the fact that in aerated concrete, as in most mineral building materials, there is significantly broader pore size distribution than in sand fill and consequently a much flatter shape to the

suction pressure curve. Hence hysteresis has less impact. Investigations by this author on specimens of natural sandstone show that roughly the same superhygroscopic equilibrium moisture contents are established regardless of whether they were reached by humidification or dehumidification of the reference specimens (Fig. 6). The effect of temperature on the suction pressure curve follows, as tests by Crausse [20] and Vetterlein [135] show, from the slight influence of temperature on surface tension (see equation 2).

Supersaturated region

Capillary saturation can only be exceeded by application of external pressure, application of a vacuum to remove trapped air or forced condensation by pushing below the condensation point. Another possibility lies in protracted soaking in water since trapped air dissolves in the water with time. There is no unique relation between capillary pressure and water content in the region of supersaturation since replacing the air bubbles in a specimen does alter its water content but not its suction pressure. Consequently the suction pressure curve of a vacuum-saturated specimen will even in the capillary water region differ from that of the suction pressure curve for a capillary saturated specimen. As tests have shown [73], no moisture equilibrium is reached through capillary transport between supersaturated and capillary-saturated regions even within 40 days. Because wetting of mineral building materials beyond the point of capillary moisture saturation occurs only as a rarity under the natural physical conditions prevailing in built structures, the region of supersaturation is ignored.

2.1.2 Moisture transport

Fig. 7 gives an overview of the transport phenomena which may take place in pores dependent on aggregate state and motive forces [56]. A number of transport phenomena are however of little relevance under the practical physical conditions of building and construction and will therefore not be looked at in this study. With the exception of the effects of fire which involve high temperatures, differences in overall pressure occur only to a modest degree under normal conditions (wind pressure) so that convective hydraulic

and gas flow may be neglected. The influence of electrokinesis on capillary transport is as yet not adequately understood. According to [4] the process of suction is accelerated by electrokinetic phenomena, but impeded according to [140]. According to [5] thermodiffusion accounts for only the negligible figure of about 0.05% of overall transport under the conditions to which built structures are normally exposed. This transport phenomenon is not to be confused with the thermally-controlled portion of vapour diffusion resulting from the fact that water vapour saturation pressure is a function of temperature. Moisture transport coefficients having temperature as the driving potential, as used by numerous authors ([55] [63] [92] [106] etc.) are only caused by formal splitting apart of the real potential, the partial pressure, into the potentials relative humidity and temperature. Likewise omitted from this study is the effect of gravitation on moisture transport. As the authors of [141] show, gravitation only begins to affect liquid transport at pore radii greater than 10^{-6} m; it can therefore be neglected in the horizontal suction experiments conducted. Fig. 8 shows the transport phenomena occurring at various moisture contents using the model of a single cylindrical capillary of varying diameter (modified after [118]).

2.1.2.1 Water vapour diffusion

As illustrated in Fig. 7, vapour diffusion as well as effusion may occur as a result of differences in partial pressure. Using the Knudsen factor, which describes the ratio of mean free path length of the water molecule and pore space diameter, it is possible to produce a breakdown into the various transport mechanisms:

$$K_n = \frac{L}{2r} \qquad (3)$$

K_n [-] Knudsen factor
L [m] mean free path
r [m] pore radius

If the mean free path length is greater than the pore space diameter, there is Knudsen molecular movement, also referred to as effusion. Transport here is marked by collisions of the water molecules with the pore wall. Under normal conditions the free path length for gases and water vapour is in the order of magnitude of 10^{-8} m. Effusion therefore takes place only in the micropore region.

Krischer [68] reports the following transport equation for effusion through cylindrical capillaries:

$$g_E = -\frac{8}{3} r \sqrt{\frac{M}{2\pi RT}} \frac{dp}{dx} \qquad (4)$$

g_E [kg/m²s]	effusion flux density
M [kg/mol]	molecular weight
R [J/mol K]	universal gas constant
T [K]	absolute temperature
p [Pa]	partial pressure of water vapour
r [m]	capillary radius

In the case of pore diameters considerably greater than the mean free path length (Kn <<1), transport is marked by collisions of the water molecules with one another. Gas transport in this „continuum flow regime" is known as water vapour diffusion. According to [130] the following is given by the general gas theory using the ideal state equation for humid air:

$$g_v = -\frac{2\sqrt{2}}{3} \frac{\sqrt{\frac{1}{M_l} + \frac{1}{M_w}}}{N_L \cdot \sigma_{L,w}^2 \cdot P_L} \left(\frac{RT}{\pi}\right)^{3/2} \frac{dp}{dx} \qquad (5)$$

g_v [kg/m²s]	vapour diffusion flux density
M_L, M_w [kg/mol]	molecular weight of air and of water
$\sigma_{L,w}$ [m]	average gas-kinetic impact diameter
P_L [Pa]	ambient atmospheric pressure
N_L [mol^{-1}]	Loschmidt number

In the intervening transition zone the two transport mechanisms occur intermixed. Because there is a pore size spectrum in most mineral building materials, which covers all three regions in a continuous manner, clear separation of the transport phenomena is scarcely possible. Moreover the driving force for both kinds of transport is partial vapour pressure. Consequently, from this point on the study employs a single common diffusion coefficient to describe effusion and water vapour diffusion in building materials.

$$g_v = -\frac{D_D}{\mu R_D T} \frac{dp}{dx} \qquad (6)$$

g_v [kg/m²s]	vapour diffusion flux density
D_D [m²/s]	vapour diffusion coefficient in air
R_D [J/kgK]	gas constant for water vapour
p [Pa]	partial pressure of water vapour
μ [-]	water vapour diffusion resistance factor

In the physics of building and construction the empirical equation by Schirmer [124] which is also established in DIN 52 615 has become most widely used for the vapour diffusion coefficient in air:

$$D_D = 2{,}3 \cdot 10^{-5} \frac{P_o}{P_L} (T/273)^{1{,}81} \qquad (7)$$

P_0 [Pa]	standard pressure
P_L [Pa]	ambient atmospheric pressure
D_D [m²/s]	vapour diffusion coefficient in air

In the case of vapour diffusion through porous material layers, diffusion flow has to overcome an increased resistance. This is due to the ratio of the area occupied by the pores to the total cross-section area (porosity), to the roundabout routes imposed by the pore structure and to cross-sectional changes in the pore ducts. Krischer and Kast [68] have introduced a constant

resistance factor incorporating these phenomena and determined experimentally. This water vapour diffusion resistance factor μ expresses the factor by which the diffusion resistance of a layer of material exceeds that of a layer of air of equal thickness. The factor D_D/R_DT represents the transport coefficient for diffusion in air defined in DIN 52 615 [26].

$$g_v = -\frac{D_D}{\mu R_D T}\frac{dp}{dx} = -\frac{\delta}{\mu}\frac{dp}{dx} \qquad (8)$$

g_v [kg/m²]	vapour diffusion flux density
μ [-]	water vapour diffusion resistance factor
δ [kg/msPa]	water vapour permeability of stagnant air
p [Pa]	partial pressure of water vapour

However if the vapour diffusion resistance δ/μ is determined from equation (8) in accordance with DIN 52615 for varying ranges of relative humidity, measured diffusion resistance shows a typical dependence on relative humidity in hygroscopic porous building materials ([81] [133] [90] [35] etc.). If the mean relative humidity in the specimen is increased, the water vapour permeability rises in a non-liner fashion, in some cases steeply. Fig. 9 shows the difference between the water vapour resistance factors determined in accordance with DIN 52615 in the dry region and determined in the moist region for various building materials plotted against degree of pore fullness (volumetric proportion of sorption water content as a fraction of total pore volume). It is abundantly clear that the water absorbed in the pores is responsible for the rise in water vapour permeability as determined in this way [71]. Husseini [54] modifies the Glaser procedure by including the dependence of the diffusion resistance factor on relative humidity and the sorption isotherm of hygroscopic materials in his nonsteady diffusion model. Philip and De Vries [106] attribute the lowering of vapour diffusion resistance measured under isothermic conditions to the increased appearance of water islets with increasing relative humidity. These water islets are said to act as a short circuit for the water vapour diffusion (see Fig. 10, top).

Whereas a number of authors ([55] [64] [98] [99] [114] etc.) likewise see the formation of water islets as a major reason for the moisture dependence of diffusion resistance, others ([17] [35] [67] [118] and [119]) suspect that the cause is to be found in surface diffusion (see Fig. 10, bottom). On examination of scanning electron microscope photos of the pore spaces of capillary-porous materials (Fig. 1 and Fig. 2), closing of the pores by the so-called water islets postulated as the cause by Philip and de Vries does not appear very probable, at least at low relative humidities (below roughly 80% relative humidity).It would seem more likely to assume that when water is taken up by absorption it is deposited as an adsorbed film on the walls of the pores and especially in the wedge-shaped spaces between adjoining crystals of the solid-matter structure (see Fig. 11). It is these wedge-shaped spaces which, as humidity rises, are capable of absorbing a great deal of water which, compared to the thin absorbing film with a thickness of only a few molecules clinging to the flat surface, is highly mobile.

If the specimen is under a partial vapour pressure gradient, there will be a diffusion transport along this gradient as given by equation (8) which is unaffected by the sorption moisture present in the pore space. Strictly speaking, this applies only as long as the open cross-section available for diffusion is not appreciably reduced in size by the water present.

Under isothermic conditions, when there is a partial vapour pressure gradient, there is always in the specimen a gradient of relative humidity or sorption content in the same direction. The transport phenomena occuring under these conditions may be clearly illustrated using the simple model of a single cylindrical capillary (see Fig. 12). Owing to the drop in partial pressure a diffusion transport takes place along the capillary in gaseous phase. In addition the existing adsorption moisture gradient produces liquid transport in the sorptive layer, likewise in the direction of the partial pressure gradient. This means however that sorption moisture on the side of higher humidity drops below equilibrium moisture content and on the other side rises above equilibrium moisture. The result is sorption on one side of the specimen and desorption on the other. It may be assumed that sorption moisture equilibrium

on the surfaces of the specimen is reached very rapidly compared to diffusion and liquid transport through the specimen cross-section. Accordingly, water vapour permeability determined under isothermic conditions prescribed in DIN 52615 results, at least at higher average relative humidity, from the sum of vapour diffusion and liquid transport overlying this diffusion.

The present study is intended to contribute to understanding of the true causes of the observed moisture dependency. Understanding of this issue is of great importance since it determines whether the customary description of moisture transport (liquid and vapour) as diffusion dependent on moisture is acceptable.

2.1.2.2 Liquid transport

In looking at the phenomena of liquid transport it is necessary, just as with moisture storage, to draw a distinction between the sorption moisture region and the capillary water region. The region of supersaturation may be omitted for the reasons discussed in Para. 2.1.1. In hygroscopic mineral building materials, surface diffusion takes place in the sorption moisture region, while capillary action occurs in the capillary water region.

Surface diffusion

Due to adsorption of water molecules on the inner surfaces, there forms, according to the BET theory [11], a sorptive film of greater or lesser thickness; the thickness increasing with rising relative humidity. With the thickness of the sorptive film there is also an increase in the mobility of the water molecules absorbed in multi layers [61]. If there is a relative humidity gradient, a mass transport takes place in the liquid film on the pore wall set in motion by the differences in layer thickness of the sorptive film. In contrast to Philip and de Vries [106], who consider surface diffusion to be negligible, mass transport through surface diffusion is of considerable significance in hygroscopic mineral building materials at relative humidities above 50% as

reported in [17] [23] [35] [118] [119] and [122], and in fact may exceed pure vapour diffusion by many times. It may be assumed that mass flow in surface diffusion is proportional to the layer thickness gradient and hence to the concentration gradient. It is therefore a diffusion transport which can be described by an equation analogous to Fick's law [122] and [119]):

$$g_{OD} = D_{OD} \frac{dw}{dx} \qquad (9)$$

g_{OD} [kg/m^{2}s]	surface diffusion flux density
D_{OD} [m^2/s]	surface diffusion coefficient
w [kg/m^3]	water content
x [m]	spatial coordinate

According to studies by Schaschek [122] and Chang [17] on the temperature dependance of surface diffusion based on investigation of adsorption energies and activation energies to overcome potential thresholds on heterogeneous surfaces, the transport intensity of surface diffusion increases as temperature rises. A further indication which suggests an increase with temperature comes from the decrease in the viscosity of the liquid with rising temperature.

Capillary conduction

The practically significant effect of capillary conduction in porous building materials has to date eluded precise theoretical description ([61] [58] [55]). The reasons for this, as previously discussed in Para. 2.1, lie in the extremely complex cavity structure with its indefinable changes in cross-section and interconnection of the transport ducts which no longer can be depicted by simple, easily treatable mathematical models. A mathematical approximation is therefore tied to certain model theories derived from and proved by experiments.

For the model of a single capillary, Cammerer [14], starting with the Bernoulli equation of hydrodynamics and the Hagen-Poiseuille law for flow through tubes, derives a differential equation for fluid movement and obtains for depth of suction an equation in the form:

$$X = B\sqrt{t} \qquad (10)$$

X [m]	depth of water penetration
B [m/√s]	water penetration coefficient
t [s]	time

This √t relationship also appears in the capillary water absorption of porous building materials having widely differing pore structures ([126] [80]). From this Schwarz [126] derives the water absorption coefficient A which is also contained in DIN 52617 [27] in accordance with the following defining equation:

$$m_w = A\sqrt{t} \qquad (11)$$

m_w [kg/m²]	amount of water absorbed
A [kg/m²√s]	water absorption coefficient

While the amount of liquid absorbed during the contact with water can indeed be calculated using Equation (11), it does not however allow any conclusions on water content distributions or capillary equilibrium phenomena. The √t mathematical calculation model assumes a precisely defined water front which penetrates into the interior of a building material. However this is not the case in actual building materials where there is always a water content gradient due to the interconnected pores varying in size, with their different capillary pressure and flow resistances (see Para. 2.1.1). Using the model of interconnected cylindrical capillaries it is possible to explain the formation of water content profiles. The liquid in a capillary-porous body is accelerated by capillary tension until an equilibrium is reached between capillary tractive force and flow resistance. In a cylindrical capillary, tractive force is

proportional to the inverse value of the radius (equation (2)). However flow resistance is proportional to the inverse value of the square of the radius (Hagen-Poiseuille law). The result of this is that the water in the larger capillaries pushes on ahead despite their lower drawing power (see Fig. 13, top). For this reason there is always a continuous decline in water content in the direction of suction.

Since the operative tractive forces of capillary action in the pore space cannot be measured directly, but since their measurable effects (gradient in water content) must have a functional relationship with them, Krischer [68] formally introduced water content as motive potential. This yields the following diffusion equation:

$$g_w = -D_{w(w)} \frac{dw}{dx} \qquad (12)$$

g_w [kg/m²s]	liquid transport flux density
$D_{w(w)}$ [m²/s]	liquid transport coefficient
w [kg/m³]	water content

In his theoretical derivation Krischer likewise assumes a capillary bundle model consisting of parallel cylindrical capillaries of varying diameter interconnected without any resistance. Equilibrium of pressure in all filled capillaries at a given cross section of the bundle is assumed. The negative pressure in the liquid is then determined by the capillary suction of the taut meniscus of the largest still-filled capillary in this cross section. This relationship between the capillary suction stress in a cross section of the bundle and the water content there results in a capillary transport coefficient D_w which is heavily dependent on water content. Cammerer [15] comes to a similar conclusion through the equation of motion in the capillary bundle. In [19] Crank shows that with this approach, the √t dependence of absorbed amount of water found experimentally can be reproduced, regardless of the form of the capillary transport coefficient. Krischer's approach does not apply however, as he himself states, to the following limiting cases:

a) water transport without water content gradient. The transport coefficient would have to be infinitely large, e.g. if transport in the water-saturated region of an individual capillary or in an area of a building material capillary saturated with water is considered.

b) water transport with discontinuous water content gradient. The transport coefficient would have to be equal to zero at the discontinuous point because of the infinite water content gradient, e.g. across the meniscus in an individual capillary, in the absence of certain intervals in the pore-size spectrum of a material or with passage of fluid through the interface of two materials of differing capillary structure.

Despite the limitations cited, an approach along the lines of equation (12) seems appropriate for the following reasons:

Case a) involving total saturation of sizeable areas of a building material rarely ever occurs under ordinary circumstances. Discontinuity in pore distribution (case b) has not been observed in mineral building materials in the water-content regions of interest. The problem of discontinuity at boundary layers may be eliminated by proper choice of the mathematical method used or by conversion to another motive force independent of material. Since this approach allows a far better depiction of the capillary transport phenomena actually occurring in capillary-porous materials, compared to the pure $\sqrt{t}$ approach, it has already been employed in numerous papers ([34] [37] [58] [64] [106] etc.) and will also be used in the course of this work.

According to studies by Crausse [20] and Vetterlein [135] the temperature-dependence of capillary transport results from the temperature-dependence of the viscosity of the fluid. The temperature-dependence of surface tension, which is only very slight, is of minor significance here.

If the supply of water is cut off, ongoing fluid transport takes place, although counter-menisci do form on the surface no longer supplied with water (see

Fig. 13, bottom). This subsequent movement of fluid occurs because the smaller pores not yet filled suck dry the larger filled pores through the cross-connections by virtue of their greater suction power. It is anticipated that this ongoing movement of fluid proceeds much more slowly than does the transport during the absorption process, so that it is necessary to apply different fluid transport coefficients for fluid transport depending on the boundary conditions (wetted or unwetted surface). Prazak [108] likewise states, based on test measurements on lime sandstone, that capillary transport is dependent on the boundary conditions involved. However he draws from this simply the conclusion that the capillary transport coefficient is not a true material characteristic.

2.2 Experimental procedures

For determining storage characteristics, moisture transport coefficients and vapour diffusion coefficients the literature contains a variety of test procedures, some differing markedly. However not all procedures are equally well-suited, or indeed suited at all, for conducting the necessary investigations for optimal success at reasonable expense. Following is a look at the various test procedures and a discussion of their suitability.

2.2.1 Determination of storage characteristics

In determining storage characteristics it is necessary to distinguish between the sorption moisture region and the capillary water region. In the sorption moisture region there is a very simple universally-used procedure. The specimen is placed in an environment regulated by means of a salt solution or a conditioning cabinet and the equilibrium moisture content determined by weighing the specimen. Varying relative humidity in stages from relatively low (<50% RH) to high humidity (up to 90% RH) yields the adsorption isotherm, or, using the reverse process, the desorption isotherm. Measurements above 95% RH should not be made since in this area the sorption isotherm for hygroscopic mineral building materials is extremely steep. In fact, small unavoidable variations in relative humidity (for example, due to variations in

temperature) by themselves cause very large changes in sorption moisture ([26] [61] [133]). Depending on the specimen material and the number of moisture stages involved, determination of a sorption isotherm may take several weeks or months due to the very slow process of establishing equilibrium moisture content. For this reason a second measuring procedure should not go unmentioned, viz. that described by Fagerlund in [29]. The measuring principle here is based on the lowering of the freezing point of the water in pores of decreasing radius. This allows formulation of a theoretical relationship between freezing point depression and radius as well as via the Kelvin relationship per equation (1) with relative humidity. Recording of a sorption isotherm can be carried out in this fashion within about 3 hours. However freezing can produce structural damage. In addition the possibility of supercooling of the liquid in the pore space has to be taken into consideration. Another major drawback of this test method lies in the relatively large outlay in measuring and recording equipment involved.

In the capillary water region, the storage function, which represents the relationship between capillary pressure and water content, has to be determined in a different manner. Kießl [55] calculates the storage function for this region from pore radii distributions determined from mercury porosimetry. Seemingly more useful by contrast is the use of water as the measuring medium (more on this in Para. 4.3). In all procedures, capillary pressure or suction pressure is controlled and water content determined after establishment of equilibrium water content. By incremental increase in suction pressure the suction pressure curve is obtained. In doing this use can be made of centrifugal force in centrifuging the specimen or a pressure or negative pressure can be applied directly to the liquid in the pore space. Measuring equipment based on osmotic phenomena may also be used (tensiometer). A good overview of the various analytical methods may be found in [21].

When a water-saturated specimen is centrifuged, centrifugal forces are exerted as a function of rotating speed and distance from centre of rotation. Under their influence water is thrown out from the side of the specimen

furthest from the axis until there is equilibrium between capillary action forces and centrifugal forces acting on the columns of liquid suspended from the menisci. This results in a water content in the specimen which increases with increasing distance from the axis of rotation, as shown in Fig. 14a ([67] [127]). Since the operative centrifugal forces are readily calculable, a number of tests involving varying rotation speeds yields the suction pressure curve. In order to centrifuge the water out of pores even as small as 10^{-7} to 10^{-8} cm in diameter, rotating speeds sometimes much higher than 10,000 rpm have to be used depending on the diameter of the centrifuge. Aside from the high cost of such centrifuges, this can easily result in high mechanical stress of the specimen material, and even its destruction. In addition, once the test has been completed the moisture profile has to be determined quickly and immediately before it changes as a result of capillary equilibrium phenomena. This problem can be avoided by using a relatively short specimen on the outer end of which is attached a saturated capillary-porous body. This achieves a given length of water column, as long as the pores of this body are fine enough. As long as specimen length is small vis-a-vis overall length the moisture gradient in the specimen can be ignored ([21] [76]) and the suction pressure curve can be determined by weighing the specimen after equilibrium is reached with an appropriate number of different rpm levels (see Fig. 14a).

So-called tensiometers are based on a different measuring technique and are used chiefly in soil science (see [21] and [113]). In tensiometers the specimen is in contact with a porous, water-saturated ceramic. This ceramic is in contact with a sealed water-filled chamber in which a manometer is located (see Fig. 14c). Water is removed from the tensiometer until suction pressure equilibrium is reached by way of the measurable underpressure which develops. Another alternative is creating a hydrostatic underpressure through a lowered water level (Fig. 14d). The drawback of both methods however lies in the only very limited suction pressure range from 0 to about 1 bar, since the achieved underpressure is limited by the vapour pressure of water.

A significantly broader suction pressure range is covered by the pressure plate apparatus (see Fig. 14e) attributable to Gardner [36] and likewise used in soil science ([6] [9] [47] [104] [123]). In a pressure vessel is a porous ceramic plate which is air-tight but water permeable (the details of the apparatus setup are discussed further in Para. 4.1.1). In this case, instead of using an underpressure, water is forced out of the water-saturated specimen placed on the plate by an overpressure until establishment of an equilibrium moisture content appropriate to the pressure. By progressively increasing pressure, the storage function up to a suction pressure of up to 100 bar can be determined in this way. In contrast to the centrifuge method described previously, this method precludes destruction of the specimen since only pressure stresses act upon the solid-matter structure.

In this research study measurement of suction pressure using the pressure plate apparatus is used for the first time in tests on solid-state bodies in the field of physics relating to structures and the building sciences. Through a comparison with mercury porosimetry the advantages of this analytical method for determination of a realistic moisture storage function are discussed in Para. 4.3.

2.2.2 Determination of vapour diffusion coefficients

Procedures for measurement of vapour diffusion coefficients are standardized in the Federal Republic of Germany under DIN 52 615 [26]. Here a distinction is drawn between dry region processes for a moisture region between 0 and 50% RH, generally known as the "dry-cup" method, and moisture region processes for a moisture region between 50 and 100% RH ("wet-cup"). Measurement takes place under isothermal conditions.

A plate-shaped specimen of the material to be tested is placed atop a vessel as its cover and made vapour-proof around the edges of the vessel (Fig. 15). A constant relative humidity is then set up in the vessel using a drying agent or a saturated salt solution. The vessels are placed in a conditioning chamber at constant temperature and humidity. Under the influence of the water

vapour partial pressure gradient between the air spaces bordering the surfaces of the specimen water vapour diffuses through the specimen. Once a steady diffusion flow is set up there is a constant weight change in the test vessel per unit of time which corresponds to the diffusion flow.

For diffusion measurements on thin layers of non-hygroscopic materials a stationary diffusion flow is established almost at once without a "start-up process." For thicker layers of hygroscopic materials, moisture equilibrium commensurate with the ambient conditions (exterior and interior) must first be established in the test specimen. The initial weight changes measured in the test vessel including the test specimen are therefore at first attributable both to changes in moisture of the test specimen and to weight changes in the sorbent inside the vessel. Separation of the two is possible by weighing the test specimen and the sorbent separately. Zehendner [142] is one author who describes a test apparatus for this. Steady diffusion is reached when the weight of the test specimen remains constant. It may under some circumstances take a long time for the steady state to be reached depending on the thickness and diffusion resistance of the test specimen. Because an initial weight change proportional to time often takes place during the start-up process, faulty interpretations are easily made if there is inadequate measuring expertise in this regard ([8] [30]).

For procedural reasons in such tests it is useful if there is a layer of air between the underside of the specimen and the drying agent/salt solution [13]. With use of a granular drying agent (e.g. silica gel) fresh drying agent can be made to emerge on the surface of the fill by shaking after each weighing. If a liquid is used, an intervening air space is necessary to prevent wetting of the specimen underside during handling.

To calculate the diffusion resistance of the layer of air, stagnant air is assumed. This is permissible for "dry cup" measurements since in this case there is increasing relative humidity from the drying agent to the specimen with resulting decreasing density of the air. In the case of "wet cup" measurements there is however beneath the surface of the specimen drier air

of higher density than above the salt solution. This may result in a convection in the air layer and hence to a lower diffusion resistance through the layer of air. Especially with specimens having low diffusion resistance, faulty interpretation of the influence of the air space can result in an underestimation of diffusion resistance.

For some materials, as shown in [85], the water vapour diffusion resistance factor can be determined with good accuracy much more quickly by way of nonsteady diffusion measurements. However this method does not work for non-homogeneous materials having a denser surface skin or coating.

Since in practice diffusion processes as a rule take place under the influence of differences in temperature and relative humidity in the air on the opposing surfaces of the building component,measurements were also carried out in the presence of a temperature gradient in the test body ([120] [138]). This method is more laborious and carries with it the danger that the diffusion value from the test will be falsified by possible presence of moisture condensation in the specimen. Moreover comparison with insulating materials against cold [13] revealed no major difference in the results from those obtained under temperature equilibrium.

In the diffusion measurements carried out under isothermic conditions, the partial vapour pressure gradient and the gradient of relative humidity and consequently also the sorption moisture gradient are all in the same direction. Differentiation between gas diffusion and fluid transport in the sorbate film to verify the aspects set out in Para. 2.1.2.1 is not possible. This would require use of a measuring apparatus which would make it possible to set up a temperature gradient over the specimen cross-section so as to create a humidity gradient and therefore also a sorption moisture gradient opposing the partial pressure gradient (see Fig. 12). In the event that in reality the superimposed fluid transport in the sorbate film led to the lowering of vapour diffusion resistance determined under isothermic conditions, a sorption moisture gradient opposed to the partial pressure gradient would have to cause a rise in the measured diffusion resistance.

2.2.3 Determination of capillary transport coefficients

According to Equation (12) the capillary transport coefficient is yielded by the mass flow of the water and the water content gradient responsible for the transport:

$$D_w = -g_w / (\frac{dw}{dx}) \qquad (13)$$

D_w [m^2/s]	liquid transport coefficient
g_w [kg/m^2s]	liquid transport flux density
w [kg/m^3]	water content

To determine this coefficient it is therefore necessary to measure the water content distribution. This makes it necessary therefore to employ a moisture measuring procedure with relatively high spatial resolution. A non-destructive and rapid measuring procedure would be desirable to be able to observe how the moisture distribution develops with time during the absorption process. Measurement of change in water content distribution with time in a single specimen also excludes the effect of the inevitable fluctuations in material characteristics of a number of specimens of a building material on determination of the capillary transport coefficient. In addition determination of water content distribution must be able to be carried out quickly enough to preclude any appreciable change in water content distribution while the measuring process is going on.

The difficulty in measuring moisture in materials is evident from the large number of varying test methods. A good overview of the physical fundamentals, the limitations of application and the pros and cons of the various methods is given in [7] [53] and [91]. In the following pages the various analytical methods under consideration are introduced and their suitability for determination of the capillary transport coefficient discusssed.

The methods of measuring material moisture may be divided into conventional methods and radiation-type procedures. The conventional methods include measurement of electrical resistance, measurement of thermal conductivity, measurement of electrical capacity, ultrasound analysis and the drying method.

Measurement of electrical resistance

The key effect of measuring resistance lies in a lowering of ohmic resistance as moisture content increases in a specimen that is almost non-conducting if dry ([2] [7] [42] [107]). Spatial resolution is scarcely attainable and the measurable phenomenon is heavily dependent on fluctuations in electrolyte content (salts). The influence of salts present can be reduced but not eliminated by using alternating current for the measurements. Moreover, measurement may cause warming of the specimen. Moisture measuring apparatus based on measurement of resistance are widely and successfully used only for recording wood moisture content.

Measurement of thermal conductivity

The increasing thermal conductivity of a material with rising moisture content is used in thermal conductivity test apparatus to determine material moisture content. A strong measurable response is obtained only from insulating materials ([1] and [137]), however measurement of moisture content distribution is possible in building materials using the hot-wire meter technique, but only with spatial resolution in the centimeter range [106]. Nevertheless there is the danger with this method that the heating necessary for measurement will influence the moisture profile.

Measurement of electrical capacity

This type of moisture measurement is based on the fact that in the frequency range below 1 Ghz the dielectric constant of water is some 10 to 40 times greater than that of most dry building materials. If the subject specimen is in a

capacitor, the change in the capacity of the capacitor is a measure of moisture content. By setting up an electrical resonant circuit, capacity is measured by determining the resonant frequency ([65] [91] [100]). This method of testing is affected only slightly by electrolyte content at a suitable test frequency. Surface roughness of the test specimen may cause randomly fluctuating distances between the specimen and the electrode which strongly affects the outcome. High moisture content levels close to the electrode may also cause erroneous measurements. This method is suitable for measuring moisture distributions with a spatial resolution of about 1 cm although the volume measured is dependent on the moisture content ([94] [100]).

Ultrasound analysis

The measurement of moisture content using ultrasound is based on the dependence of sound absorption, as well as its speed of propagation, on moisture. Because measurement of absorption is much more prone to error, measurement of sound speed is used more frequently ([7] [38] [91]). As tentative investigations of this author have also shown, this method of measurement is quite imprecise, is very dependent on the composition and structure of the test material and has practically no spatial resolution.

Kiln method

The kiln method, i.e. determination of moisture content by drying of the specimen in a kiln, still offers the most accurate method of testing and is therefore mostly used as a reference procedure ([7] [91]). An assessment of various relevant parameters such as drying temperature, time of year and possible flooding of the kiln with pre-dried air may be found in [84]. Although determination of the moisture distribution is only possible by destruction of the specimen, i.e. dividing of the specimen into the number of pieces required for the desired spatial resolution, this method is used frequently because of its accuracy, simplicity and affordability ([10] [37]).

The tracer method

In this method the absorption tests are conducted with water containing dissolved radioisotopes. Depth of penetration is determined from darkening of a special film placed on the specimen or from scanning of the specimen using a special detector. This requires use of gamma emitters as radioisotopes, since because of their low penetration power, beta emitters would only allow measurement of surface moisture content. Moreover, the half-life period of the isotopes used has to be sufficiently large relative to absorption time ([7] [38] [46]). This method may suffer from chromatography phenomena, i.e. penetration different for water and the tracer. Repetition of measurements is difficult due to contamination of the specimens and experiments of this nature may only be carried out in special radioisotope laboratories.

X-ray analysis

The absorption of X-rays depends on the density and the atomic number of the irradiated material. Water has a markedly lower X-ray absorption coefficient than do building materials. Computer tomography developed by Hounsfield [52] for the field of medicine makes possible two-dimensional pictures having high spatial resolution [102]. However due to the low absorption coefficient of water, moisture content can only be measured with very low resolution at relatively high outlay in terms of equipment and radiation safety ([109] [117]).

The microwave method

When irradiated with microwaves, water yields a high level of attenuation since the water molecules are excited into rotation. In the process the energy of the microwaves is transformed into heat. This can be used to determine the water content. A full description of the microwave test method may be found in [89]. With this method the density and the structure of the specimen material have a great influence on the outcome so that a calibration curve has to be established for each material [3]. Moreover, sharp boundaries between

dry and moist material may cause adulteration of the results because of diffraction effects [139]. Radiation levels must be restricted to the extent of not causing moisture migration due to warming. It is for this reason that this method allows achievement of acceptably high rates of measurement on very thin specimens only. The microwave technique makes it possible to measure moisture content distribution with a spatial resolution of about 1 cm with good sensitivity at high measuring accuracy. The influence of temperature and density may be taken into consideration to some degree by simultaneous recording of the phase shift created by of material ([59] [60] [136] and [139]).

Gamma-ray attenuation

Gamma-ray attenuation is the most widespread method of non-destructive measurement of material moisture content distribution ([78] [101] [110] [128]). It is based on the moisture dependency of absorption and scattering of gamma rays, with ^{241}Am, ^{60}Co and ^{137}Cs most frequently used as emitters. However the absorption coefficient of water is approximately the same as that of dry solids. Hence this method may be looked upon as a method of measuring density. Moisture content is determined from the difference of densities of moist and dry building material. In the case of materials showing wide differences in density, it is necessary to carry out a dry measurement involving precise site location. This can cause considerable difficulty especially in materials which swell greatly. With materials which over time change their solid structure and hence their density (e.g. from hydration in concrete or mortar), reliable determination of water content is not really possible with this method. An additional drawback of this method lies in the outlay required for radiation safety. New developments in test equipment allow determination of moisture content distribution with spatial resolution in the millimeter range at acceptable sampling speeds ([22] [24] [62] [129]).

Neutron scanning

High-energy neutrons, the so-called fast neutrons, interact with atoms upon passage through material. They are scattered, slowed down or diffuse. This

creates thermal neutrons having altered direction of travel and reduced energy. Water is most effective at braking fast neutrons; its braking power exceeds that of other commonly occuring elements by more than a factor of one hundred. Hence, for mineral building materials, measurement of thermal neutrons represents a direct measurement method for water ([7] [50] [132]). In general parlance a method of measuring moisture content is referred to as a direct measuring method for water when the test signal is influenced only, or at least almost only, by water content. Applied in this way, however, this method does not yield any spatial resolution. Dependent on moisture content, moisture is measured within a sphere with a radius of 20 to 50 cm around the emitter. High resolution can only be achieved if a specimen is irradiated with thermal neutrons instead of fast neutrons. After passage through the subject specimen, the neutrons penetrate a photographic plate which includes a conversion film. Neutron bombardment causes electrons to be be produced in the conversion film. These cause darkening of the photographic layer ([134] [143]). Drawbacks of the neutron method include the effect of a number of elements such as chlorine, lithium, iron and potassium on the test signal as well as the outlay required for equipment and radiation safety. Moreover, the method using thermal neutrons is an indirect measurement of water content similar to that of gamma-ray irradiation.

Nuclear Magnetic Resonance

Nuclear magnetic resonance is a test procedure long known in the fields of biology, chemistry and medicine as a spectroscopic method ([43] [49] [51] [66]). Less complex equipment units not suited to spectroscopy are also used in the food industry, materials science and soil science ([48] [77] [96] [103] [131]). Nuclear magnetic resonance is based on the angular momentum of the positively charged protons (spin) and the resultant magnetic moment. In an external constant magnetic field the hydrogen nuclei act like precessing magnetic dipoles; there are two allowed proton energy levels corresponding to orientation of their magnetic moment parallel or opposed to the direction of the applied magnetic field. An alternating magnetic field of a specified frequency, at right angles to the constant field, induces transitions between

the two energy levels. The high frequency energy hereby absorbed by the specimen is dependent on the number of protons in the specimen and can serve as a measure of moisture content since hydrogen nuclei in building materials in general occur only in the form of water. A detailed description of the test principle is given in Para. 6.1.1. Like the neutron irradiation method, this method is a direct method of measuring moisture content, albeit without its hazardous biological effects. It is further distinguished by its high accuracy at high measuring speed and low sensitivity to temperature ([69] [116] [121]). Good spatial resolution, as will be shown in this work, is possible using a special modified probe.

The criteria for non-destructive, high-accuracy measurement of moisture content offering good spatial resolution and a high measurement speed needed in determining capillary transport coefficients can only be met at reasonable cost by the gamma-ray method and by NMR. In contrast to gamma-ray irradiation, measurement by nuclear magnetic resonance, being a direct method, allows measurement of moisture content without the need for dry measurement. This and the absence of any hazardous radiation are the reasons for the first-time use of NMR in the present work for investigations in the field of building materials and structures.

To determine whether, depending on the boundary condition, capillary transport involves two different transport mechanisms (see Para. 2.1.2.2) it has been necessary to set up a test apparatus allowing rapid recording of moisture profiles. This was designed to make it possible to determine moisture content distributions during the absorption process even on building materials which absorb rapidly without the distribution changing appreciably during the test period. From the chronologically measured distributions it is possible to determine the transport coefficients for capillary penetration by liquid when the surface is wetted. If the supply of liquid is stopped after a sufficient amount has been absorbed, the transport coefficients describing subsequent moisture redistribution may be determined in the same way.

3. Building materials investigated

All investigations involved the same selection of building materials. Four types of natural sandstone (Baumberger, Obernkirchner, Rüthener and Sander) were selected so as to encompass, as far as their moisture-related properties are concerned, the broad array of natural sandstones used in building and construction. To represent man-made building materials, specimens of mineral materials commonly used in masonry (sand-lime brick, aerated concrete and clay brick) were chosen. Gypsum is used as an example of a material used in interior work. Following is a brief description of these materials.

The Baumberger sandstone is a yellowish-grey, arenaceous limestone from the Upper Cretaceous period having chiefly calcitic cement. It is finely porous and has a high absorptive capacity compared to the other types of sandstone. It has only poor to moderate resistance to weathering, showing such weathering phenomena as incrustation, wearing away, scaling and gypsum efflorescence [41]. Examples of its use include the cathedrals of Cologne and Münster.

The Obernkirchner sandstone is a coarse-silt to fine-sand, greyish-white to yellowish-white unstratified sandstone from the Lower Cretaceous period having high quartz content and primarily siliceous cement. This sandstone, which is likewise finely porous, has the lowest sorption capacity of any sandstone investigated here. It is used in the Rathaus [town hall] of Bremen and in numerous religious and secular buildings in Bückeberg and has good to very good resistance to weathering. Weathering phenomena include flaking and formation of cavities in fossil-rich strata [41].

The Rüthener sandstone is a greyish-green, moderately arenaceous sandstone from the Upper Cretaceous period having high quarz content and barytic-siliceous-argillaceous cement. This coarse-pored sandstone has a markedly high capillary saturation and a very high water absorption coefficient. It is used in many buildings and in many gravestones in the

Rüthen area, has very good resistance to weathering and shows encrustation, thin flaking and wearing away as typical weathering phenomena [41].

The Sander Sandstone from Sand is a brownish to olive green finely to moderately arenaceous sandstone from the middle Keuper (in the late Triassic period) having a mostly argillaceous cement. This fine-pored sandstone has a relatively high absorption capacity and a low water absorption coefficient. It is used in the Residence and the Ursuline Convent in Würzburg and in Schloß Seehof castle near Bamberg among others and shows a moderately good, occasionally good resistance to weathering with numerous weathering phenomena such as wearing away, crumbling, scaling, cracking and efflorescence [41].

Sand-lime brick is a building brick made of lime and silicic additives, which are thoroughly mixed, then moulded, compacted and cured under steam pressure. They are made solid or hollow in various densities and strength grades and depending on the application also made as frost-resistant sand-lime brick or facing brick. A solid brick having an apparent specific gravity of about 1900 kg/m^3 was chosen. At 29 % by volume, porosity is higher than in natural sandstones. Capillary saturation and the water absorption coefficient are comparable to those of the Baumberger sandstone.

To make aerated concrete, finely ground quartz sand is thoroughly mixed with cement, lime, water and an aerating agent and poured into moulds. Hydrogen is produced in the mixture, aerating it. The raw blocks are removed from the moulds and the various building products are cut from them. The products are cured in an autoclave under steam pressure. Because of its high porosity, aerated concrete has good thermal insulating properties. Investigations were carried out on an aerated concrete having a density of about 600 kg/m^3 and a porosity of roughly 72 % by volume. Because there is a significant volume of large pores without appreciable absorption capacity, capillary saturation and the water absorption coefficient are markedly lower than the high porosity would suggest.

Clay brick is one of the oldest man-made building materials. It is made of clay, loam or clay compounds, moulded with or without additives and fired. Firing at higher temperatures can produce sintering which makes the brick resistant to frost. The addition of sawdust or polystyrene beads can lower apparent specific gravity and thermal conductivity. The solid brick investigated with a specific gravity of about 1700 kg/m^3 has a porosity of roughly 38% by volume and a water capillary saturation of almost the same size. The sorption capacity of this material is very low; by contrast the water absorption coefficient is relatively high (see Table 1).

Gypsum is a material used in interior work primarily in the form of gypsum wallboard. The gypsum is applied to a heavy paper backing and dried in a stream of warm, dry air. Gypsum has a very high capillary saturation of about 40% by volume and a large water absorption coefficient with only a very low sorption capacity.

The moisture-related basic characteristics of the materials just discussed are listed in Table 1.

4. Determination of storage characteristics

Because wetting of mineral building materials beyond capillary saturation occurs only in isolated instances under normal conditions in building and construction, only the sorption moisture region and the capillary water region are discussed here. Different measuring methods have to be employed for the two regions. Determination of the sorption isotherm is quite well known and the measuring method standardized in DIN 52 620 [28] and as a result no further description of the method is given here.

A relatively comprehensive catalogue of sorption isotherms may be found in [44]. For some materials albeit the variation is relatively large, necessitating new measurements in some instances. Table 2 contains a listing of

adsorption moisture content figures at various relative humidities for the building materials investigated.

The moisture storage function in the capillary moisture region is determined using a pressure-plate apparatus. Using selected examples of salt-impregnated and non salt-impregnated natural sandstones the capillary pressure determined with the pressure-plate apparatus is compared with the test data from mercury porosimetry to illustrate the benefits and drawbacks of this measuring method. From the outcome of the sorption measurements and the pressure plate measurements a moisture storage function is developed encompassing all significant moisture storage characteristics of a porous building material all the way up to capillary moisture saturation.

4.1 Pressure plate measurement

Following is a description of the measuring principle, the equipment setup and the procedure involved in measuring capillary pressure.

4.1.1 Measuring principle

In capillary-porous, hygroscopic materials with continuous pore-size distribution, a maximum size of pores still filled with water can be correlated with every moisture content right up to capillary saturation. This correlation is predicated on the notion that all pores accessible to moisture are interconnected and the smaller pores having the higher capillary pressure draw water from the larger pores until capillary pressure equilibrium is reached for a specific moisture content. For the region of superhygroscopic moisture there exists a characteristic relationship; the so-called capillary pressure curve. Using the capillary pressure measuring setup, this curve is determined from dehumidification of initially saturated specimens by applying varying overpressures, with the corresponding equilibrium moisture content being determined for each pressure increment.

To calculate the relationship between moisture content and maximum pore-size still filled, the following model is used. The pore volume of the capillary-porous body consists of a bundle of unbranched capillary tubes of varying radii (cylindrical pore model). The elevation h of water in a capillary of radius r is given by:

$$h = \frac{2\sigma \cos\theta}{r\rho g} \qquad (14)$$

σ [N/m] surface tension (for water: $72{,}75 \cdot 10^{-3}$ N/m at 20 °C)
ρ [kg/m^3] density (for water: 1000 kg/m^3)
g [m/s^2] acceleration due to gravity
θ [°] wetting angle (for fully wetting liquids: 0°)

Because hydrostatic pressure at maximum attainable elevation must be equal to the pressure needed to empty this capillary, the pressure can be correlated with a radius up to which all of the larger pores are emptied. For water, this yields the following approximation equation:

$$r = 1{,}5 \cdot 10^{-6} / P_{ü} \qquad (15)$$

r [m] pore radius
$P_{ü}$ [bar] applied overpressure

Since normally there are no cylindrical unbranched capillaries in a capillary-porous body, the cylindrical pore model inherently has certain problems. Sometimes there can be considerable variation in diameter along the length of the capillaries. The pressure which has to be applied to empty the volume behind a constriction (the neck of the pore) is determined by the cross-sectional dimensions of this constriction in the pore. Thus equation (15) gives a correlation between the volume of water forced out and the radius of the pore-neck through which it was emptied [125]. However, since the same model shows the same systematic error when used in mercury porosimetry, we have the requisite conditions for a comparison between measurement of

suction pressure and mercury porosimetry. The conversion of capillary pressure to a pore radius only serves to illustrate the experimental results; the choice of pore model has no effect on the applicability of the suction pressure curve.

4.1.2 Equipment setup

The experimental apparatus for measuring suction pressure consists of three pressure vessels, diameter about 25 cm, for pressures up to 5 bar, 15 bar and 100 bar. Pressure is generated up to 15 bar by a compressor and with a gas bottle above this level. Pressure reducers are used to maintain constant pressure. The schematic layout of a pressure vessel and a photographic view are shown in Fig.16. Depending on its size and the number of specimens involved, each pressure vessel contains one to three ceramic plates. They are selected as to porosity so that after saturation their water permeability is as high as possible but not permitting the passage of air up to the maximum applied pressure. The plates are sealed with a rubber membrane on one side and connected to the outside by a hose. To achieve a good capillary contact between the underside of the specimen and the plate, the underside of the specimen is normally coated with porcelain clay and the specimen pressed against the plate. However because this can dirty the specimen and cause errors in weighing, after a thick layer of porcellain clay has been applied, the plate is covered with a very fine cloth through which very little of the clay can pass. Once the plate is moistened this produces a soft bed into which the specimens can be pressed. This likewise assures good hygroscopic contact while significantly reducing the clay adhering to the specimen.

4.1.3 Procedure and specimen material

The specimen material to be investigated is cut into pieces about 4 x 4 x 1 cm^3 in size. Greater thicknesses than 1 cm are to be avoided since this can significantly increase measuring time. Ten specimens of each type are used so that averaging will even out discrepancies in measurement. The dry weight of the specimen tablets is determined, following which they are saturated with

water under standard pressure, weighed and pressed onto the cloth. The plate is installed in the pressure vessel and the first pressure level applied. The water is now forced out of the specimens, through the plate and out through the hose. In two to four days a state of equilibrium is reached dependent on the dimensions of the specimens and their porosity characteristics, marked by cessation of water movement out of the vessel. The specimens are then removed from the plate, cleaned of any clay sticking to them and weighed, yielding the water loss for the particular pressure level. The specimens are then returned to the vessel to set the next pressure level. This procedure is repeated from the lowest pressure level to the highest. Overall measurements are taken at up to 10 pressure levels between 0.015 bar and 100 bar, covering a pore-radius range between 10^{-4} m and 1.5×10^{-8} m. From the readings for weight loss, pore volume or - expressed in terms of overall porosity - relative pore volume can be determined for each pressure stage and hence from equation (15) for the corresponding capillary radius range.

4.2 Results of pressure plate measurements

Figs. 17 and 18 show equilibrium moisture content for the four natural sandstones and the man-made materials plotted against the pressure applied in the test apparatus for measuring suction pressure. Also shown on the graphs are capillary saturation and as second abscissa the pore radius corresponding to pressure from equation (15).

It is evident from Fig. 17 that water is not seen being forced out of the Baumberger sandstone until a pressure of 0.5 bar, i.e. this sandstone has no appreciable volume of pores of radius greater than 3×10^{-6} m. From this point on, equilibrium moisture content drops continuously for the entire remainder of the pressure range. This means that there must be uniformly distributed pore-space volume over the full pore-radius range from 3×10^{-6} m to 1.5×10^{-8} m.

The curve is different for the Obernkirchner sandstone. From a pressure of 0.5 bar there is a very sharp drop in equilibrium moisture content and at a presure of 1.5 bar a moisture content of less than 30 % of capillary saturation has already been reached. When pressure is increased to 5 bar it falls again down to about 10% of capillary saturation and changes only slightly from there on. Hence the majority of the pores in the Obernkirchner sandstone must be in a radius range between 3×10^{-6} m and 10^{-7} m.

Even when pressure is increased from 50 to 150 mbar there is a sharp drop noticeable in the coarse-pored Rüthener sandstone and at a pressure of 0.5 bar one quarter of capillary saturation has already been reached. This means that half of all the pores in the Rüthener sandstone lie in the radius range between 3×10^{-5} m and 1.5×10^{-5} m and another quarter in the adjacent region up to 3×10^{-6} m.

In the Sander sandstone, equilibrium moisture content declines steadily over the entire pressure range. Hence this sandstone does not have a pronounced maximum in pore radii distribution.

The suction pressure curve for gypsum (see Fig. 18) is very similar to that of the Baumberger sandstone. The drop at 0.5 bar is somewhat steeper however and continues up to a moisture content of less than 5% of capillary saturation. Gypsum can therefore only have a low sorption capacity.

In sand-lime brick there is only a modest decline up to a pressure of 15 bar followed by a steep drop to the maximum pressure of 100 bar. This means that the largest proportion of the pores lies between 10^{-7} m and 1.5×10^{-8} m.

Aerated concrete likewise shows only a modest decline up to a pressure of 5 bar. Beyond this, equilibrium moisture content drops continuously as far as a moisture content of about 20% of capillary saturation when 100 bar is reached. In the large visible pores of aerated concrete there is hence no capillary transport; an observation confirmed as well by the large difference between capillary saturation and maximum water saturation for this material.

The majority of the capillary-active pores thus lies in the radius range between 10^{-7} m and 1.5×10^{-8} m.

Clay brick behaves in a manner very similar to that of gypsum, except that upon reaching 100 bar pressure there still exists an equilibrium moisture content of approximately 15% of capillary saturation.

4.3 Comparison with mercury intrusion porosimetry

To illustrate the advantages of pressure plate measurement vis-a-vis Hg porosimetry, measurements are carried out on salt-impregnated and non salt-impregnated sandstone materials. It is anticipated that salt content exerts an appreciable influence on water storage behaviour. To begin with, following is a brief description of mercury intrusion porosimetry, specimen preparation and the experimental procedure. The test results from the two methods are then compared and the method-related differences shown while taking into account the effects of the type of stone and the influences of salt in the pore spaces of the various stones. A full description of these investigations may be found in [70].

4.3.1 Description of mercury intrusion porosimetry

Mercury intrusion porosimetry is well-known and used frequently and operates on the principle of mercury intrusion being dependent on pressure. The operative principle is also based on the capillary law; the cylindrical pore model is usually applied here, too. Mercury, being a non-wetting liquid, is forced into the porous specimen material and the volume taken up by the specimen registered for each pressure level. Controlling increases in pressure and recording and analysis of the test data are done by computer. A mercury porosimeter operates over a range from 0.15 to 2000 bar, corresponding to a radius range of 5×10^{-5} m to 3.7×10^{-9} m. It takes from 2 to 4 hours to complete measurement of a specimen to acquire up to 630 test points over the full pressure range.

4.3.2 Specimen preparation and experimental procedure

The investigations are carried out on two different types of sandstone - the Obernkirchner and the Rüthener sandstone - markedly different in their porosity characteristics, each involving unimpregnated specimens as well as others saturated with Epsomite ($MgSO_4;7H_2O$) or with Nitrokalite (KNO_3). Salt-impregnation of the Rüthener sandstone is done in a 3% Epsomite solution and a 3% Nitrokalite solution; that of the Obernkirchner sandstone in a 3% solution of Epsomite and a 25% solution of Nitrokalite. Using these concentrations it is possible to achieve roughly the same quantity of absorbed salt in each of the specimens. The specimens, initially rod-shaped and measuring $4 \times 4 \times 20$ cm^3, are saturated with the respective salt solution, then dried in dry air at 40 °C to constant mass, weighed and then returned to the salt solution. This process is repeated until there is no longer any appreciable increase in mass. To measure capillary pressure the specimens are cut to size at about $4 \times 4 \times 1$ cm^3. For mercury pressure porosimetry, 5 to 10 g of specimen material is sufficient each time. For each of the test methods, specimens are cut from the same sample to assure complete comparability of the data.

As initial information on the materials investigated, Table 3 shows the porosity characteristics of the unimpregnated, recently quarried specimens of rock measured using a helium pycnometer as well as data on the average amounts of salt absorbed by the specimens under the preparation described.

4.3.3 Measurement results and evaluation

Fig. 19 shows the results of these investigations for the two test methods and types of rock in the form of an integrated pore-size distribution. From this the moisture storage function can be calculated for the superhygroscopic region. Whereas mercury porosimetry always encompasses all of the reachable pore space, it is possible with the pressure plate apparatus to look only at the pore-space available for natural moisture storage phenomena by starting with capillary-saturated specimens. In Fig. 19 the results obtained from the freshly

quarried stones using the two test methods are shown as solid lines. The distributions found using the suction pressure apparatus are somewhat more angular due to the small number of pressure levels involved but show the same characteristics as those from Hg porosimetry. In the Obernkirchner sandstone, both methods show a sharp drop in the pore-radius range between 3×10^{-6} m and 1.5×10^{-6} m; the drop lies between 3×10^{-7} m and 3×10^{-6} m for the Rüthener sandstone.

In addition to the distributions for the unimpregnated specimens, Fig. 19 also shows those for the salt-impregnated specimens. The curves found for the Obernkirchner sandstone (Fig. 19, top left) using mercury-intrusion porosimetry are almost identical up to a filled pore radius of about 3×10^{-6} m and there are practically no noticeable salt effects. Beyond this point, the curves diverge only slightly toward a differing overall porosity. Here the curves for the salt-impregnated specimens are also close together, hence showing scarcely any differences according to type of salt. In the pressure plate method there is likewise scarcely any difference among the curves for the salt-impregnated specimens, though they do differ from that of the unimpregnated specimen, especially in the lower pore-radius range $< 10^{-5}$ m (Fig. 19, top right).

The differing results from the two methods of measurement are especially evident in the Rüthener sandstone (Fig. 19, bottom). Using Hg-pressure porosimetry all curves for salt-impregnated and unimpregnated rock are close together. The shapes of the curves differ markedly however when measured using pressure plate apparatus; the salt-impregnated specimens are scarcely differing in the upper pore-radius range though differing distinctly from the unimpregnated specimen. In the lower radius range the specimen impregnated with KNO_3 seems, in contrast to the one impregnated with $MgSO_4$, to have capillary storage characteristics barely differing from those of the unimpregnated specimen.
For interpretation of these results the reader is directed to the appropriate remarks on differential pore-radius distributions contained in [70]. Comparison of the test results from the two methods shows that despite its

more basic manual measuring procedure and the consequent lower number of test points, the pressure plate method yields results which are certainly comparable to those of mercury-pressure porosimetry. An investigation of reproducibility accuracy using multiple measurements was not conducted because of the lengthy measurement time involved. The use of water as the operating medium assures a more realistic result since, as under natural conditions, it covers the true interaction between water and pore wall including substances possibly in the pores, especially hydrophilic or hydrophobic ones. This is particularly evident with salt-impregnated specimens as the test results described indicate. Moreover the use of capillary saturated specimen material also only includes in the analysis the pore-space available to capillary transport. In Table 4 the main points of the two analytical methods are again compared in terms of their characteristic features.

4.4 Determination of storage function from pressure plate measurement and sorption measurement

The sorption isotherm and the suction pressure curve both give moisture content as a function of true motive potentials, relative humidity φ as the ratio of vapour pressure to saturation vapour pressure and the capillary radius r as a quantity characterising capillary pressure. The two parameters are connected to one another through Kelvin's thermodynamic equilibrium condition mentioned previously (see equation (1)). This means that moisture content may be expressed in a standardized fashion in both the hygroscopic and the superhygroscopic moisture regions as a function either of φ or r. Universally applicable and beetter amenable to an intuitive grasp in practical work is the choice of relative humidity as general moisture storage potential. In non capillary-active building materials, as in most insulating materials for example, vapour pressure or relative humidity, but not capillary pressure, is defined. Using the example of sand-lime brick, Fig. 20 [57] shows how the moisture storage function is composed of:

- the sorption isotherm (top left, indicating the value for capillary saturation) and
- the suction pressure curve (top right, indicating relative humidity for the respective pore radii per the Kelvin equation).

Because suction pressure measurement deals only with a relative humidity range between 93% and 100% as a result of the non-linear relationship between pore-size and relative humidity, this means that this choice of depiction yields a steep curve for its results. To better compare the moisture storage functions of various building materials, capillary radius is therefore chosen instead as moisture storage potential for Figs. 21 and 22 and the moisture storage function is developed similarly.

The moisture storage functions shown in Fig. 21 for natural sandstone and in Fig. 22 for the man-made building materials all show a seamless transition (without steps or breaks) from the hygroscopic moisture region in which storage function is determined through sorption measurements, to the superhygroscopic region with pressure plate measurement as the analytical method. This applies both to materials having low sorption capacity (e.g. Obernkirchner sandstone and gypsum) and to those having high sorption capacity (such as Baumberger sandstone and sand-lime brick). Despite the use of two different analytical methods, this allows determination of a uniform moisture storage function which contains all of the practically significant moisture storage characteristics for a porous building material up to capillary saturation and which can be expressed as a function of a genuine potential variable independent of material (either relative humidity or pore radius).

5. Determination of water vapour diffusion coefficients

The points on moisture transport discussed in Para. 2.2.2 can only be verified by measurements in a temperature gradient since under isothermic conditions the operative gradients for vapour transport and for liquid transport are always in the same direction. To do this, measurements were carried out

using two different newly developed test equipment systems allowing gradients for vapour transport and liquid transport in the same direction and in opposite directions. Further evidence for the validity of the thesis that a liquid transport is superimposed on diffusion transport is given by way of new interpretation of the test results of other authors on the temperature-dependence of diffusion readings and on dew-point measurements in churches [72].

5.1 Measurement in a moisture and temperature gradient

For measurement in a moisture and temperature gradient, this author developed a suitable test apparatus. The equipment setup and the test procedure as well as the results obtained using it are described in the following paragraphs.

5.1.1 Equipment setup and measuring procedure

The measuring apparatus shown in Fig. 23 makes it possible to set up specific vapour pressure and sorption moisture gradients or humidity gradients even in opposing directions, in a specimen of material through application of a temperature difference. Through the bottom of a glass diffusion vessel having a specimen of building material on the top, the interior surface of the specimen is warmed to a specific temperature with the aid of an adjustable lamp. The vessel is insulated on the sides to create unidimensional conditions. The relative humidity inside is generated by a saturated salt solution in an annular glass container on the bottom of the vessel. The setup stands in a climatic chamber which controls the external climatic conditions. Thermoelements are used to record the temperatures and the partial vapour pressures are determined by dew-point mirror.

Use of an external heating unit is necessary because with a resistive heater in the vessel large temperature gradients in the vessel would result in a “storm in a teacup” situation. This would make investigation of diffusion

transport impossible. With the type of heating used here, temperature differences between the underside of the specimen, interior airspace, brine and glass bottom are always less than 2 K. The investigations are carried out under varying boundary conditions on round specimens of gypsum and Baumberger sandstone 9 cm in diameter and 1 and 2 cm in thickness respectively. Mass flow is determined by weighing the diffusion vessel.

5.1.2 Results of the diffusion measurements

The boundary parameters and test results for same-direction and opposing gradients are shown in Table 5 for the specimen materials mentioned, with the diffusion resistance factor μ calculated on the basis of the diffusion equation (8) from measured mass flow. For gypsum, same-direction gradients yield a μ-value of 6.3 and opposing gradients a value of 22. This corroborates theoretical studies suggesting that opposing gradients result in a reduction in total mass flow (see Fig. 12).

From the measurements on the Baumberger sandstone, in which both measurements were carried out under non-isothermic conditions with opposing gradients but differing vapour pressure differences, it can be seen that a lowering of vapour pressure difference from 3.2 to 1.5 mbar causes the μ-value calculated in accordance with equation (8) to rise from 29 to 160. This extreme effect may be understood by looking at the respective difference in mass flow between the measured non-isothermic case and the calculated isothermic case. Each of these was predicated on the same vapour pressure difference:

$$\Delta g = 1{,}07 - 0{,}57 = 0{,}50\ g/m^2h \qquad (16)$$

$$\Delta g = 0{,}50 - 0{,}05 = 0{,}45\ g/m^2h \qquad (17)$$

Δg [g/m^{2}h] mass flux difference

The difference of roughly the same size in both cases reflects liquid transport running counter to diffusion and independent of it in the non-

isothermic state. Because in the case of the lower vapour pressure difference the transport of liquid running counter is almost as large as diffusion flow, instruments only record a very small total mass flow from which is calculated an extremely large μ-value.

5.2 Further proofs for the thesis of liquid transport superimposed on diffusion

Experimental results from a second test apparatus provide further proof that the increase in water vapour permeability observed under isothermic conditions involves transport of liquid superimposed on diffusion. Additional evidence is also provided by new interpretations of test results reported by other authors.

5.2.1 The double chamber test

The test setup shown in Fig. 24 is simpler than the one already described (Fig. 23). Two chambers are separated from one another by the specimen material. In the lower chamber relative humidity is kept constant by a supersaturated salt solution. This chamber is cooled in a cooling bath having a bath temperature of 5°C so as to create an air temperature beneath the specimen of about 13°C. The air in the upper chamber is at room temperature. Particle board is used as a specimen material since in addition to a high sorption capacity it has good insulating qualities. The specimen is 9 cm in diameter and 16 mm in thickness. In both chambers dew point or water vapour partial pressure is measured by means of a lithium chloride sensor which operates something in the manner of a dew-point mirror.

If there is pure diffusion transport there must be equal water vapour partial pressure in the two chambers; the relative humidity in the upper chamber being lower because of the higher temperature. If a liquid transport is superimposed on diffusion because of the gradient in relative humidity or in

sorption water content from the lower to the upper chamber, a higher water vapour partial pressure and hence a higher dew-point temperature is to be expected in the upper warmer chamber. In fact this test did record a difference in dew-point of between 1 and 2 K.

5.2.2 Temperature-dependence of measured vapour diffusion coefficients

According to Schirmer [124] the following equation describes the effect of temperature on the vapour diffusion coefficient of air D_D:

$$D_D = 8{,}8 \cdot 10^{-10} \cdot T^{1{,}81} \left[m^2 / s \right] \qquad (18)$$

T [K] absolute temperature
D_D [m^2/s] water vapour diffusion coefficient in air

Substituting Equation (18) in Equation (8) yields:

$$g_v = -\frac{1}{\mu} \cdot \frac{8{,}8 \cdot 10^{-10}}{R_D} T^{0{,}81} \cdot \frac{dp}{dx} = -\frac{\delta}{\mu} \frac{dp}{dx} \qquad (19)$$

Water vapour permeability would have to rise with increasing temperature.

R.C. McLean, G.H. Galbraith and C. Sanders [90] have determined the water vapour permeability of different materials at various temperatures (10, 15, 20 and 25°C) and a variety of moisture ranges (0 to 60, 60 to 100, 60 to 93 and 80 to 100 % RH). Fig. 25 shows the change in measured values for water vapour permeability compared to the value measured in each case at 20°C for plasterboard, wood and insulating material. During the measurements there was a humidity gradient from 60 to 93 % over the specimen cross section. This humidity range was chosen because in the other ranges there was either a very low sorption water content (0 to 60 % RH) or in the case of measurements at 100% RH on one side of the specimen there was a danger of skewed test results from water vapour condensation on the surface of the specimen due to slight temperature fluctuations.

The insulating material, which has only a low sorption moisture content even in these high moisture ranges, shows, as anticipated from Equation (19), an increase in water vapour permeability with rising temperature. In plasterboard and to an even greater extent in wood however, the behaviour is the opposite.

On the assumption that in this moisture range a liquid transport is superimposed on diffusion, this behaviour may be explained as follows:
Total mass flow may be expressed as:

$$g = g_v + g_w = -\frac{D_D}{\mu RT} \frac{dp}{dx} - D_w \cdot \frac{dw}{dx} = -\frac{\delta}{\mu} \frac{dp}{dx} - D_w \frac{dw}{dx} \qquad (20)$$

g [kg/m^2s] total mass flux density
g_v [kg/m^2s] vapour flux density
g_w [kg/m^2s] liquid flux density
D_D [m^2/s] vapour diffusion coefficient in air
D_w [m^2/s] liquid transport coefficient
δ [kg/msPa] water vapour permeability of stagnant air
μ [-] water vapour diffusion resistance factor

From total mass flow relative to the water vapour partial pressure gradients, fictitious water vapour permeability works out to:

$$\delta^* = -\frac{D_D}{\mu RT} + \frac{g_w}{dp/dx} \qquad (21)$$

δ^* [kg/msPa] fictitious water vapour permeability

The liquid transport coefficient D_w slightly increases through the temperature-dependence of the viscosity of water, whereas the slope of the sorption isotherm declines slightly with temperature. This means that the liquid transport component barely changes with temperature. By contrast the water vapour partial pressure gradient is known to rise very steeply as a result of the exponential dependency of water vapour partial pressure on temperature.

This causes a sharp drop in the liquid transport component of water vapour permeability calculated from equation (21); the result is water vapour permeability which falls with temperature.

Tests involving paper membranes [122] also support these conclusions. The top diagram of Fig. 26 shows diffusion flow through the membrane as a function of partial pressure difference. Contrary to the laws of gas diffusion, it drops with rising temperature. If the moisture-related increase (moisture flow minus moisture flow under dry conditions) is plotted against relative humidity (Fig. 26, bottom) temperature-dependence is in accord with the regular laws of physics.

5.2.3 Dew-point investigations in churches

H. Künzel and D. Holz [83] have conducted studies on numerous churches. Fig. 27 shows typical profiles for dew-point temperatures inside and outside churches for a heated church and an unheated church. In an unheated church (Fig. 27, left) the interior dew-point curve follows the dew-point temperature curve outside the church, although of course the peaks are somewhat damped. By contrast, dew-point temperature in a heated church (Fig. 27, right) runs markedly above the dew-point temperature curve outside the church during the heating period in the first and fourth quarters. The investigations revealed that moisture released from congregations increases the humidity of the air only very slightly. From this they took it that the higher dew-point temperature is due to desorption of moisture stored in the walls. This alone cannot be the cause however since in this case the walls would have to re-absorb during the rest of the time the moisture given off. In this period dew-point temperature in the church interior would have to be below that of the outside air.

This phenomenon can only be explained by the movement of moisture from the outside air through the walls into the building. Here diffusion cannot be the cause of the transport since it cannot work against a partial pressure

gradient. By contrast heating of the church creates a gradient of relative humidity from the outside to the inside. Outside, relative humidity is high at about 80%, typical for the heating period, whereas humidity in the interior of the church has dropped markedly due to the increase in temperature. As a result of this a sorption moisture profile develops in the wall which causes a liquid transport from the outside of the wall to the inside. The transported water is acquired from the outside through sorption and increases the moisture content of the air in the interior through desorption from the interior surfaces (see also Fig. 12).

5.3 Diffusion coefficient independent of material moisture content

The results shown demonstrate that the increase in water vapour permeability recorded under isothermic conditions per DIN 52 615 [26] with increase in average material moisture content is due to a moisture transport in liquid phase superimposed on diffusion.

Because differing transport potentials are at work in the two transport mechanisms, an integrated description of the two transport phenomena as moisture-dependent diffusion is not acceptable. As discussed in Para. 5.1.2, a reduction in moisture transport as a result of moisture content may occur under non-isothermic conditions, the normal situation specifically during the heating period. This is because under these conditions liquid transport counter to diffusion can take place. Consequently using the diffusion equation alone with a diffusion resistance independent of vapour pressure gradients cannot describe the transport phenomenon for non-isothermic conditions. Even under isothermic conditions as well, where the gradients for vapour and moisture transport are parallel, inclusion of moisture transport in the vapour diffusion equation by way of a moisture-dependent diffusion resistance factor can produce errors in calculations. Specifically, if the calculations are done with temperatures different from those at which the coefficients were determined experimentally (cf. Para. 5.2.2).

For these reasons it is useful to postulate a diffusion coefficient independent of material moisture and to take into account surface diffusion in calculating liquid transport. Requisite for this of course is that vapour and liquid transport do not affect each other. In the sorption moisture region this criterion is essentially fulfilled for most building materials since rate of diffusion is controlled principally by the larger pores, whereas liquid transport takes place largely independent of this through the micropores and in the film of water absorbed in the narrow interstice corners. In the capillary water region diffusion resistance independent of moisture can no longer be postulated since here diffusion is clearly impeded by the water present. However in this moisture range capillary transport is in general greater than diffusion by several orders of magnitude, so that for calculations in this region moisture-related changes in the diffusion coefficient can have only a slight influence on the outcome.

Consequently the diffusion transport coefficient has to be determined under conditions having no (appreciable) liquid transport taking place. In most building materials there is only a slight sorption moisture content up to a relative humidity of 50%. Hence the diffusion resistance coefficient determined in accordance with DIN 62 615 in the dry region (0 to 50% RH) may be looked on as a true material coefficient describing diffusion.

5.4 Determination of liquid transport coefficients in the sorption moisture region from diffusion resistance measurements and comparison with NMR investigations

On the assumption that vapour diffusion is described by the vapour diffusion resistance coefficient recorded in the dry zone, and that decline in the diffusion resistance coefficient is due to a superimposed liquid transport, it must be possible to calculate the liquid transport coefficients in the sorption moisture region by determining fictitious vapour diffusion resistance coefficients μ^* in a manner similar to measurement per DIN 52 615 in higher moisture regions [26]. The difference between mass flows measured in higher

moisture regions and those measured in the dry zone must be attributable to liquid transport:

$$\Delta g = g_w = -\left(\frac{1}{\mu} - \frac{1}{\mu^*}\right) \cdot \frac{D_D}{RT} \frac{dp}{dx} = -\left(\frac{1}{\mu} - \frac{1}{\mu^*}\right) \cdot \frac{D_D p_s}{RT} \cdot \frac{d\varphi}{dx} \qquad (22)$$

Δg [kg/m^{2}s]	mass flux density difference
D_D [m^2/s]	water vapour diffusion coefficient in air
μ [-]	water vapour diffusion resistance factor
μ^* [-]	fictitious water vapour diffusion resistance factor (with liquid transport)
R [J/kgK]	gas constant for water vapour
T [K]	absolute temperature
p_s [Pa]	saturation vapour pressure
φ [-]	relative humidity

For transport in the liquid phase we have:

$$g_w = -D_w \frac{d_W}{dx} \qquad (23)$$

D_w [m^2/s] liquid transport coefficient

This yields the following defining equation for the liquid transport coefficient:

$$D_w = \frac{D_D p_s}{RT}\left(\frac{1}{\mu} - \frac{1}{\mu^*}\right) / \frac{dw}{d\varphi} \qquad (24)$$

Consequently for calculation of the transport coefficients, one must also know the sorption isotherm for determining operative water content gradients.

Table 6 shows vapour diffusion resistance coefficients measured in various regions of relative humidity. For some building materials the differences from

the value in the dry region are only slight, so that evaluation using equation (24) does not appear to be meaningful. This slight diminution in the diffusion resistance coefficient in the higher moisture region is due to a low sorption water content and/or a very high degree of permeability to vapour diffusion.

Fig. 28 shows the transport coefficients calculated from the diffusion measurements per equation (24) using the Baumberger sandstone and the sand-lime brick as examples together, in advance, with the transport coefficients determined for redistribution of water using the NMR equipment system. The coefficients determined using the two methods show amazingly close agreement for sand-lime brick. In this instance the transport coefficient was determined only from the dry cup and wet cup methods. In the case of the Baumberger sandstone there is likewise close agreement in the upper hygroscopic moisture region. Only at low moisture levels do the transport coefficients determined from diffusion measurements decline to somewhat lower values. Table 7 lists the liquid transport coefficients for the materials examined for the hygroscopic region. They were determined using equation (24) from isothermic diffusion measurements in the dry and moist regions. All of the transport coefficients are relatively small.

6. **Determination of liquid transport coefficients**

Through the taking up of liquid water, quantities of water greater by several orders of magnitude per unit of time than those moved by diffusion are transported into most mineral building materials. Although, apart from natural stone facades or external masonry walls of double-leaf contructions exposed to natural weather, highly absorbent building materials are usually protected against exposure to heavy rains by proper design and construction, it is useful to take a closer look at this transport phenomenon. For example, sufficient moisture to cause problems for structures can even result from minor deficiencies as a result of improperly installed sealing, caulking and the like or from small cracks which may appear over time, because of the great intensity of this type of transport. The capillary activity of building materials

may however also be beneficial because water forming within the material from a drop in temperature below dew-point becomes spread over broader areas hence avoiding excessive local concentration.

6.1 Measurement of water content distribution using nuclear magnetic resonance

To determine liquid transport coefficients dependent on water content it is necessary to measure water content distributions in the specimen body during the transport process. This calls for analytical apparatus capable of providing rapid recording of moisture profiles with good spatial resolution. To do this an apparatus employing measurement by nuclear magnetic resonance was set up. In contrast to nearly all other methods for measuring material moisture, this method may be viewed as a direct method for measuring the water content present in a building material.

6.1.1 Physical principle of measurement

All atomic nuclei having an uneven number of protons or neutrons (roughly two-thirds of all stable atomic nuclei) have an angular momentum (spin) and connected with it a magnetic moment resulting from their spatially unevenly distributed charges. Simplified, one may imagine the atomic nuclei as rotating bar magnets (magnetic dipoles) forming a symmetric magnetic field around their axis of rotation. As long as no external magnetic field is present, the poles of these bar magnets are pointing statistically in every possible spatial direction. If an external magnetic field B_0 is applied, the magnetic nuclear dipoles try to align themselves (see Fig. 29). However, according to the laws of quantum mechanics only very specific orientations relative to a preferred orientation are allowed. In hydrogen atoms (protons) only two directions are permitted, one more parallel to the applied magnetic field and one more antiparallel. The dipoles precess like tilted gyros in a cone-shaped envelope about the B_0 axis (see Fig. 30). The parallel alignment is that of lower energy, with the energy difference of the two alignments being proportional to the magnetic field strength. At absolute zero temperature all nuclear magnetic

moments are aligned parallel to the external magnetic field. At higher temperatures this ceases to be the case since thermal energy considerably disrupts the regular alignment. If for example water is introduced into a magnetic field of flux density 1 T, for every ten million nuclei in the higher energy level there will be ten million and eleven nuclei in the lower at room temperature. However since there are 6.7×10^{22} hydrogen atoms in one cm^3 of water the result is nonetheless an excess of 3.7×10^{16} magnetic moments parallel to the external magnetic field. This excess results in macroscopic nuclear magnetization having the nuclear magnetization vector M_Z parallel to the applied external field (Z-direction).

In pulsed nuclear resonance, this nuclear magnetization is disturbed by applying a high frequency pulse via a measuring coil. The frequency of the pulse must correspond with the precession frequency of the dipoles (resonance frequency); it is proportional to the field strength of the applied magnetic field. Via the length of the pulses the deflection of the macroscopic nuclear magnetization may be varied. If the pulse is switched off when the nuclear magnetization vector is at right angles to the magnetic field (angle of deflection = 90°, hence 90°-pulse), the nuclei precess about the static field at a maximum vertex angle. Maximum voltage is then induced in the measuring coil. This voltage is proportional to the number of hydrogen nuclei in the test volume.

Once the high-frequency pulse ceases, the excited nuclei return to their original positions with a time-behaviour which may be described by a relaxation equation of the form:

$$M_{z(t)} = M_{z0}(1 - e^{-t/T_1}) \qquad (25)$$

$M_{z(t)}$ [T] macroscopic nuclear magnetization vector in Z-direction
M_{z0} [T] macroscopic nuclear magnetization vector prior to pulse
T_1 [s] longitudinal relaxation time

incorporating the relaxation time T_1. During relaxation, the energy corresponding to the difference between the two alignments is released. T_1 is chiefly dependent on the physical bonding of the hydrogen nucleus, i.e. in the case of water on whether it is present as a solid (ice) or in liquid form but also on bonding to the pore walls and hence on pore diameter. This relaxation time is of importance for the nuclear resonance experiment in that following each excitation of the nuclei, all nuclei have to have returned to their original alignments before the start of the next measurement. Hence longitudinal relaxation is definitive for the speed at which the measurements can be conducted. In general, time between measurements should be roughly five times the T_1 relaxation time [97].

In nuclear magnetic resonance a second relaxation process takes place: transverse relaxation. Between the nuclei precessing at right angles to the static field an energy exchange takes place, the individual nuclei change their precession frequency and phase angle; the result is a "fanning out" of the magnetization vector. During this process there is no change in the total energy of the spin system. However, there is a decrease in the magnetization responsible for the voltage induced in the measuring coil. Because transverse relaxation occurs much more rapidly (except for free water) the time-behaviour of the measuring signal is in large measure determined by it and shows an exponential decline. Fig. 31 shows a typical measuring signal generally referred to as FID (free induction decay).

$$FID = FID_0 \cdot \exp^{-t/T_2} \qquad (26)$$

FID [V] free induction decay (measuring signal)
FID_0 [V] measuring signal immediately following pulse
T_2 [s] transverse relaxation time

Transverse relaxation too is dependent on the physical and chemical bonding of the nucleus (see Table 8). If components having various T_2 relaxation times are present, this gives a measuring signal composed of the overlapping exponential curves of the individual components. If the measuring curve is

separated into the individual exponential curves, the relative content of the individual components may be determined. This is for example routinely used in the food industry to determine the fat/water content of margarine [16]. Since the relaxation times, as previously described, are also strongly dependent on the physical bonds of the water in the pore space and hence on pore-space size, it is conceivable that determining them would make it possible to gain information on the relative content of bound/free water or a kind of pore size distribution. This is however not possible as investigations by this author have shown. Since in mineral building materials there is always a continuous pore size distribution over a sizeable region, the measuring signal is an overlapping of numerous relaxation curves. Separating them at reasonable cost and with reasonable accuracy is impossible. Table 8 shows the orders of magnitude of longitudinal and transverse relaxation times for water in a variety of bound conditions.

It has only been possible to present the fundamental principles of nuclear magnetic resonance in simplified form and to the extent necessary for understanding of this paper. The behaviour of atomic nuclei cannot be explained solely by way of classical physics; to properly describe it reference must be made to the laws of quantum physics. A more complete description may be found in the relevant literature of the field and in the standard books ([31] [33] [43] [95] [97]).

6.1.2 Equipment setup

The heart of the equipment setup is an NMR unit consisting of an electronic control unit and a permanent magnet with measuring coil. In the measuring field of the permanent magnet, magnetic field strength is 0.235 Tesla, meaning that the resonance frequency for hydrogen nuclei is about 10 MHz. The magnet is thermostatically set at 40^{0}C to prevent temperature from affecting the magnetic field. Field strength can be readjusted by means of a pair of Helmholtz coils at the poles of the permanent magnet. The measuring head is located between the poles of the magnet. Because good spatial resolution is necessary for determining water content distributions, a special

measuring head was developed. Its coil length is only 3 mm in contrast to the 25 mm standard for this type of unit. Moreover use of a fully open measuring head and placing of a matching opening in the base of the magnet housing allows stepwise scanning of the specimen. The open diameter of the measuring coil of about 30 mm hence allows the use of prismatic specimens having sectional dimensions up to 20 x 20 mm^2 or cylindrical specimens 30 mm in diameter. The magnet is mounted on a sliding carriage in such a way that the opening with the measuring head lies horizontally in the direction of travel of the carriage. The carriage is positioned by a step motor. Thus the measuring coil can be gradually passed over the specimen to record distributions. The specimen itself is suspended horizontally and hooked up to a glass liquid supply system to allow free water absorption without gravitational influences. Capillary liquid flow is determined by continuous weighing of the reservoir container from its mass loss, corresponding to determination of the water absorption coefficient (A value) from a suction test. Weighing provides a check of the liquid distributions recorded in the specimen. Fig. 32 shows a schematic sketch of the setup.
The control unit operated by a microprocessor has a quartz oscillator to generate the resonance frequency. Pulse length is set by potentiometer and like field strength adjustment of the magnet has to be controlled through the signal profile displayed by a storage oscilloscope hooked up to it. The alternating voltage induced in the coil by the test specimen after the high frequency impulse is rectified and the user can choose between diode rectification and phase-sensitive rectification. Higher measuring sensitivity is attained using phase-sensitive rectification but fluctuations in field strength and temperature have a greater influence on the test signal than using diode rectification. The rectified signal is then digitized for the microprocessor using an analog-digital converter (ADC). Since the ADC only has an operating range of -5.1 to +5.2 volts, the signal has to be attenuated further so that this range is not exceeded.

This unit makes it possible to register and average a number of signals to improve signal-to-noise ratio S/R after the equation

$$S/R \approx \sqrt{n} \qquad (27)$$

n [-] number of measurements

In recording distributions therefore as many measurements are made at each test point as are possible without taking too much time for the measurements. Here of course the interval between measurements is also a big factor. It has to be selected to assure that all nuclei have returned to their original alignments before the next measurement is taken. The amplitude of the FID signal (Fig. 31) is recorded as a measurement signal at a time set on the unit. This point in time must in any event be later than the dead time of the measuring coil (resulting from switchover from sending of the pulse to receiving of the desired signal). Choosing different times allows variation of the effect of a possible signal of the solid-state matrix on the result.

A personal computer having four serial interfaces is used to operate the entire system. Connected to these interfaces are the step motor control, the operating electronics for starting measurement, NMR control and the weighing unit. A menu-operated program was developed to record the test data, performing the following functions:

1. positioning of the measuring unit,
2. initiation of NMR analysis via the operating electronics,
3. receipt of the NMR signal,
4. recording of the test data from the weighing unit,
5. recording of liquid distributions at constant root time intervals
6. graphic display of NMR signal over specimen length and recorded liquid volume over the root of time, with automatic scaling of axes
7. storage of data.

A second NMR test unit was also set up suitable for investigating larger specimens measuring 5 x 5 cm^2 in section. In contrast to the system just described this called for an electromagnet weighing about 700 kg. In this case it is not the magnet which is moved but the specimen by means of a sliding carriage. This set-up is less well suited for long-term studies since there is a drift of the power supply and hence of the magnetic field. If diode rectification, which is more insensitive to changes in field strength, is selected, the magnetic field has to be adjusted roughly every two to three hours. The magnet has a field strength double that of the "little" NMR and consequently a somewhat greater measuring sensitivity. Except for the differences discussed, this analytical setup is identical to the first apparatus. Fig. 33 shows a photographic view of the two units.

6.1.3 Accuracy of measurement, limits of applicability

A comparison of water content figures derived using traditional gravimetric means and the NMR apparatus on the same specimens is shown in Fig. 34 for two different natural sandstones (one fine-pored, of good sorption capacity and one coarse-pored, of lesser sorption capacity). The same calibration curve can be used for both sandstones. This shows the advantage of a direct method of measurement for moisture content. The NMR method can be looked on as such for most building materials. A dry analysis does not have to be carried out and a new calibration curve plotted for every material. This does not apply to materials containing hydrogen nuclei (e.g wood, plastics).

Fig. 35 shows the high measuring accuracy of this method. The Fig. shows measurement of moisture content in the hygroscopic region for a variety of natural sandstones. Material moisture content can be determined to an accuracy of more than 0.2 % by volume. The signal-to-noise ratio and hence the attainable measuring accuracy can be varied with the number of individual measurements to be averaged.

Of course, the spatial resolution capability of the test equipment, too, is of importance in determining moisture distributions. The NMR unit measures not only inside the short 3 mm measuring coil, but ahead of it and behind it as well since it is there too that the hydrogen nucleii are excited to resonance and hence also contribute to the measurement signal. Spatial resolution was determined using a very thin saturated filter paper passed by millimeters through the measuring head. Fig. 36 shows the sensitivity curves determined in this manner for the two NMR units. Both units yield a curve which can be approximated very well by a Gauss function in each case. Half-width at half-maximum for the relative sensitivity of the two measuring units is about $\pm$ 6 mm and $\pm$ 7.5 mm respectively. Fig. 37 shows a comparison between measurement of water content distribution using the NMR unit and measurement by gamma testing. The measurements were taken one immediately after the other on the same specimen after an absorption period of several hours. The specimen measured had 5 x 5 cm^2 in section and 25 cm in length. Scanning of the specimen took about 5 mins for NMR and 25 mins for gamma testing. The gamma testing unit used achieved a spatial resolution of one millimeter [62]. Nevertheless the two distributions measured show only very slight differences, if the first millimeters of the specimen are ignored. This shows that the spatial resolution of the NMR unit is completely adequate for determining the moisture distributions of common building materials which usually do not involve moisture gradients on a millimeter scale. Because in suction testing the moisture gradient becomes ever flatter with increasing depth of penetration, a possible problem of spatial resolution being too low can in most cases be mitigated by making absorption time longer.

As investigations by this author have shown, it is not possible, despite knowing the response function limiting the spatial resolution of the measuring equipment, to calculate from the measured profiles the true water content distributions which differ slightly from them. It is however very possible to take the reverse tack and to determine from the calculated distributions those profiles which would be yielded by the NMR unit in measuring these distributions. To allow optimal comparison between calculation and

measurement, all calculated distributions were "NMR corrected" in this manner.

Problems can occur in the measurement of building materials containing coarse-grained aggregates. Frequently aggregates are used which in part exceed one centimeter in diameter. At a maximum sectional size of 5 x 5 cm^2 the specimen can in this case no longer be viewed as homogeneous. The so-called gel pores in concrete pose another problem. These pores are extremely small in diameter. As previously discussed, the transverse relaxation time of water drops off sharply in pores of decreasing pore diameter. In very small pores, relaxation time can become so short that even within the dead time of the measuring coil the hydrogen nuclei are already relaxed so far that they can no longer be detected by the measuring coil, or only just barely. This results in a calibration curve, as the tentative studies on concrete shown in Fig. 38 also indicate, which does not pass through the zero point and possibly is not even a straight line.

6.1.4 Procedure

Moisture-distribution measurements to determine transport coefficients were carried out using the "little" NMR unit on dried specimens sealed on the sides with epoxy resin and having a sectional area of 2 x 2 cm^2 and a length of 10 to 15 cm. The appropriate attenuation of the NMR signal and the necessary time interval between measurements are determined from saturated test specimens. For most materials an interval of 0.2 sec is sufficient. For the chosen number of 25 measurements per point this means a measuring time of 5 sec. Measurement is made every 4 mm; i.e. for a specimen 15 cm in length there are about 40 sampling points. Combined with the positioning time of the carriage this yields a total measuring time for a moisture profile of less than 5 minutes. However, a longer measuring-time interval of sometimes as much as a full second is required for highly absorbent coarse-pored materials which are just those with the fastest changes in the moisture distribution. To reach an acceptably short measuring-time despite this, the number of measurements to be averaged has to be reduced accordingly. Usually this

does not present any problem in that these materials frequently have a very high capillary saturation which results in a better signal-to-noise ratio.

The specimen is connected with the glass liquid supply system by way of a shrinkable PVC plastic tubing some sealing compound being placed between the tubing and the specimen. Once the specimen holder has been properly adjusted so that the magnet with the measuring coil can be passed over the specimen without difficulty, a dry measurement is carried out. This dry measurement is necessary since, containing hydrogen nuclei, both the epoxy resin and the sealing compound give an NMR signal which has to be subtracted from the subsequent measurements.

Following input of the NMR parameters (signal attenuation, number of measurements to be averaged, interval between individual NMR measurements) the liquid supply is opened and the face of the specimen fully wetted. Immediately thereafter the test routine is begun. The specimen is scanned in the direction of absorption. Recording of moisture profiles is repeated at constant root-time intervals to obtain constant spacing of the profiles despite the absorption process becoming slower and slower ($\sqrt{t}$ law). The profiles recorded are displayed at once on the computer monitor. Once the liquid has penetrated deeply enough and enough profiles to determine the capillary transport coefficients have been recorded, sampling can be stopped. To provide meaningful evaluation, penetration of about 6 to 12 centimeters is necessary. Depending on the absorption capacity of the specimen material, a test period from under 2 hours up to as much as several days may be needed.

After interruption of the water supply, the process of subsequent moisture redistribution begins in the specimen. This transport phenomenon, which is considerably slower, may also be observed through subsequent determination of moisture distribution using the NMR unit. However this requires a test period from roughly one day to as much as several weeks depending on the specimen material. Observation time is limited as a result of the simultaneous process of diffusion which causes drying of the specimen through the open sectional surface on the end of the specimen. Once the total moisture content

of the specimen has dropped by more than 5%, the sampling operation is discontinued.

6.2 Measurement results

In the following discussion of measurement results the four natural varieties of stone and the four different man-made building materials are combined into two composite graphs made up of the four individual graphs each. This means of depiction is also used to show the capillary transport coefficients. Also plotted on the graphs in addition to the test points are calculated moisture distributions which are discussed in more detail in Para. 6.3.1.

6.2.1 Absorption of water

Figs. 39 and 40 show the test results for natural sandstones and man-made materials. The moisture distributions measured over the length of the specimens at specific times in the absorption process clearly show that water does not penetrate in the form of a "definite moisture front." Fully in accord with theoretical approaches to describing capillary penetration in porous building materials having varying pore size, it penetrates in a complex way with gradients changing over space and time. The natural sandstones show a behaviour similar to one another. On the absorbing face of the specimen a constant moisture content corresponding to capillary saturation quickly establishes itself. Moisture content declines continuously in the direction of absorption. The measured water content distributions all have a convex shape. As depth of penetration increases, the curves become flatter. The individual types of sandstone differ in rate of penetration and steepness of the resultant curves.

Baumberger and Sander sandstone have the lowest rate of penetration. That Baumberger sandstone has about the same rate of penetration as Sander sandstone despite its water absorption coefficient which is roughly twice as large is due to its water absorption capacity which also is nearly double that of Sander (cf. Table 1). Because of its very low absorption capacity with only

slightly higher water absorption coefficient, Obernkirchner sandstone has a markedly higher rate of penetration. With its very high A-value, Rüthener sandstone shows the highest rate of penetration and the steepest water content profiles.

Of the man-made building materials, gypsum and sand-lime brick behave in a manner similar to the natural sandstones (see Fig. 40). With its somewhat higher capillary saturation but also its higher A-value, sand-lime brick behaves in a manner somewhat comparable to Baumberger sandstone. At 400 kg/m^3 gypsum has the greatest water absorption capacity of all the materials considered here, though because of its relatively high A-value it still does not have a low rate of penetration.

Water penetration presents a different picture for aerated concrete. Though for short absorption times this material does show a water absorption behaviour comparable to the results already presented, this changes once the absorption times exceed 24 hours. The moisture content of the absorbing surface climbs above capillary saturation to 375 kg/m^3, and at capillary saturation and below this at about 200 kg/m^3 moisture plateaus form which migrate into the interior of the material as absorption time increases. After an absorption period of eight days (192 hrs), moisture content of the absorbing surface rises further to a water content of 450 kg/m^3 with a third moisture plateau beginning to form at 375 kg/m^3.

In the case of brick a moisture plateau also forms, albeit after only roughly one hour of absorption time. This plateau, with a shape somewhat less distinct than that of aerated concrete, appears at about half the capillary saturation. Here no change in water content is evident on the absorbing surface.

An explanation for the peculiar behaviour of aerated concrete and clay brick could not be found in the course of this research work. Studies of the pore radii distribution in clay brick using mercury porosimetry produced two pore

radii frequency maxima. This could be an explanation for the appearance of water content plateaus.

6.2.2 Redistribution of water

To investigate redistribution the specimens are first supplied with water up to the time t = 0 until a penetration depth of roughly one-third of the specimen length is reached. Application of water from outside is then discontinued. The test curves for water content distribution at the start of redistribution are marked in Figs. 41 and 42 with time t = 0. In the process of redistribution the smaller pores with their greater suction power suck dry the larger, full pores. The result of this is that water penetrates further into the specimen whereas water content in the front portion of the specimen falls. If the water content profiles shown are compared with the profiles obtained during the absorption process, the markedly greater time intervals are conspicuous.

While the behaviour of gypsum and sand-lime brick is comparable to that of the natural sandstones with respect to redistribution as well, here again it differs from it in the case of aerated concrete and clay brick. At the start of redistribution, the water content of aerated concrete shows only an indistinct moisture plateau at a water content of about 210 kg/m^3 after an absorption time of seven and a half hours. This plateau continues to grow until after a redistribution time of something over one day the water content at no point in the specimen exceeds the value of this plateau. A new plateau then forms at 175 kg/m^3. In the case of clay brick there is no moisture plateau visible at the start of redistribution. It then appears however after eight hours at approximately the same moisture content as in the absorption process along with an additional plateau at a moisture content of roughly 30 kg/m^3.

6.3 Determination of liquid transport coefficients

Two methods are commonly used to calculate capillary transport coefficients from recorded water content distributions varying with time. Using a

Boltzmann transformation, equation (12) becomes an ordinary differential equation

$$-\frac{1}{2}\lambda\frac{dw}{d\lambda}=\frac{d\left(D_{w(w)}dw/d\lambda\right)}{d\lambda} \qquad (28)$$

$D_{w(w)}$ [m^2/s] liquid transport coefficient
w [kg/m^3] water content

with the Boltzmann variable $\lambda = x/\sqrt{t}$. This equation applies to penetration of liquid into a body extending infinitely in the direction of absorption, having constant initial water content and constant water content on the absorbing surface. In addition, capillary transport must be a function of water content only; a criterion synonymous with linear water absorption over the root of time [19]. The method of calculating transport coefficients using the Boltzmann transformation is not applicable to the redistribution process which is why another method is utilized. Equation (12) may be solved directly for D_w:

$$D_w = -g_{w(x,t)}/\left(\frac{dw_{(x,t)}}{dx}\right) \qquad (29)$$

$g_{w(x,t)}$ [kg/m^2s] liquid flux density

For any point in time the transport coefficient is given by the ratio of mass flow and water content gradient. This ratio is independent of time if capillary transport can be described by a diffusion equation. The water content gradient in equation (29) may be determined directly for every measuring time and every sampling location from the recorded profiles.

To allow better evaluation a regression curve is passed through the test points; the curves are read in using a digitizing board having a data point spacing of 0.1 mm. This regression method is used because a mathematical regression for the full moisture range would only be possible if different equations were used for different areas. However this would result in

discontinuity in the first derivative at the interfaces and hence to physically inexplicable forms of the capillary transport function (as in Kumaran [79] for example).

The mass transport $g_{w(x,t)}$ may be determined from profiles determined at two different points in time t_1 and t_2:

$$g_{w(x,t=\frac{t_1+t_2}{2})}=\frac{1}{(t_2-t_1)}\int_{a=x}^{\infty}\left(w_{(a,t_2)}-w_{(a,t_1)}\right)da \qquad (30)$$

The upper limit of integration may be replaced by the location of the moisture front since a further integration cannot result in any change.

6.3.1 Coefficients for absorption

Fig. 43 shows the transport coefficients determined in this fashion for the various types of sandstone. In all cases the transport coefficient is heavily dependent on water content. At capillary saturation the transport coefficient is above that in the hygroscopic moisture region by roughly two orders of magnitude.

The moisture transport coefficients of the Baumberger sandstone and of the Sander sandstone, both of which have approximately the same rate of penetration, show a similar pattern. Obernkirchner sandstone, which despite its low water absorption capacity does have a slightly higher water absorption coefficient than Baumberger sandstone, accordingly has a considerably higher transport coefficient. As anticipated, the high water absorption coefficient of Rüthener sandstone also results in transport coefficients higher by more than an order of magnitude.

For the transport coefficients shown in Fig. 44 for the man-made building materials, sand-lime brick and gypsum show transport coefficients comparable to the natural sandstones. As anticipated, aerated concrete by contrast presents a different image. For the moisture contents of the moisture

plateaus where extremely low gradients appear (see Fig. 40), very high transport coefficients are resulting. Moreover the moisture transport function is a function not only of water content but also of time, since the plateaus only form with time and the water content of the absorbing surface changes constantly. Behaviour of this nature can no longer be described by a diffusion equation. For clay brick as well, the plateau which forms at half saturation, yields an increase of the correspondent transport coefficient. But the time-dependence is only slight. According to Kießl [56] the capillary transport coefficients for most building materials can be approximated very well by an exponential function. To verify this an exponential approximation is included in Figs. 43 and 44 for all building materials (with the exception of aerated concrete and clay brick). The exponential function is chosen so that water content distributions calculated using it show the least deviations from the measured profiles. The calculated distributions are shown in Figs. 39 and 40 and show sufficiently good agreement for many applications. In [74] a procedure for determining from the water absorption coefficient a good exponential approximation for the capillary transport coefficient is reported.

6.3.2 Coefficients for redistribution

The transport coefficients for redistribution are shown in Figs. 45 and 46 for the four types of sandstone and the four man-made building materials. Since during redistribution the maximum water content on the front side of the specimen is decreasing steadily, the transport coefficients can only be determined up to a maximum moisture content which is falling more and more with subsequent redistribution. For redistribution as well the transport coefficient curves for Baumberger sandstone and the Sander sandstone are similar. As would be anticipated, the transport coefficients for Rüthener sandstone are higher. Despite the lower A-value, the transport coefficients for redistribution in Obernkirchner sandstone are somewhat higher than those for the Rüthener sandstone.

The transport coefficients of gypsum lie above those of Baumberger sandstone, though by contrast they are just beneath them in the case of sand-

lime brick. The recorded profiles of aerated concrete and to a great extent the profiles of clay brick as well yield transport coefficients which change with time, making mathematical description of the transport phenomena impossible at present.

Exponential approximations of the transport coefficients are also included for redistribution in the four types of sandstone as well as for gypsum and the sand-lime brick. As is evident from Figs. 41 and 42 the moisture profiles calculated in this manner are in very close agreement with the recorded curves. In contrast to the exponential approximations of the transport coefficients for the moistening process, there is however still no known means of approximating these for redistribution from simple experiments operating without measurement of moisture profiles.

6.3.3 Comparison of the coefficients for absorption and redistribution

Comparison of Figs. 43 and 44 with 45 and 46 shows that the transport coefficients for redistribution of moisture are always smaller than those for absorption. For Baumberger and Sander sandstone the transport coefficients are lower by a factor of about 5; for Obernkirchner sandstone by contrast only by a factor of 2 and for the Rüthener sandstone by a factor of about 15.

For sand-lime brick and gypsum the transport coefficients likewise differ as for Baumberger sandstone by a factor of about 5. The comparison is more difficult in the case of aerated concrete and clay brick due to the large range covered by the calculated transport coefficients. If the average curves of the coefficients for absorption and redistribution of moisture are compared respectively, the transport coefficients for absorption of aerated concrete are higher by roughly a factor of 20, that of clay brick on the other hand by about two powers of ten. The extreme difference between absorption and redistribution in the case of clay brick may be explained by its pore structure. Unlike the other building materials, clay brick actually has cylindrical capillaries. Redistribution of moisture takes place only through the few cross-connections between the capillaries, whereas by contrast in the other building

materials redistribution of the liquid also takes place in the grain interstice corners of each capillary (see Fig. 11).

However, in the hygroscopic moisture region as well the measured transport coefficients for absorption are also higher than those for redistribution. In this region, where liquid transport takes place in the sorbate film, differentiation between absorption and redistribution of moisture can not be justified in a physically meaningful manner. Fig. 48 shows a comparison of the profiles calculated using the measured transport coefficients for absorption (Fig. 47) for the Baumberger, Rüthener and Sander sandstones as well as for gypsum. These materials were chosen because exponential approximations for them do not yield perfect agreement of calculation and measurement (see Figs. 39 and 40). Whereas in the higher moisture region a better situation is reached, the curves are all too flat in the hygroscopic moisture region. This indicates that in this region the transport coefficients were chosen too high. It is however not surprising that in this region the transport coefficients recorded are not correct. The point is that the transport taking place in the hygroscopic moisture region is smaller than total transport by several orders of magnitude. Even at high levels of computational accuracy errors occur in this moisture region in determining mass flow density from equation (30) and in calculating the transport coefficients from equation (29). In this region the transport function has to be corrected by transport coefficients determined by another method. On the assumption that the transport coefficients determined from diffusion studies are valid for absorption in this region as well, a corrected transport function can be plotted. Included in Fig. 47 is the liquid transport coefficient for each of the four building materials calculated from isothermic diffusion measurements in the dry and moist regions. A straight line is drawn through this point to intersect the transport function determined from NMR studies at the water content corresponding to the end of hygroscopic moisture content (sorption moisture content at 95% RH). This line is extended downward to intersect with the ordinate. For the hygroscopic moisture region the values indicated by a dotted line are to be used for the transport function; above it the values of the solid line. The water content profiles calculated

using these transport functions show better agreement in the hygroscopic moisture region, as illustrated in Fig. 49.

For redistribution as well it is possible to improve the agreement between calculation and measurement if, in place of the exponential approximations, the transport function determined from the recorded moisture profiles is used (see Fig. 50). Instead of gypsum, for which there is already good agreement in the redistribution profiles with the exponential approximation and the measured ones (see Fig. 42), sand-lime brick is shown in this figure. Correction in the hygroscopic moisture region is not necessary in this instance since the transport coefficients determined from water content profiles differ only slightly from the values calculated from diffusion analyses.

7. Examples of calculations on moisture balance using the new coefficients and comparison with practical results

Table 9 lists the measurement accuracies for all the instruments used here for determining moisture transport and moisture storrage parameters. Usability of the measured coefficients depends not only on the precision of their measurement, however. Before they come into general use, the newly defined material transport coefficients and storage functions have to be validated by way of practical examples involving experimental investigation into the moisture behaviour of building components to show that they are not only valid under simplified laboratory conditions. This calls for a computation method which allows prediction of the moisture behaviour of building components even under complex conditions using these material characteristics. The computer program developed by H.M. Künzel [88] meets this criterion and has been successful in showing good agreement between calculated and experimental results in numerous applications ([86] [87] [88]).

To validate material coefficients only those test examples are suitable for which the initial and boundary parameters and the composition of the building components are well documented and the material coefficients are available.

No material coefficients for moisture redistribution are to be found in the literature; nor are the materials used any longer available for a new determination of material coefficients. Consequently, this author conducted his own experimental investigations which serve as the basis for the computations.

7.1 Natural stone wall section with natural weathering

The first example illustrates the investigation of moisture behaviour in a section of west-facing natural stone facade by H.M. Künzel [88]. To calculate the moisture behaviour of the facade section of Sander sandstone, the measured storage function shown in Fig. 21 (bottom right) and the liquid transport coefficients shown in Fig. 47 (bottom left) and Fig. 45 (bottom right) were used for the absorption process and the redistribution of moisture, respectively, where used. The other material characteristics needed are listed in Table 10.

The experiment was carried out on prisms of stone 25 cm in length, with sealed flanks, having a sectional area of 5 x 5 cm^2. These prisms were installed in dry condition in the west facade of an unheated test hall. The inner face of the prisms was sealed to protect it against condensation while the outer face was exposed to natural weathering. From the moment of installation on continuous recording was made of the solar radiation (western exposure), outside air temperature and humidity, and driving rain which was measured by a drop-counter integrated into the facade at the same height as the prisms. These climatic data are shown in Fig. 51 (top) in the form of daily average values or totals for an observation period of 80 days. In this same period room air temperature declined relatively steadily from 21°C to 10°C. The humidity of the interior air is not significant since the prisms are sealed on the back. The moisture uptake and release behaviour of the natural stone prisms under the conditions described was recorded by regular weighing of the prisms. In addition, the moisture profiles in the prisms were recorded by NMR at specific intervals. To calculate the moisture behaviour of a natural stone facade under the conditions described here, average hourly values of

the recorded climatic parameters were used. As transfer coefficients for heat and moisture the values from Table 11 were used.

Fig. 51 (bottom) shows the calculated curve for the water content of the natural stone facade averaged over the total width of 25 cm in comparison with the measured moisture change of three natural stone prisms for an observation period of 80 days following the start of exposure. Measurement and calculation, which agree relatively well, show a rise (interrupted by brief periods of drying) in water content due to driving rain (most apparent in the middle of Fig. 51) which has still not reached a state of equilibrium even after 80 days. The moisture profiles established in the facade specimens are shown in Fig. 52 for four distinct points in time. The profile at Time 1 shows the moisture of the stone after the first period of rain. Similar to the situation in a laboratory absorption test this shows a narrow moisture front. At Time 2 - following a lengthy period of fine weather - this moisture front has flattened out by the time it reaches the middle of the prism as a result of drying and redistribution. The chart at Time 3 shows a moisture profile in stormy weather with low relative humidity, known in the foothill areas of the Alps as the foehn. Evident here is the steep water content gradient in the surface zone resulting from the high rate of drying under these climatic conditions. The moisture profile at the end of the 80-day observation period (Time 4) shows a relatively uniform moisture gradient in the facade with approximately capillary water saturation of the exterior surface while there continues to be only very low water content in the area of the interior surface. At all four points in time there is excellent agreement between measurement and calculation. In addition to showing the applicability of the computer program, this clearly shows that the transport coefficients used permit good prediction of the moisture behaviour of building materials even under complex climatic boundary conditions. In this example the storage function is not of any great significance, however, since the test specimen involved is monolithic.

7.2 Liquid transport across the boundary layers of two capillary-porous materials in contact with one another

Until now comparisons between measurements and calculations have for the most part only been made for moisture transport in monolithic materials. One exception to this is Kießl [55] who compares the measured profile for the capillary water absorption of two solid clay bricks having a 1 cm mortar joint between them [80] with computed figures. The comparison ends however at the point of full moistening of this thin mortar joint. To fill this gap, measurements of water absorption across the boundary layers of two capillary-porous materials in contact with one another were carried out and compared with computed values.

The investigations, described in detail in [75], were conducted using three different kinds of natural sandstone: Rüthener, Baumberger and Obernkirchner. For each combination of two materials specimens measuring 5 x 5 cm^2 in section and of varying lengths were cut. The sides of all specimens were sealed with epoxy resin to provide unidimensional conditions. To get a good hygric contact, two different specimens were fastened together in each case with moistened china clay powder between them and dried. A water absorption test was then carried out, with the open end of the shorter specimen piece being placed in contact with water (see Fig. 53). Water absorption as a function of time was determined by weighing. As preliminary tests indicated, the thin layer of china clay has no appreciable effect on the process of water absorption.

7.2.1 Measurement results

Figs. 54 and 55 show the profiles for water absorption as plotted points obtained from successive weighings. Fig. 54 (left) shows water absorption for the combination of 2 cm of Rüthener sandstone and 18 cm of Baumberger sandstone. Following a brief absorption period by the Rüthener sandstone with its high water absorption coefficient, water reaches the Baumberger sandstone as can be seen from the sharp bend in the curve. From there on

the Baumberger sandstone takes up water almost totally unaffected by the Rüthener sandstone.

The Baumberger/Rüthener sandstone combination, as shown in figure 54 (right), behaves in a different fashion. In this case the Baumberger sandstone has a major influence on the absorption behaviour of the Rüthener sandstone. Despite its large water absorption coefficient, the Rüthener sandstone in fact takes up water more slowly than does the Baumberger sandstone. As absorption time increases or as depth of water penetration increases the water absorption rate of the Rüthener sandstone increases. This phenomenon is anticipated since with increasing depth of penetration the decreasing rate of flow causes a decrease in the flow resistance which is considerably higher compared to Rüthener sandstone.

For the combination of 4 cm of Obernkirchner and 16 cm of Baumberger, two materials having almost the same water absorption coefficients but differing suction pressure, absorption behaviour is similar to that of a homogeneous material (see Fig. 55, left). For the reverse combination, by contrast, behaviour is comparable to the Baumberger/Rüthener combination. The reason for this is that in this case as well a material having low suction pressure has to draw the water through a material having high suction pressure and high flow resistance.

7.2.2 Computed results

The computations were made using the moisture transport program [88]. As Table 12 illustrates, the water absorption coefficient of each type of sandstone varies in a certain range. To increase accuracy, the water absorption coefficient measured with each individual specimen was used for the computations. From this coefficient the exponential approximations for the liquid transport coefficients were computed as described in [74]; variations in

the coefficients are included in Table 12. The computed results are shown as a solid line in Figs. 54 and 55. In all cases there is excellent agreement between computation and measurement; the characteristic behaviour and the absorbed volume are accurately reproduced (with very slight deviations only).

Computations in which the transport coefficients and the suction pressure curve were varied showed the suction pressure curve (water retention curve) exerting a dominant influence on the computed behaviour of the water absorption profile. This shows that an accurate determination of the storage function, e.g. using the pressure plate apparatus, is of critical importance when moisture transport for two capillary-active building materials in contact with one another has to be calculated.

8. Summary and Conclusions

The aim of this work was to determine the storage and moisture transport coefficients of porous mineral building materials necessary for calculation of moisture balance. For this purpose the state of knowledge on the mechanisms of moisture storage and transport is first discussed through a critical analysis of the literature. Moisture movement in porous building materials due to air flow, gravitation, differences in hydraulic pressure and osmotic or electrokinetic phenomena is excluded since as a rule it is insignificant for analyses in the field of building materials and structures. On the basis of new approaches by the author, new measuring methods are developed for the field of building science. Some of the measurements results lead to new transport coefficients properly based in physics and in some instances these may also be determined or approximated using simple, classical means.

The storage of moisture in building materials is characterized by three regions. The first region marks so-called hygroscopic equilibrium moisture contents. Next to this for capillary-active materials comes the capillary water region with water contents up to capillary saturation. Capillary saturation may only be exceeded by application of an overpressure or an underpressure, artificially induced condensation from falling below dew-point or extremely long submersion in water. Because hygric equilibrium conditions no longer exist in this supersaturated region, there is also no defining a definitive storage function. The storage function for the hygroscopic moisture region is characterized by the sorption isotherm. Gravimetric determination of the sorption isotherm, which is relatively simple but mostly time-consuming, is feasible to an upper limit of 95% RH. Because the sorption isotherms of most building materials are extremely steep at higher relative humidities, clearly defined sorption measurement and correlation of water content figures with relative humidity are no longer possible above this value. Consequently the moisture storage function of the capillary water region must therefore be determined in a different manner. In capillary-porous hygroscopic building materials having continuous pore-size distribution, a correlation can be made all the way up to capillary saturation between every water content value and a

maximum pore size still filled with water. This correlation is based on the fact that all pores reached by water are connected and that the smaller pores with their greater suction power draw water from the larger pores until capillary pressure equilibrium is reached for a specific water content. For the region of superhygroscopic water contents this produces a characteristic functional relationship, the so-called suction pressure curve or water retention curve. To determine this suction pressure curve a unit for measuring suction pressure familiar in the field of soil science and modified for this purpose is used for the first time in building physics. In contrast to mercury pressure porosimetry, this method, which uses water as the measuring medium, assures a more realistic description.It allows for the interactions between water and pore walls in a way which is identical with natural conditions. It also makes it possible to document not total pore space but the pore space accessible to moisture transport by basing the analysis on capillary saturated specimens.

The sorption isotherm and the suction pressure curve express water content as a function of true potential parameters not dependent on material: relative humidity and capillary pressure respectively. The two parameters are linked by Kelvin's thermodynamic equilibrium condition. This makes it possible to combine the sorption isotherm and the suction pressure curve into a storage function continuous over the whole region and including all the practically significant moisture storage characteristics of a porous building material up to capillary water saturation.

Measurements of the water vapour diffusion resistance of porous hygroscopic building materials per DIN 52 615 for the most part show smaller diffusion resistances in the moist region than in the dry region. This increase in water vapour permeability determined under isothermic conditions is generally attributed to moisture phenomena which increase vapour diffusion flow. However with isothermic diffusion measurements in the higher moisture region the development of a sorption moisture gradient on the pore walls of hygroscopic building materials occurs. A sort of transport in liquid phase take place in this sorbate film. The operative potential of this liquid transport is relative humidity; its gradient operating under isothermic conditions in the

same direction as the water vapour partial pressure gradient driving diffusion. If this liquid transport superimposed on diffusion is responsible for the increase in total mass flow recorded under isothermic conditions, then in the case of opposing gradients of vapour pressure and relative humidity (non-isothermic conditions), a reduced mass flow would have to be recorded. By way of investigations using a test apparatus specially developed for this purepose to induce a temperature gradient through the cross-section of the specimen so as to create a relative humidity gradient and hence sorption moisture gradient running counter to the partial pressure gradient, these considerations are worked out clearly for the first time and confirmed. In addition, other studies by the author and interpretation of other authors' findings are used to offer further evidence of the correctness of this novel interpretation. Consequently only a water vapour diffusion resistance factor determined in the dry region without liquid transport can be looked on as the true material coefficient for diffusion transport.

Study of liquid transport in porous building materials calls for a diversified approach. Essentially, a distinction has to be made among three phenomena: capillary action upon water contact with the major transport intensities being in the high water-content regions; subsequent liquid water redistribution without moistening, and sorption moisture transport having transport intensities which are relatively small yet in the order of magnitude of diffusion. Accurate description of water content distributions varying in time and space under natural conditions requires liquid transport coefficients dependent on water content. To determine the transport coefficients two NMR test units are designed and set up. With their high measuring accuracy and speed of measurement, these make it possible to record continuously and in non-destructive fashion water content distributions in prismatic test specimens during capillary absorption and also, after shut-off of the water supply, during subsequent redistribution of moisture. From these distributions, recorded at different points in time, it is possible to determine the liquid transport coefficients for absorption and redistribution in a short time. It emerges that the transport coefficients for redistribution are in most cases lower than those for absorption. The moisture transport functions for

absorption and redistribution converge in the hygroscopic moisture region since liquid transport takes place there in the sorbate phase and distinguishing between absorption and redistribution is no longer physically meaningful. Both absorption and redistribution show moisture transport functions which rise with moisture content sometimes over several powers of ten. Often, the functions can also be approximated with acceptable accuracy by way of a simple exponential function. This makes it possible to work out an exponential approximation for absorption from the water absorption coefficient, whereas there is still no known simple method of approximation for redistribution.

The newly defined transport coefficients and storage functions are validated using practical examples to show that they are valid not only under simplified laboratory conditions but in practice as well. The first example involves the moisture behaviour of a section of a west-facing natural stone facade under conditions of natural weathering over a period of 80 days. The water content curves and distributions calculated using the transport coefficients and storage function determined in the laboratory show good agreement with the measured curves and distributions. In the second example moisture transport across the boundary layer of two specimens of differing capillary-active building materials in hygric contact with one another is investigated. In this example as well, where in particular the influence of the suction pressure of the materials used is of prime importance, the computed water content curves reproduce the measured values accurately.

The results of the investigations carried out into the moisture storage and transport processes of capillary-porous mineral building materials yield the following conclusions as to the use of the coefficients for calculating moisture balance:

- For the calculation of liquid transport through the boundary layer of two capillary-active materials in contact with one another, use of an accurate moisture storage function is essential. Particularly in the superhygroscopic moisture region, accurate evaluation, preferably involving a measuring method employing water as the measuring medium, is of great importance.

- For hygroscopic building materials under practical, non-isothermic conditions, the traditional description of moisture transport in the hygroscopic moisture region (liquid and vapour) as moisture-dependent diffusion is not acceptable. Calculated results obtained in this fashion are incorrect. Diffusion and moisture calculations have to be carried out separately for these materials as diffusion and liquid transport. Diffusion has to be calculated using a diffusion resistance factor determined in the dry region. For calculation of the simultaneous transport in liquid phase, liquid transport coefficients have to be used.

- In calculating liquid transport, it is necessary to distinguish between two types of transport: absorption and redistribution. For both types of transport there are moisture-dependent and to some extent widely differing transport coefficients. The functions of the liquid transport coefficients of the two types of transport are the same in the hygroscopic moisture region for physical reasons. For this region determination of the coefficients from diffusion analyses is preferable. Both for redistribution and for the absorption process the transport coefficients may be approximated by an exponential function with an accuracy adequate for numerous applications. In this regard it is possible for some building materials to derive the exponential approximation for the absorption process from the water absorption coefficients.

All in all, this work has been able to significantly refine and enhance the analytical methods used in the field of moisture science. Whereas to date mainly standardized water vapour diffusion investigations or suction tests have been used in the area of physics relating to the building sciences, in particular the NMR moisture analysis used here for the first time established the basis for specific determination of those hygric material characteristics which are indispensible for the theoretical study of moisture transport phenomena in building materials and building components.

9. Literature

[1] Achtziger, J.: Messung der Wärmeleitfähigkeit von Schaumkunststoffen mit beliebigem Feuchtigkeitsgehalt. Kunststoffe im Bau (1971), H. 23, S.19-22.

[2] Altmann, K.: Neues Feuchtigkeitsmeßverfahren für Bauteile. Die Bautechnik 47 (1970), H. 8, S. 269-272.

[3] Apel, P., Schmidt, J.: Feuchtemessungen an Betonzuschlagstoffen mit der Mikrowellenmeßtechnik. BWT 25 (1982), H. 5, S. 12-13.

[4] Augustin, H.: Elektrokinetische Vorgänge im Mauerwerk. Bauphysik 3 (1981), H. 5, S. 174-177.

[5] Auracher, H.: Wasserdampfdiffusion und Reifbildung in porösen Stoffen. VDI-Forschungsheft 566 (1974).

[6] Belgith, A., Le Fur, B.: Etude de la diffusivité dans un milieu poreux en fonction de la teneur en eau et de la temperature. C.R.A.S.T. 268 (1989).

[7] Berliner, M.A.: Feuchtemessung. VEB Verlag Technik, Berlin (1980).

[8] Bertelsen, N.H.: Moisture Transport Measured by Cup-Methods. Round Robin Tests and Uncertainties. Building Technology, Technological Institute Lyngby/Dänemark, Nov. (1987).

[9] Bomberg, M.: Water flow through porous materials. Division of Building Technology, Lund/Schweden, Institute of Technology, Report 21 (1972).

[10] Bruce, R.R., Klute, A.: The Measurement of Soil Moisture Diffusivity. Soil Science Society Proceedings 20 (1956), H. 1, S. 458-462.

[11] Brunauer, S., Emmett, P.H. und Teller, E.: Adsorption of Gases in Multimolecular Layers. Journ. Amer. Chem. Soc. 60 (1938), H. 2, S. 309-319.

[12] Brunauer, S., Mikhail, R. Sh., Bodor, E.E.: Pore Structure Analysis without a Pore Shape Model. Journ. of Colloid and Interface Science 24 (1967), H. 4, S. 451-463.

[13] Cammerer, J.S., Görling P.: Die Messung der Durchlässigkeit von Kälteschutzstoffen für Wasserdampfdiffusion. Kältetechnik 3 (1951), H. 1, S. 2-7.

[14] Cammerer, W.F.: Die kapillare Flüssigkeitsbewegung in porösen Körpern. VDI-Forschung 29 (1963), H. 500.

[15] Cammerer, W.F.: Untersuchungsergebnisse über die kapillare Leitfähigkeit von Baustoffen. Wärme und Stoffübertr. 9 (1976),H. 2, S. 159-166.

[16] McCarten, J.: Fat Analysis in Margarine Base Products. Minispec Application Note 1, Bruker Physik AG, Karlsruhe.

[17] Chang, S.C., Hutcheon, N.B.: Dependance of Water Vapour Permeability on Temperature and Humidity. ASHRAE Journ. Sect. Heating, Piping & Air Conditioning 28 (1956), H. 3, S. 149-155.

[18] Cohan, L.H.: Hysteresis and the Capillary Theory of Adsorption of Vapors. Journ. American. Chem. Soc. 66 (1944), H. 66, S. 98-105.

[19] Crank, J.: The mathematics of diffusion. Oxford University Press (1975).

[20] Crausse, P.: Etude fondamentale des transferts couplés de chaleur et d'humidité en milieu poreux. Dissertation L' Institut National Polytechnique de Toulouse (1983).

[21] Croney, D., Coleman, J.D., Bridge, P.M.: The suction of moisture held in the soil and other porous materials. Road Res. Techn. Paper No. 24. Her Majesty's Stationary Office, London (1952).

[22] Davidson, J.H. et al.: Gamma-Radiation Attenuation for Measuring Bulk Density and Transient Water Flow in Porous Materials. Journal of Geophysical Research Vol 68 (1968), H. 16, S. 4777-4783.

[23] Derjaguin B.V. et al.: Effect of film transfer upon evaporation of liquids from capillaries. Bulletin Rilem No. 29 (1965), H. 29, S. 93-98.

[24] Descamps, F.: Moisture Content Measurement using Gamma Ray Attenuation. Research Report (1990). Katholieke Universiteit Leuven, Laboratorium Bouwfysica.

[25] DIN 4108 Wärmeschutz im Hochbau. August 1981.

[26] DIN 52615 Bestimmung der Wasserdampfdurchlässigkeit von Bau- und Dämmstoffen. November 1987.

[27] DIN 52617 Bestimmung des Wasseraufnahmekoeffizienten von Baustoffen. Mai 1987.

[28] DIN 52620 Bestimmung des Bezugsfeuchtegehaltes von Baustoffen. April 1991.

[29] Fagerlund, G.: Determination of pore-size distribution from freezing-point depression. Matériaux et construction 6 (1973), H. 33, S. 215-225.

[30] Fanney, A.H. et al.: Measurements of moisture diffusion in building materials. ASHRAE Transactions 97 (1991), H. 2, S. 99-112.

[31] Farrar, T.C., Becker, E.D.: Pulse and Fourier Transform NMR. New York, London Academic Press (1971).

[32] Fitzner, B.: Untersuchungen der Zusammenhänge zwischen Hohlraumgefüge von Naturstein und physikalischen Verwitterungsvorgängen. Mitteilung zur Ingenieurgeologie und Hydrogeologie (1988), H. 29.

[33] Fukushima, E., Roeder, S.: Experimental Pulse NMR. Addison-Wesley Publishing Company Inc. London (1981).

[34] Gagarin, V.G., Mogutov, V.A.: Unsteady Movement of Fluid in Building Materials. Proceedings of the ICHMT Symposium "Heat and Mass Transfer in Building Materials and Structures". Hemisphere Publishing Corporation, New York (1990), S. 43-62.

[35] Galbraith, G.H., McLean, R.C.: Realistic Vapour Permeability Values. Heat and Mass Transfer. CI/SfB (L27) UDC 697147, S. 98-103.

[36] Gardner, W.R.: Calculation of capillary conductivity from pressure plate flow out data. Soil Sci. Soc. Amer. Proc. 20 (1956).H. 3, S. 317-320.

[37] Garrecht, H.: Porenstrukturmodelle für den Feuchtehaushalt von Baustoffen mit und ohne Salzbefrachtung und rechnerische Anwendung auf Mauerwerk. Diss. Universität Karlsruhe (1992).

[38] Gèmesi, J.: Untersuchung der Kapillarerscheinungen in Beton mit zerstörungsfreien Methoden. Wissenschaftliche Zeitschrift der Hochschule für Bauwesen, Leipzig (1969), H. 3, S. 175-177.

[39] Gertis, K. und Werner, H.: Die Problematik der Porenanalyse von Baustoffen. Schriftenreihe Deutscher Ausschuß für Stahlbeton (1972), H. 258, S. 6-36.

[40] Glaser, H.: Graphisches Verfahren zur Untersuchung von Diffusionsvorgängen. Kältetechnik 11 (1959), H. 10, S. 345-349.

[41] Grimm, W.D.: Bildatlas wichtiger Denkmalgesteine der Bundesrepublik Deutschland. Arbeitsheft 50 (1990), Bayerisches Landesamt für Denkmalpflege, München.

[42] Grüneberg, H., Lehmann, S.: Zur Entwicklung eines elektrischen Bodenfeuchtegebers für die automatische Beregnungssteuerung. Automatisierungspraxis 12 (1975), H. 5, S. 123-124.

[43] Günther, H.: NMR-Spektroskopie. Georg Thieme Verlag, Stuttgart - New York (1983).

[44] Hansen, K. K.: Sorption isotherms Catalogue. Technical report 162/86, Technical University of Denmark (1986).

[45] Harmathy, T.Z.: Moisture Sorption of Building Materials. NRC Canada, Div. Building Research, Techn. paper No. 242 (1967).

[46] Hart, H.: Radioaktive Isotope in der Betriebsmeßtechnik. 2. Auflage Berlin VEB Verlag Technik (1962).

[47] Hartge, K.H.: Die physikalische Untersuchung von Böden. Enke Verlag Stuttgart (1971).

[48] Harz, H.P., Weisser, H.: Einsatz von Kernresonanzspektrometern in der Lebensmittelindustrie. ZFL 37 (1986), H. 4, S. 278-281.

[49] Hausser, K.H.: Kernmagnetische Resonanz in Biologie und Medizin. Physik. Blätter 42 (1986), H. 7, S. 225-233.

[50] Henrich, G.: Feuchteschäden zerstörungsfrei analysiert mit der Neutronensonde. Bautenschutz+Bausanierung 12 (1989), H. 1, S. 24-27.

[51] Holz, M., Knuttel. B.: Gepulste Kernspinresonanz. Physikalische Blätter 38 (1982), H. 12, S. 368-374.

[52] Hounsfield, G.N.: Computerized Transverse Axial Scanning (Tomography): Part I. Description of System. British Journal Radiology 46 (1973), H. 552, S. 1016-1022.

[53] Hundt, J., Buschmann, J.: Moisture Measurement in Concrete. Materiaux et Constructions 4 (1971), H. 22, S. 253-259.

[54] Husseini, F.: Feuchteverteilung in porösen Baustoffen aufgrund instationärer Wasserdampfdiffusion. Diss. Universität Dortmund (1982).

[55] Kießl, K., Gertis, K.: Feuchtetransport in Baustoffen. Eine Literaturauswertung zur rechnerischen Erfassung hygrischer Transportphänomene. Forschungsberichte aus dem Fachbereich Bauwesen 13 (1980), Universität Essen Gesamthochschule.

[56] Kießl, K.: Kapillarer und dampfförmiger Feuchtetransport in mehrschichtigen Bauteilen. Diss. Universität Gesamthochschule Essen (1983).

[57] Kießl, K., Krus, M., Künzel, H.M.: Weiterentwickelte Meß- und Rechenansätze zur Feuchtebeurteilung von Bauteilen. Praktische Anwendungsbeispiele. Bauphysik 15 (1993), H. 2, S. 61-67.

[58] Kießl, K., Gertis, K.: Isothermer Feuchtetransport in porösen Baustoffen. Sonderdruck aus "Deutscher Ausschuß für Stahlbeton" (1976), H. 258, S. 86-110.

[59] Klein, A.: Microwave Determination of Moisture in Coal. Comparison of Attenuation and Phase Measurement. Journal of Microwave Power 16 (1981), H. 3 und 4, S. 290-304.

[60] Klein, A.: Erfahrungen beim Einsatz von Meßgeräten zur Schnellbestimmung des Wassergehaltes. Aufbereitungstechnik 28 (1987), H. 1, S. 10-16.

[61] Klopfer, H.: Wassertransport durch Diffusion in Feststoffen. Bauverlag GmbH. Wiesbaden (1974).

[62] Kober, K., Mehlhorn, L.: Radiometrische Feuchtemessung in Bauteilen mit hoher räumlicher Auflösung. Bauphysik 13 (1991), H. 2, S. 43-49.

[63] Kohonen, R.: A method to analyze the transient hygrothermal behaviour of building materials and components. Diss. Helsinki University Espoo (1984).

[64] Kooi van der, J.: Moisture Transport in Cellular Concrete Roofs. Diss. TH Eindhoven (1971).

[65] Krause, D. et al.: Kapazitive Messung des Wassergehaltes von Böden in Kulturgefäßen. GIT Fachz. Labor 29 (1985), H. 2, S. 91-105.

[66] Krestel, E.: Bildgebende Systeme für die medizinische Diagnostik. Siemens AG Berlin, München (1980).

[67] Krischer, O. und Mahler, K.: Über die Bestimmung des Diffusionswiderstandes und der kapillaren Flüssigkeitsleitzahl aus stationären und instationären Vorgängen. VDI-Forschungsheft 473 (1959), Ausgabe B, Band 25.

[68] Krischer, O. und Kast, W.: Die wissenschaftlichen Grundlagen der Trocknungstechnik. 3. Auflage, Springer Verlag Berlin (1978).

[69] Krus, M. und Kießl, K.: NMR-Messung kapillarer Flüssigkeitsbewegungen in porösen Gesteinen und Ableitung neuer Kapillartransport-Kenngrößen. Jahresberichte aus dem Forschungsprogramm Steinzerfall - Steinkonservierung (1989), Band 1, Verlag Ernst & Sohn, S. 39-45.

[70] Krus, M. und Kießl, K.: Vergleichende Untersuchungen zur Bestimmung der Porenradienverteilung von Natursandstein mittels Saugspannungsmessung und Quecksilber-Druckporosimetrie. IBP-Bericht FtB-11/1991.

[71] Krus, M. und Kießl, K.: Ist der Diffusionswiderstand von Baustoffen wirklich feuchteabhängig? IBP-Mitteilung 18 (1991) Nr. 208.

[72] Krus, M.: Does vapour diffusion really depend on moisture content? IEA-Annex 24 Projekt, Report T3-D-92/02.

[73] Krus, M. und Künzel, H.M.: Liquid water transport above capillary saturation. IEA-Annex 24 Projekt, Report T3-D-92/03.

[74] Krus, M.: Determination of D_w from A-value. IEA-Annex 25 Projekt, Report T3-D93/01.

[75] Krus, M., Künzel, H.M., Klier, M.: Liquid Transport Over the Boundary Layers of Two Different Hygroscopic Capillary Active Materials. IEA-Annex 24 Projekt, Report T1-D93/08.

[76] Ksenshek, O.S. et al.: Centrifugal Method for Finding Pore-size Distribution Function in Porous Media. Russian Journal of Phys. Chem. 41 (1967), H. 7, S. 856-863.

[77] Kuhn, K.: Kernresonanzmessungen und Wasseraktivitätsbestimmungen zur Aufklärung des Trocknungsverhaltens von Kartoffeln. Diss. Universität Hamburg (1986).

[78] Kumaran, M.K., Bomberg, M.: A Gamma-Spectrometer for Determination of Density Distribution and Moisture Distribution in Building Materials. Proc. of the International Symposium on Moisture and Humidity, Washington D.C., (1985), S. 485-490.

[79] Kumaran, M.K.: Moisture diffusivity of gypsum board from gammy-ray attenuation measurements. IEA-Annex 24 Projekt, Report T3-CA-93/03.

[80] Künzel, H. und Schwarz, B.: Die Feuchtigkeitsaufnahme von Baustoffen bei Beregnung. Berichte aus der Bauforschung (1968) H. 51, S. 99-113, Verlag Wilhelm Ernst & Sohn, Berlin.

[81] Künzel, H. und Bernhardt, P.: Wasserdampfdurchlässigkeit von Baustoffen bei verschiedenen Feuchtezuständen. Berichte aus der Bauforschung (1973), H. 80, S. 15-19, Verlag Wilhelm Ernst & Sohn, Berlin.

[82] Künzel, H.: Zusammenhang zwischen der Feuchtigkeit von Außenbauteilen in der Praxis und den Sorptionseigenschaften der Baustoffe. Bauphysik 4 (1982), H. 3, S. 101-107.

[83] Künzel, H. und Holz, D.: Bauphysikalische Untersuchungen in unbeheizten und beheizten Kirchen alter Bauart. IBP-Bericht FB-32/1991.

[84] Künzel, H.M. und Kießl, K.: Ist Vakuumtrocknung günstiger als Konvektionstrocknung? Untersuchungsergebnisse für Natursteine. Bauphysik 12 (1990), H. 1, S. 27-30.

[85] Künzel, H.M. und Kießl, K.: Bestimmung des Wasserdampfdiffusionswiderstandes von mineralischen Baustoffen aus Sorptionsversuchen. Bauphysik 12 (1990), H. 5, S. 140-144.

[86] Künzel, H.M.: Heat and Moisture Transfer in Porous Media; a comparison of measurement and calculation and its consequences for the treatment of vapour diffusion. IEA-Annex 24 Projekt, Report T1-D92/01.

[87] Künzel, H.M.: Rechnerische Untersuchungen des Langzeit-Feuchteverhaltens von Wärmedämmschichten in Umkehrdächern mit Begrünung. IBP-Bericht FtB-23/1993.

[88] Künzel, H.M.: Verfahren zur ein- und zweidimensionalen Berechnung des gekoppelten Wärme- und Feuchtetransports in Bauteilen mit einfachen Kennwerten. Diss. Universität Stuttgart (1994).

[89] Kupfer, K.: Feuchtemessung an Zuschlagstoffen für die Betonherstellung unter Verwendung der Mikrowellenmeßtechnik. Diss. Hochschule für Architektur und Bauwesen Wismar (1990).

[90] McLean, R.C., Galbraith, G.H., Sanders, C.: Moisture transmission testing of building materials and the presentation of vapour permeability values. Building Research And Practice. The Journal of CIB, No. 2 (1990).

[91] Lück, W.: Feuchtigkeit. Verlag R. Oldenbourg, München (1964).

[92] Luikov, A.V.: Systems of Differential Equations of Heat and Mass Transfer in Capillary Porous Bodies (Review). Intern. Journ. Heat & Mass Transfer 18 (1975), H. 1, S. 1-14, Pergamon Press.

[93] Lykow, A.W.: Transporterscheinungen in kapillarporösen Körpern. Akademie Verlag Berlin (1958).

[94] Mahler, K.: Über die Bestimmung des Diffusionswiderstandes und der kapillaren Flüssigkeitsleitzahl aus stationären und instationären Vorgängen. Diss. Technische Hochschule Darmstadt 1958.

[95] Martin, M.: Practical NMR Spectroscopy. Heyden Verlag London, Philadelphia, Rheine (1980).

[96] Matzkanin, G.A.: Application of Spatially Localized NMR to Nondestructive Evaluation. Proc. of the second World Conf. on NDT, 3-8. Nov. 1985, Las Vegas.

[97] Michel, D.: Grundlagen und Methoden der kernmagnetischen Resonanz. Akademie-Verlag Berlin (1981).

[98] Molenda, C.H.A., Crausse, P. und Lemarchand, D.: The influence of capillary hysteresis effects on the humidity and heat coupled transfer in a non-saturated porous medium. Intern. Journal Heat & Mass Transfer 35 (1992), H. 6, S. 1385-1396.

[99] Neiß, J.: Numerische Simulation des Wärme- und Feuchtetransports und der Eisbildung in Böden. Fortschrittsbericht VDI-Z. 3 (1982), H. 73, S. 1-293.

[100] Neue, J.: Anwendung des dielektrischen Meßprinzips zur Bestimmung der Feuchtigkeitsverteilung in Baumaterial. 2. Bauklimatisches Symposium der Sektion Architektur. Schriftenreihe der Sektion Architektur der TU Dresden (1978), H. 11, S.133-143.

[101] Nielsen, A.F.: Gamma-Ray-Attenuation Used for Measuring the Moisture Content and Homogeneity of Porous Concrete. Building Science 7 (1972), H. 4, S. 257-263.

[102] Ostman, E.: The Use of Computed Tomography in Non-destructive Testing of Polymeric Materials, Aluminium and Concrete. 2. Intern. Conference on Testing, Evaluation and Quality Control of Composites - TEQC 87. University of Surrey, Guildford, U.K., 22.-24. Sept. 1987.

[103] Paetzold, R.F., Matzkanin, G.A., De Los Santos, A.: Surface Soil Water Content Measurement Using Pulsed NMR Techniques. Soil Science Society of America Journal 49 (1985), H. 3, S. 537-540.

[104] Peck, A.J.: Diffusivity Determination by a New Outflow Method. Proc. Wageningen Symposium (1969), S. 191-202.

[105] Perrin, B. et al.: Détermination du Coefficient de Diffusion Isotherme de l'Humidité dans des Matériaux de Construction. Matériaux et Construction Vol. 16 (1983), H. 91, S. 27-33.

[106] Philip, J.R., de Vries, D.A.: Moisture Movement in Porous Materials under Temperature Gradients. Transactions, Amer. Geophysical Union 38 (1957), H. 2, S. 222-232.

[107] Pratt, A.W.: Some observations on the variation of the thermal conductivity of porous inorganic solids with moisture content. Thermal Conductivity Conference. National Physical Laboratory, Great Britain, (1964).

[108] Prazak, J. et al.: Bemerkungen zur Beschreibung des Flüssigtransportes in porösen Baumaterialien. Gesundheits-Ingenieur 110 (1989), H. 6, S. 308-312.

[109] Queisser, A.: Zerstörungsfreie Materialuntersuchungen an Natursandstein mittels Computertomographie. Bautenschutz und Bausanierung 11(1988), S. 54-60.

[110] Quenard, D., Sallee, H.: A Gamma-Ray Spectrometer for Measurement of the Water Diffusivity of Cementitious Material. Mat. Res. Soc. Symp. Proc. 137 (1989), S. 165-169.

[111] Rao, K.S.: Hysteresis in Sorption. Journ. Phys. Chem. 45 (1941), H. 45, S. 500-539.

[112] Reinhardt, H.W., Gaber, K.: Equivalent pore size characterizing the pore size distribution of cement mortar. Advances in Cementitious Materials, Sidney Mindess (ed.), Ceramic Transactions, Am. Ceram. Soc., Westerville 16 (1990), S. 319-335.

[113] Richards, L.A.: Methods of measuring soil moisture tension. Soil Science 68 (1949), H. 68, S. 95-112.

[114] Ricken, D.: Ein einfaches Berechnungsverfahren für die instationäre Wasserdampfdiffusion. Bauphysik 13 (1991), H. 2, S. 33-37.

[115] Rode, C.: Combined heat and moisture transfer in building constructions. Diss. Technical University of Denmark (1990).

[116] Rollwitz, W.C.: Moisture Measurement in various hygroscopic materials using nuclear magnetic resonance. Humidity and Moisture, Vol. 2 (1965), New York.

[117] Roos, H., Niesel, K., Hoffmann, D.: Über Phänomene des Feuchtigkeitstransports in Ziegeln und Mauerwerk. GIT Fachz. f. d. Lab. 32 (1988), H. 5, S. 16-21.

[118] Rose, D.A.: Water movement in porous materials. Brit. Journal Appl. Phys., Vol. 14 (1963), H. 5, S. 256-262.

[119] Rowell, R.L. et al.: Gas and Vapour Permeability: Surface Flow Through Porous Media. Journ. of Colloid and Interface Sc. 37 (1971), H. 1, S. 242-246.

[120] Rowley, F.B. und Lund, C.E.: Vapour Transmission Analysis of Structural Insulating Board. Bulletin Nr. 22 (1944), University of Minnesota.

[121] Schaefer, K.: Messung des Wassergehaltes und der Wasserbindung in Papier mit Hilfe der gepulsten Kernresonanz-Spektroskopie. Diplomarbeit Lehrstuhl für Brauereianlagen und Lebensmittelverpackungstechnik, Weihenstephan (1988).

[122] Schaschek, H.: Bewegungsmechanismus von Wasserdampf in porösen blattförmigen Materialien. Chemie-Ingenieur-Technik 28 (1956), H. 11, S. 698-702.

[123] Scheffer, F. und Schachtschabel, P.: Lehrbuch der Bodenkunde. Enke-Verlag Stuttgart (1976).

[124] Schirmer, R.: Diffusionszahl von Wasserdampf-Luft-Gemischen und die Verdampfungsgeschwindigkeit. 2. VDI Beil. Verfahrenstechnik (1938), H. 6, S. 170-177.

[125] Schubert, H.: Kapillarität in porösen Feststoffsystemen. Springer-Verlag Berlin (1982).

[126] Schwarz, B.: Die kapillare Wasseraufnahme von Baustoffen. Gesundheits-Ingenieur 93 (1972), H. 7, S. 206-211.

[127] Sommer, E.: Beitrag zur Frage der kapillaren Flüssigkeitsbewegung in porigen Stoffen bei Be- und Entfeuchtungsvorgängen. Diss. TU Darmstadt (1971).

[128] Stroosnijder, L. und De Swart, J.G.: Column Scanning with Simultaneous Use of ^{241}Am and ^{137}Cs Gamma radiation. Soil Science 118 (1978), H. 2, S. 61-69.

[129] De Swart, J.G. und Groenevelt, P.: Column Scanning with 60 KeV Gamma Radiation. Soil Sci. Vol. 112 (1971), H. 6, S. 419-424.

[130] Timofijew, D.P.: Adsorptionskinetik. VEB-Verlag Leipzig (1967).

[131] Timur, A.: Pulsed NMR Studies of Porosity, Movable Fluid and Permeability of Sandstones. Journal of Petroleum Techn. 21 (1969); H. 5, S. 775-786.

[132] Trost, A.: Industrielle Feuchtemessung mit Neutronen. Zeitschrift für Instrumentenkunde 73 (1965), H. 12, S. 329-336.

[133] Tveit, A.: Measurements of moisture sorption and moisture permeability of porous materials. Norwegian Building Research Institute, Oslo (1966), Rapport 45.

[134] Tyvoniak, J. et al.: Feuchtemessung mittels Neutronenradiographie. Bautenschutz + Bausanierung 14 (1991), H. 2, S. 20-23.

[135] Vetterlein, E.: Untersuchungen über den Einfluß der Temperatur auf die kapillare Leitfähigkeit und Wasserbindung in Böden. Albrecht-Thaer-Arch., 12 (1968), H. 5-6, S. 385-400.

[136] Volkwein, A.: Untersuchungen über das Eindringen von Wasser und Chlorid in Beton. Bericht aus dem Bauforschungsinstitut (1991) Technische Universität München, H. 1, S. 1-131.

[137] Vos, B.H.: Meßmethoden zur Bestimmung des Wärmedurchlaßwiderstandes, des Feuchtegehaltes und der Feuchteverteilung. Gesundheits-Ingenieur 89 (1968), H. 3, S. 74-80 und H. 4, S. 115-118.

[138] Wißmann W.: Über das Verhalten von Baustoffen gegen Feuchtigkeitseinwirkungen aus der umgebenden Luft. Diss. TH Darmstadt (1964).

[139] Wittig, G. und Lingott, H.: Untersuchungen mit Mikrowellen zur Feuchtewanderung in Baustoffproben. Bauphysik 14 (1992), H. 2, S. 45-49.

[140] Wittmann, H.: Kann das Prinzip der Elektroosmose zur Trockenlegung von Mauerwerk angewendet werden? Bautenschutz und Bausanierung 4 (1981), H. 4, S. 126-132.

[141] Zacharias, B., Venzmer, H.: Ein Kapillarmodell zur Abschätzung der Wirkung äußerer Kräfte auf den kapillaren Feuchtetransport. Tagung "Feuchtegeschädigte Wände", TH Wismar (1989).

[142] Zehendner, H.: Ein Meßverfahren zur Bestimmung des Wasserdampf-Diffusionswiderstandsfaktors von Bau- und Wärmedämmstoffen. Kältetechnik-Klimatisierung 19 (1967), H. 5, S.141-146.

[143] Zeilinger, A.: Untersuchung des Feuchtetransports in Beton des SNR-300 durch Neutronentransmission. Kerntechnik 18 (1976), H. 3, S. 119-125.

9.1 Translation of German titles in the literature

[1] Measurement of thermal conductivity of plastic foam having arbitrary moisture content.

[2] A new method of measuring moisture for building components.

[3] Measurements of moisture in concrete aggregates using the microwave method.

[4] Electrokinetic phenomena in masonry.

[5] Water vapour diffusion and white frost in porous materials.

[6] Study of diffusivity in a porous medium as a function of water content and temperature.

[7] The measurement of moisture.

[13] Measurement of the permeability of insulating materials for water vapour diffusion.

[14] Capillary fluid movement in porous bodies.

[15] Results of investigations into the capillary conductivity of building materials.

[20] Basic study of combined heat and humidity transfer in porous media.

[25] DIN 4108 Insulation in building construction.

[26] DIN 52 615 Determination of the water vapour permeability in building materials and insulaton products.

[27] DIN 52 617 Determination of water absorption coefficient of building materials.

[28] DIN 52 620 Determination of the reference moisture content of building materials.

[32] Investigations into the relationships between the cavity structure of natural stone and physical weathering phenomena.

[37] Pore structure models for the moisture balance of building materials with and without salt loads, and calculative application for masonry.

[38] Investigation of capillary phenomena in concrete using non-destructive methods.

[39] Problems of pore analysis in building materials.

[40] Graphic method for investigation of diffusion phenomena.

[41] Illustrated atlas of significant monument stones of the Federal Republic of Germany.

[42] Development of an electric soil moisture sensor for automatic sprinkler control.

[43] NMR spectroscopy.

[46] Radioactive isotopes in industrial measuring technology.

[47] The physical study of the soil.

[48] The use of nuclear resonance spectrometers in the food industry.

[49] Nuclear magnetic resonance in biology and medicine.

[50] Moisture damage analyzed non-destructively using the neutron probe.

[51] Pulsed nuclear magnetic resonance.

[54] Moisture distribution in porous building materials as a result of unsteady-state water vapour diffusion.

[55] Moisture transport in building materials. An analysis of the literature on calculative study of hygric transport phenomena.

[56] Capillary and vaporous moisture transport in multi-layer building components.

[57] Advanced measurement and calculation techniques for the evaluation of moisture in building components. Practical examples.

[58] Isothermic moisture transport in porous building materials.

[60] Experiences using measuring equipment for rapid determination of water content.

[61] Water transport by diffusion in solids.

[62] Radiometric moisture measurement in building components with high spatial resolution.

[65] Capacitive measurement of the water content of soils in planting pots.

[66] Imaging systems for medical diagnostics.

[67] On the determination of diffusion resistance and the capillary liquid conductivity coefficient from steady-state and unsteady-state phenomena.

[68] The scientific principles of drying technology.

[69] NMR measurement of capillary penetration behaviour of liquids in porous stone and derivation of new capillary transport coefficients.

[70] Comparative investigations to determine the pore radius distribution of natural sandstone by way of suction pressure measurement and mercury pressure porosimetry.

[71] Is the diffusion resistance of building materials really dependent on moisture?

[77] Nuclear resonance studies and water activity analyses to explain the drying behaviour of potatoes.

[80] The moisture uptake of building materials under irrigation.

[81] Water vapour permeability of building materials in various moisture conditions.

[82] Relationship between the moisture of outdoor building components in practice and the sorption characteristics of the building materials.

[83] Investigations into temperature and moisture in heated and unheated old style churches.

[84] Is vacuum drying more effective than convection drying?

[85] Determination of water vapour diffusion resistance of mineral building materials through sorption experiments.

[87] Calculative examinations of the long-term moisture behaviour of insulation layers in inverted roofs with plant cover.

[88] Simultaneous Heat and Moisture Transport in Building Components. One-and two-dimensional calculation using simple parameters.

[89] Moisture measurement on aggregates for the making of concrete using the microwave method.

[91] Moisture.

[93] Transport phenomena in capillary porous material.

[94] Determination of diffusion resistance and the capillary liquid conductivity coefficient from steady-state and unsteady-state phenomena.

[97] Basic principles and methods of nuclear magnetic resonance.

[99] Numerical simulation of heat and moisture transport and the formation of ice in soils.

[100] Using the dielectric measuring principle to determine moisture distribution in building materials.

[105] Determination of the isothermic diffusion coefficient for moisture in building materials.

[108] Notes on the description of liquid transport in porous building materials.

[109] Non-destructive materials testing on natural sandstone using computer tomography.

[114] A simple calculative method for unsteady-state water vapour diffusion.

[117] On phenomena of moisture transport in brick and masonry.

[121] Measurement of water content and water bonding in paper using pulsed nuclear resonance spectroscopy.

[122] The transport mechanism of water vapour in porous leaf-shaped materials.

[123] Textbook of soil science.

[124] Diffusion coefficient of water vapour - air mixtures and rate of vapourization.

[125] Capillarity in porous solid-matter systems.

[126] The capillary water absorption of building materials.

[127] Contribution to the question of capillary liquid transport in porous materials during humidification and dehumidification processes.

[130] Adsorption kinetics.

[132] Industrial moisture measurement with neutrons.

[134] Moisture measurement via neutron radiography.

[135] Investigations into the effect of temperature on capillary conductivity and water absorption in soils.

[136] Examining the penetration of water and chloride in concrete.

[137] Test methods for determining thermal conductivity resistance, moisture content and moisture distribution.

[138] The behaviour of building materials vis-a-vis the action of atmospheric moisture.

[139] Investigations with microwaves on moisture migration in specimens of building materials.

[140] Can the principle of electro-osmosis be used for drying of masonry?

[141] A capillary model for estimating the effect of external forces on capillary moisture transport.

[142] A measuring method for determining the water vapour diffusion resistance factor of building and thermal insulating materials.

[143] Investigation of moisture transport in concrete of the SNR-300 through neutron transmission.

Table 1 Tabulation of „classical" moisture-related material coefficients for the materials investigated. The water absorption coefficient A and the vapour diffusion resistance factor μ were determined in accordance with DIN 52 617 [27] or DIN 52 615 [26] respectively.

material	bulk density [kg/m³]	porosity [vol.-%]	capillary saturation [kg/m³]	A-value [kg/m²√s]	vapour diffusion resistance factor	
					dry-cup (3 to 50 % r.F.)	wet-cup (50 to 93 % r.F.)
Baumberger	1980	23	210	0.044	20	14
Obernkirchner	2150	14	110	0.046	32	28
Rüthener	1950	24	200	0.30	17	13
Sander	2120	17	130	0.02	33	22
gypsum	850	65	400	0.29	8.3	7.3
sand-lime brick	1900	29	250	0.045	28	18
aerated concrete	600	72	290	0.09	7.6	6.7
solid clay brick	1700	38	370	0.25	9.5	8

Table 2 Tabulation of sorption moisture contents for the building materials investigated, determined at various relative humidities.

material	sorption moisture content in [kg/m³] at					
	10 % RH	30% RH	50 %RH	65 % RH	80 % RH	90 % RH
Baumberger	8.5	17.6	-	27.5	35.6	43.1
Obernkirchner	0.6	1.3	-	2.6	3.4	4.3
Rüthener	1.8	4.5	-	8	12.4	16.9
Sander	4.4	10.2	-	15.2	-	22.6
gypsum	-	-	3.6	5.2	6.3	11
sand-lime brick	-	-	17	18	24.9	40.2
aerated concrete	-	-	7.3	12.5	17	38
solid clay brick	-	-	7.5	8.4	18	34

Table 3 Tabulation of the porosity coefficients and the amount of absorbed salt of the varieties of stone investigated for comparison of pressure plate measurement and mercury intrusion porosimetry.

stone variety	bulk density [kg/m^3]	porosity [vol.-%]	capillary saturation [kg/m^3]	absorbed amount of salt [mass-%]	
				$MgSO_4 \cdot 7H_2O$	KNO_3
Obernkirchner sandstone	2150	14	110	0.16	0.39
Rüthener sandstone	1950	24	210	0.19	0.41

Table 4 Comparison of parameters for pressure plate measurement and mercury intrusion porosimetry.

parameter	pressure plate measurement	mercury intrusion porosimetry
analytical medium	water	mercury
pore space encompassed	only water-filled pores	all pores
influence of salt	measurable	no measurable response
hydrophobic effects	measurable	no measurable response
moisture condition	wet	dry
rate of measurement	low (ca. 4 weeks)	high (ca. 3 hrs)
accuraly	medium	high
gradation	coarse	fine
pore radius range [µm]	0.015 to 30	0.004 too 50

Table 5 Parameters and results for diffusion mass flux densities and μ-values in gypsum wallboard and Baumberger sandstone. The non-isothermic diffusion resistance coefficients were determined from measured mass flows on the basis of equation (1). The isothermic diffusion resistance coefficient was determined at an average relative humidity of 63 % and the mass flow calculated from it.

material	parameter							results	
	ϑ_1 [°C]	ϑ_2 [°C]	φ_1 [%]	φ_2 [%]	p_{D1} [mbar]	p_{D2} [mbar]	gradients φ und p_D	g [g/m²h]	μ [-]
gypsum	24	18	50	75	14.9	15.5	parallel	0.86	6.3
measured non-isothermic	26.5	18	50	75	17.3	15.5	opposing	0.41	22
Baumberger	27	17	50	75	17.7	14,5	opposing	0.57	29
measured non-isothermic	25	17	50	75	16.0	14.5	opposing	0.05	160
Baumberger	23		average value ca. 63 %		Δp_D = 3.2		parallel	1.07	16
calculated isothermic					Δp_D = 1.5		parallel	0.50	16

ϑ_1, φ_1, p_{D1}: temperature, relative humidity, partial vapour pressure in the diffusion vessel

ϑ_2, φ_2, p_{D2}: temperature, relative humidity, partial vapour pressure in the conditioning chamber

g: total mass flux

Table 6 Vapour diffusion resistance coefficients for the materials investigated, measured per DIN 52 615 [26] in the dry-cup and wet-cup region as well as in other moisture regions above the dry-cup region. The differences in the results from the dry-cup region measurements are attributable to liquid transport phenomena and may be used to determine the liquid transport coefficients in the hygroscopic moisture region.

material	vapour diffusion resistance coefficients			
	dry-cup region		wet-cup region	
	3 to 50 % RH	44 to 63 % RH	50 to 93 % RH	80 to 90 % RH
Baumberger	20	17	14	8,8
Obernkirchner	32	30	28	18
Rüthener	17	16	13	9.4
Sander	33	30	22	13
gypsum	8.3	-	7.3	-
sand-lime brick	28	24	18	13
aerated concrete	7.6	-	6.7	-
solid clay brick	9.5	8.8	8	6.9

Table 7 Liquid transport coefficients determined from isothermic diffusion measurements in the dry-cup and wet-cup regions using equation (24). The sorption isotherm must be known for calculation (see Table 2).

material	water content [kg/m^3]	liquid transport coefficient [m^2/s]
Baumberger	31	$2.5 \cdot 10^{-10}$
Obernkirchner	7.7	$1.9 \cdot 10^{-10}$
Rüthener	14	$2.9 \cdot 10^{-10}$
Sander	22	$1.8 \cdot 10^{-10}$
gypsum	10	$3.5 \cdot 10^{-10}$
sand-lime brick	30	$1.8 \cdot 10^{-10}$
aerated concrete	44	$1.1 \cdot 10^{-10}$
solid clay brick	35	$2.6 \cdot 10^{-10}$

Table 8 Orders of magnitude of longitudinal relaxation time T_1 (from [77] and transverse relaxation time T_2 (from [121]) of water in various bound states.

bound state of water	longitudinal relaxation time	transverse relaxation time
solid (ice)/firmly bound water	about one hundred millisecs	a few microsecs
lightly bound water	about one hundred millisecs	a few microsecs
unbound pore water	about one second	several hundred microseconds
free water	a few seconds	a few seconds

Table 9 Tabulation of measuring accuracy for all measured variables needed for the determination of moisture transport and storage coefficients.

measured variable	used measuring instrument	measuring accuracy
temperature	copper constantan thermocouple	±0,2 K
pressure	manometer	to 0.3 bar ± 5 mbar to 5 bar ± 0.1 bar to 15 bar ± 0.2 bar to 100 bar ± 0.5 bar
relative humidity	capacitive humidity sensor	± 1 % RH
weight	balance	to 500 g ± 2 mg to 2000 g ± 20 mg
dew point temperature	dew point mirror	± 0.1 K
	LiCl-sensor	+ 0.2 K
water content	NMR-equipment	≥ ± 0.1 vol.-%

Table 10 Tabulation of additionalmaterial coefficients of Sander sandstone necessary for the example of calculation.

material coefficient	Sander sandstone
specific heat capacity [J/kgK]	850
thermal conductivity [W/mK]	1.6
moisture increase [%/m.-%]	8
short wave adsorption coefficient	dry: 0.71 wet: 0.83

Table 11 Mean surface transfer coefficents for calculation of heat and moisture exchange between ambient air and outdoor and indoor building component surfaces respectively [87].

building component surface	transfer coefficients	
	heat transfer α [W/m^{2}K]	water vapour transfer β_p [kg/m^{2}sPa]
outdoors	17	$75 \cdot 10^{-9}$
indoors	8	$25 \cdot 10^{-9}$

Table 12 Tabulation of the spread in the water absorption coefficients of the sandstone specimens used for the sample calculation. From these water absorption coefficients the spread in the exponential approximations of the liquid transport coefficients was calculated.

variety of sandstone	water absorption coefficient [kg/m$^2\sqrt{s}$]	liquid transport coefficient	
		D_{wo} [m^2/s]	D_{wf} [m^2/s]
Baumberger	0.040 - 0.048	$6.0 - 7.2 \cdot 10^{-10}$	$1.05 - 1.30 \cdot 10^{-7}$
Obernkirchner	0.042 - 0.050	$1.8 - 2.2 \cdot 10^{-9}$	$5.8 - 7.0 \cdot 10^{-7}$
Rüthener	0.28 - 0.35	$5.4 - 6.2 \cdot 10^{-10}$	$1.5 - 2.3 \cdot 10^{-5}$

D_{wo}: liquid transport coefficient for dry material
D_{wf}: liquid transport coefficient at capillary saturation

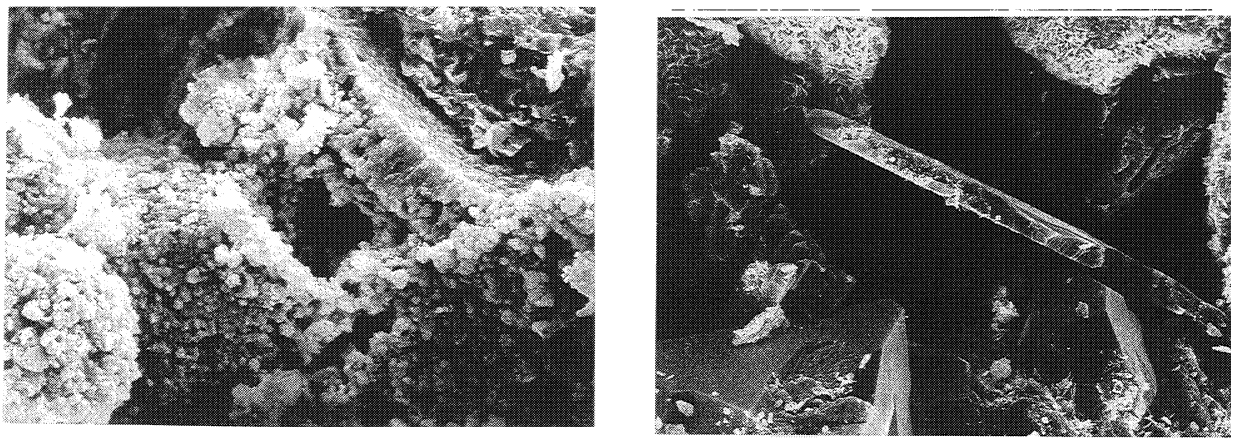

Fig 2 Scanning electron microscop photographs [41] of Baumberger sandstone with 850 x magnification (left) and Sander sandstone with 450 x magnification (right). Despite their very similar genesis the two sandstones show marked differences in their pore space structure.

Fig. 1 Scanning electron microscope photograph of aerated concrete [38] with 22 x magnification (left) and 11,000 x magnification (right). Whereas the pores in the structure of the material give a roundish impression at low magnification, the microstructure visible at high magnification is marked by spiky needles. Use of a cylindrical pore model to describe pore structure seems unsuitable in this case.

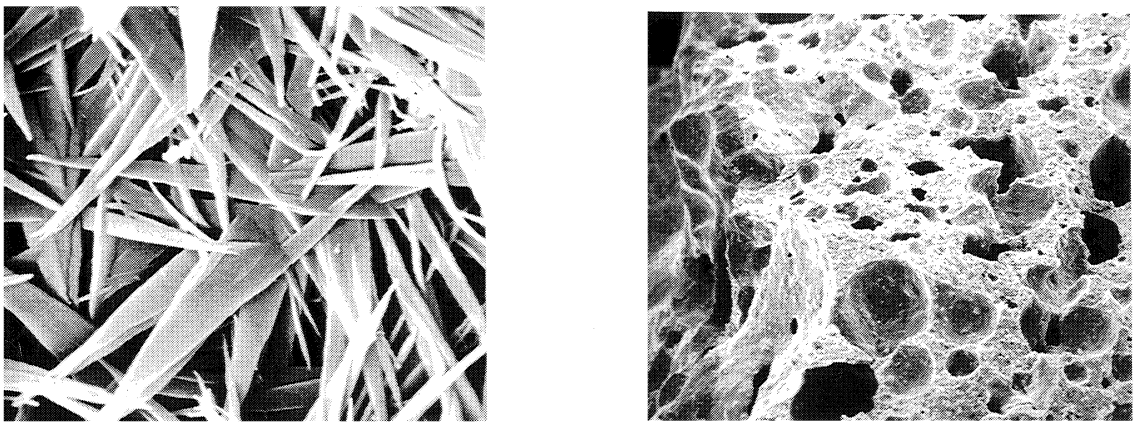

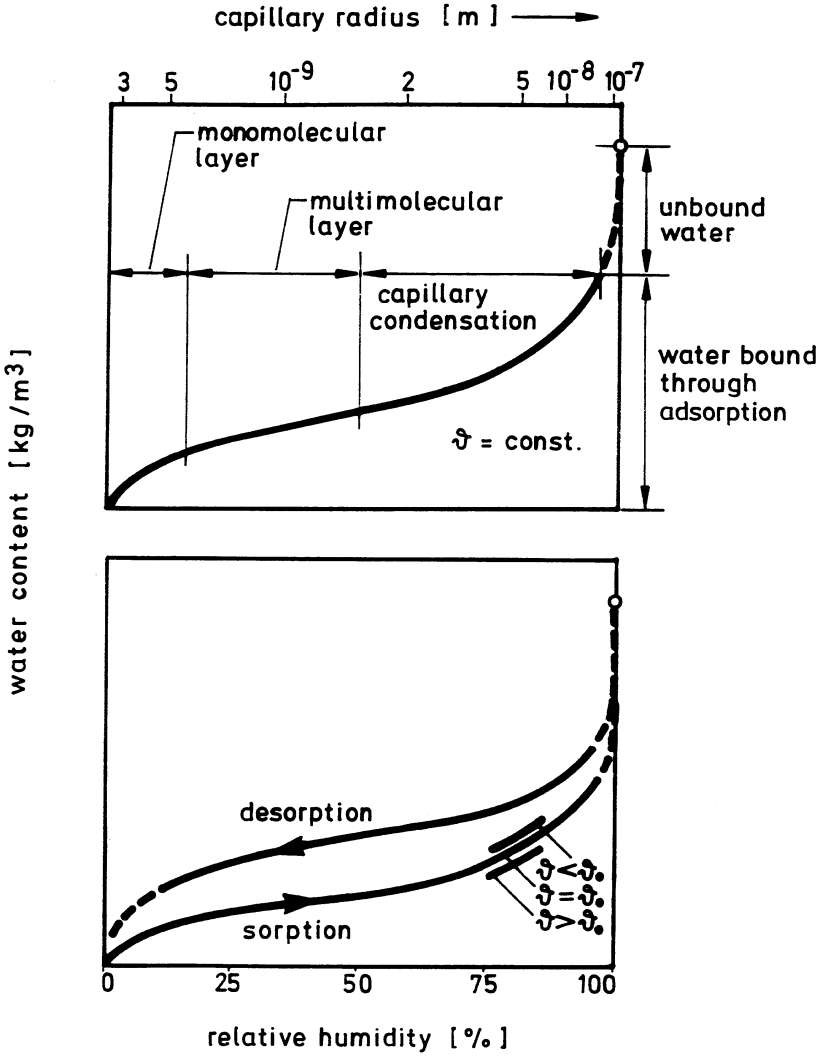

Fig. 3 Schematic representation of a typical sorption isotherm for hygroscopic porous building materials [56].
Above: Areas of moisture absorption with indication of approximate pore radii (using cylindrical pore model).
Below: Temperature influence and hysteresis effect between moisture absorption and desorption

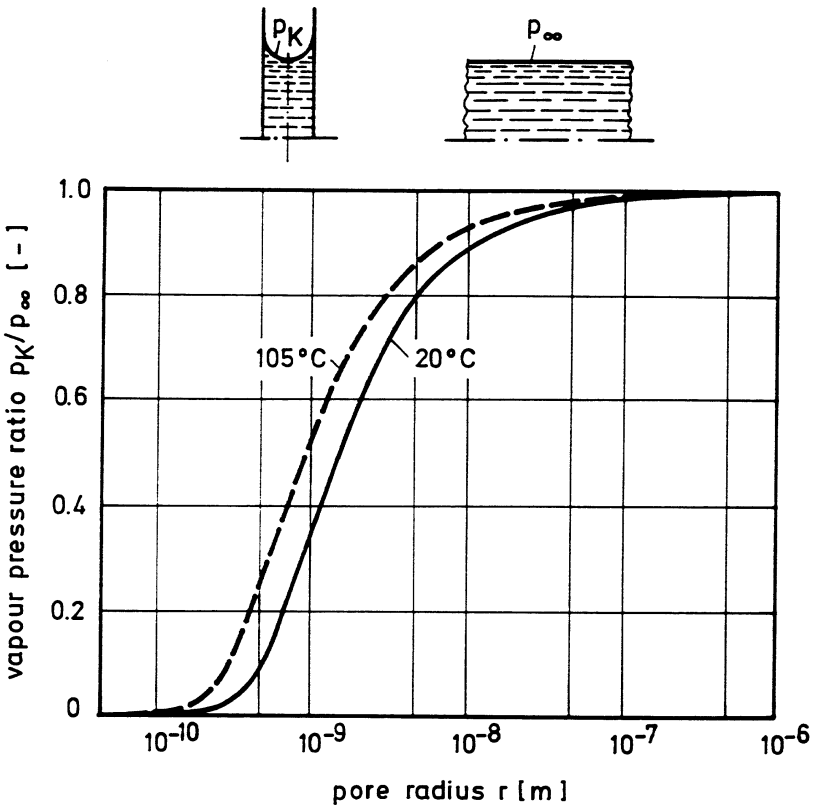

Fig. 4 Ratio of saturation vapour pressure over a curved water surface (meniscus) to that over a flat water surface as a function of capillary radius. Wetting angle $\theta = 0$ assumed [56].
p_k: vapour pressure over a meniscus having a radius of curvature p_k
$p\infty$: vapour pressure over a water surface having a radius of curvature $p_{k\to\infty}$

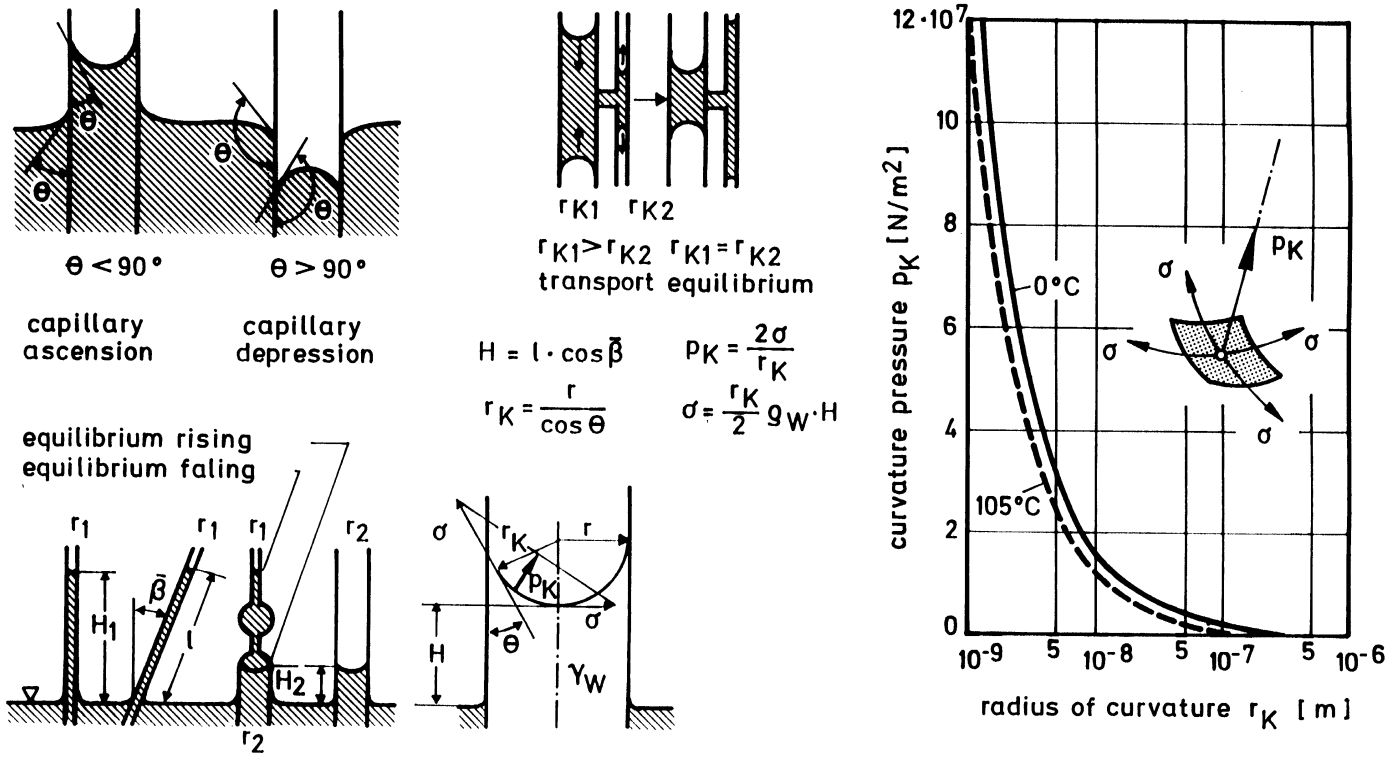

Fig.5 Compilation of the principal capillary phenomena for simple cyndrical capillaries [55]

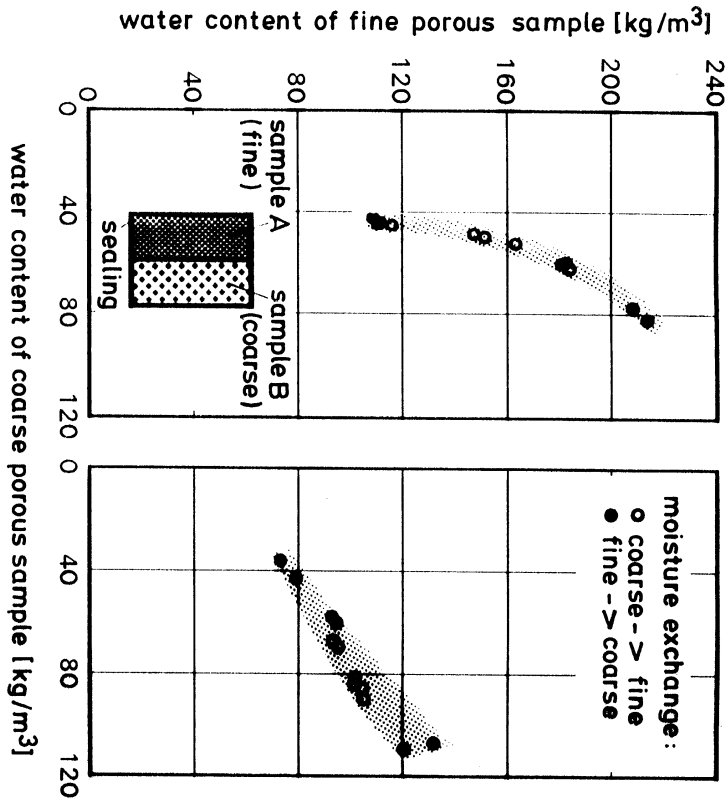

Fig. 6 Superhygroscopic equilibrium moisture content to two building materials in capillary contact (coarse and fine pored sandstones having large (left) and small (right) differences in porosity (from [87]).
The initial water contents of the specimens were chosen in such a way that in each case one half of the coarse-pored reference specimen reached equilibrium water content through absorption of moisture and the other half through release of moisture. The narrow areas (shaded) showing location of the states of equilibrium, independent of the initial moisture situation, suggest an insignificant hysteresis in capillary moisture exchance in natural sandstones. The shaded area indicates the spread recorded in the measurements.

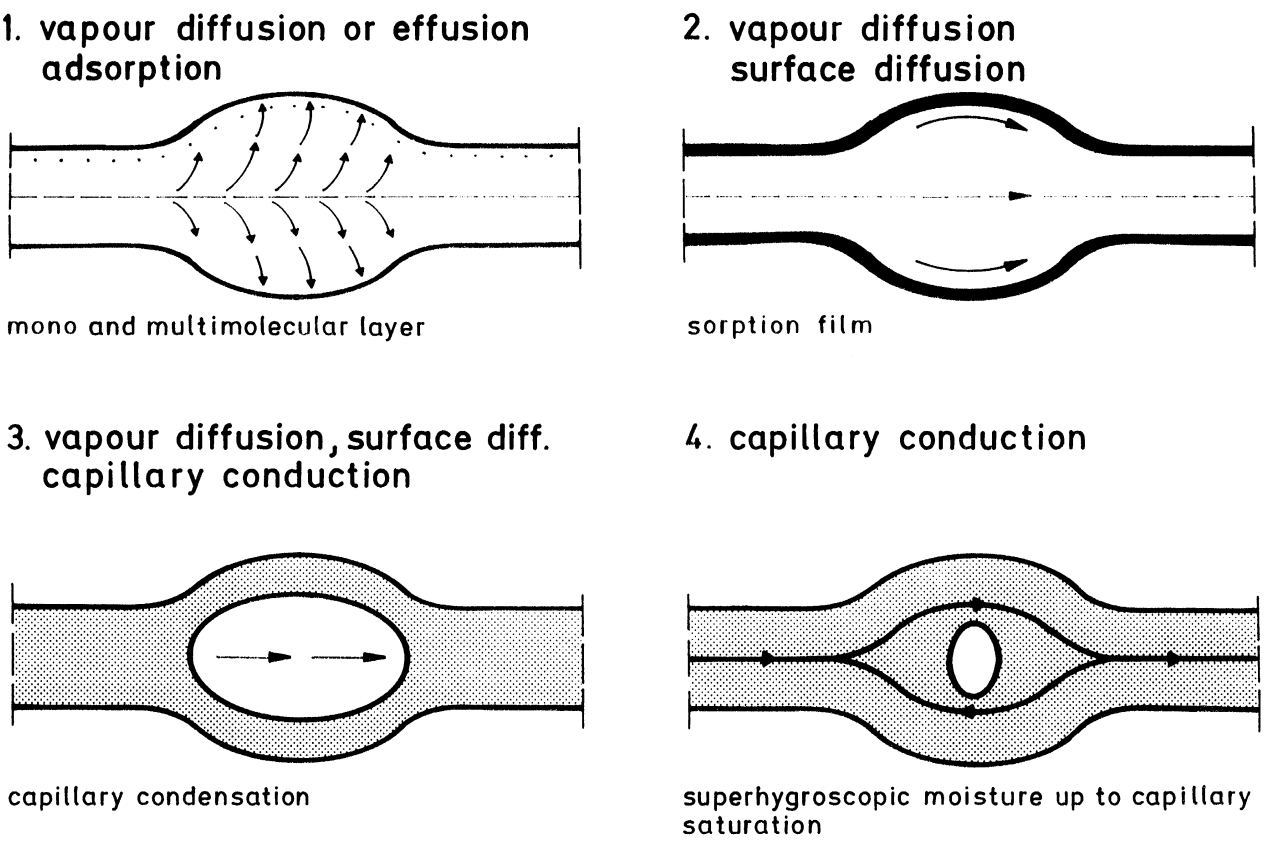

Fig. 8 Transport phenomena occurring at various moisture contents, shown for the model of a cylindrical capillary of varying diameter, modified after [118].

Fig. 7 Schematic overview of the moisture transport phenomena in porous mineral building materials (modified after [56]). The transport phenomena highlighted by shading are investigated in this work.

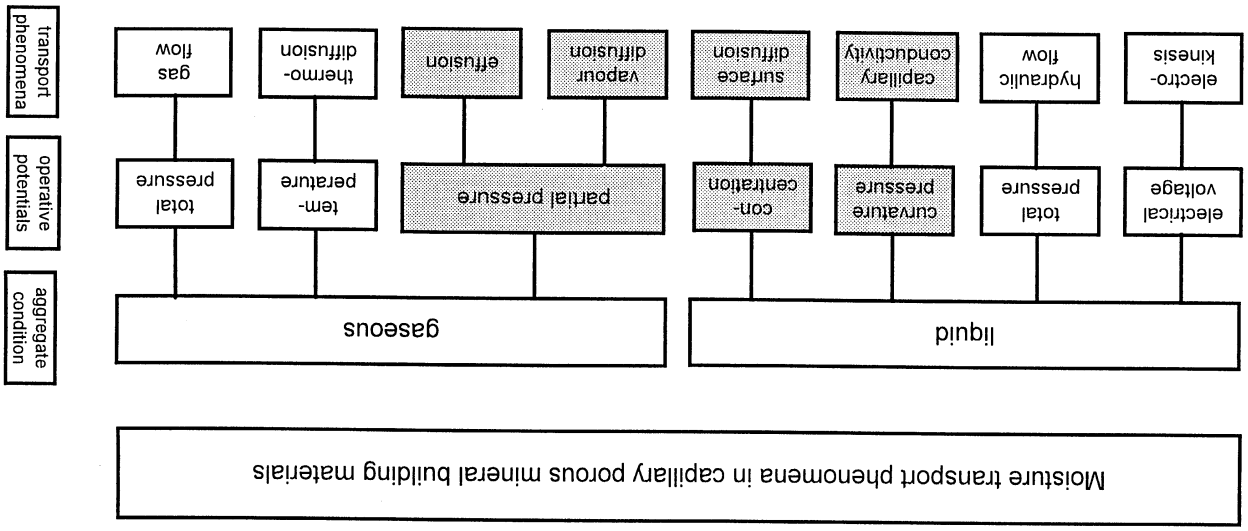

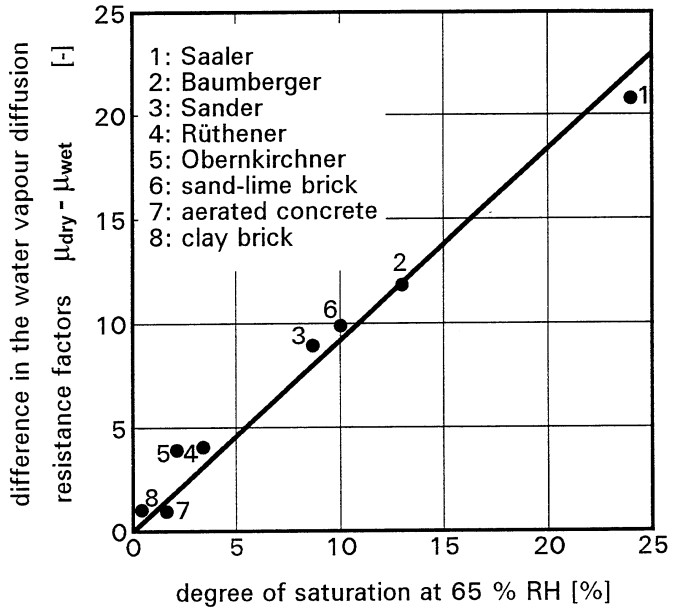

Fig. 9 Differences in the water vapour diffusion resistance factors of various natural sandstones and building materials as a function of sorption-related degree of saturation at 65% RH determined under DIN 52 615 [26] in the dry region (μ_{dry}) and in the moist region (μ_{wet}) respectively.

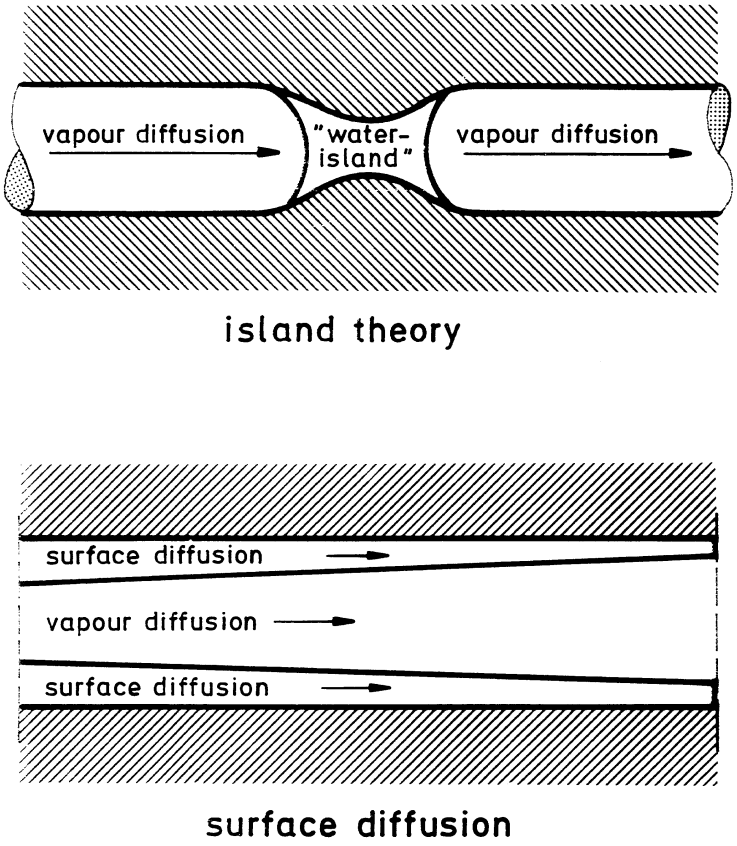

Fig. 10 Model explaining the rise in water vapour permeability observed in hygroscopic building materials with increasing moisture content.
Top: island theory - the water islands act as a short circuit for vapour transport (from [106]).
Bottom: surface diffusion is superimposed on a vapour diffusion (from [119]).

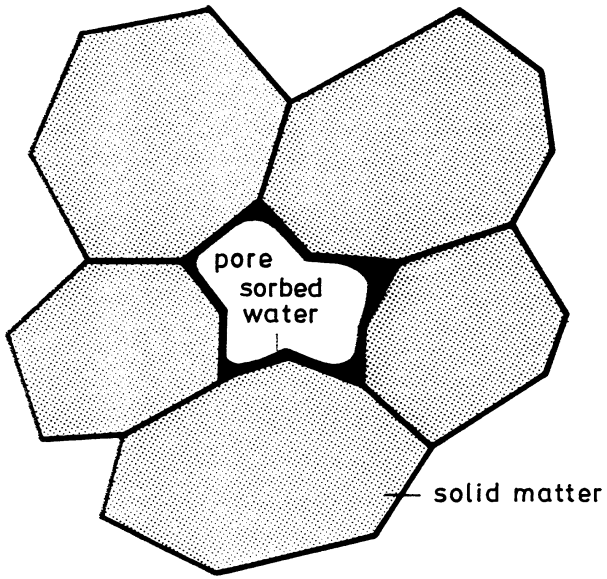

Fig. 11 Pore model with sorbate film and gusset water absorbed through sorption. In contrast to the thin sorbate film on the flat pore surfaces, the thickness of the layer of water in the pore space gussets is large enough to permit moisture transport

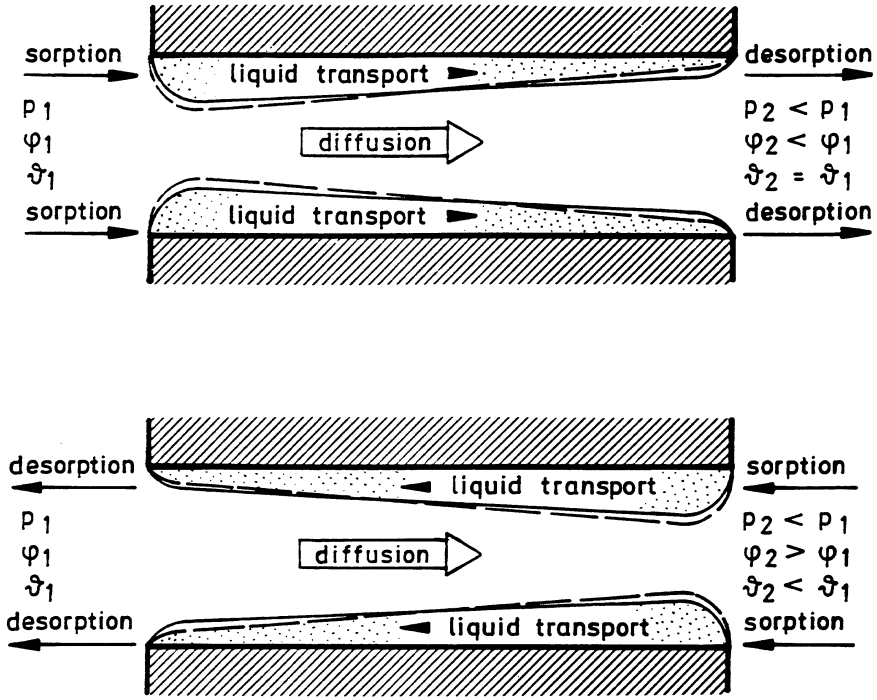

Fig. 12 Model for superimposed liquid and vapour transport in the pore space of hygroscopic building materials under isothermic (top) and non-isothermic (bottom) conditions. The dashed line represents the sorption moisture equilibrium wich would develop without liquid transport in the sorbed phase. The solid line shows the dynamic equilibrium established as a result of liquid transport. Liquid mass flow is maintained by sorption on the side of higher atmospheric humidities and desorption on the side of lower atmospheric humidities.

p_1, p_2 water vapour partial pressure on both sides
φ_1, φ_2 relative humidity on both sides
δ_1, δ_2 air temperature on both sides

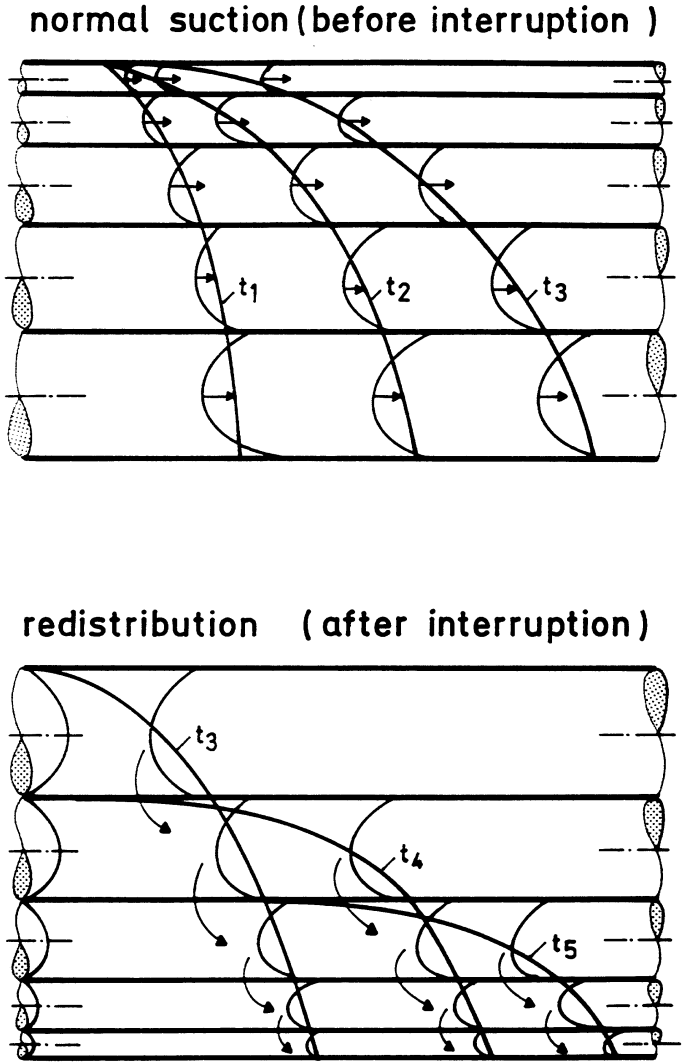

Fig. 13 Capillary transport phenomena depicted for the model of cylindrical capillaries of varying diameter in contact with one another.
Above: Due to lower flow resistance the larger capillaries draw at a higher rate. A continuous moisture distribution develops in the direction of suction.
Below: Following interruption of the water supply there is subsequent liquid distribution or dispersion. Smaller capillaries not yet filled suck dry the larger capillaries because of their greater drawing power.

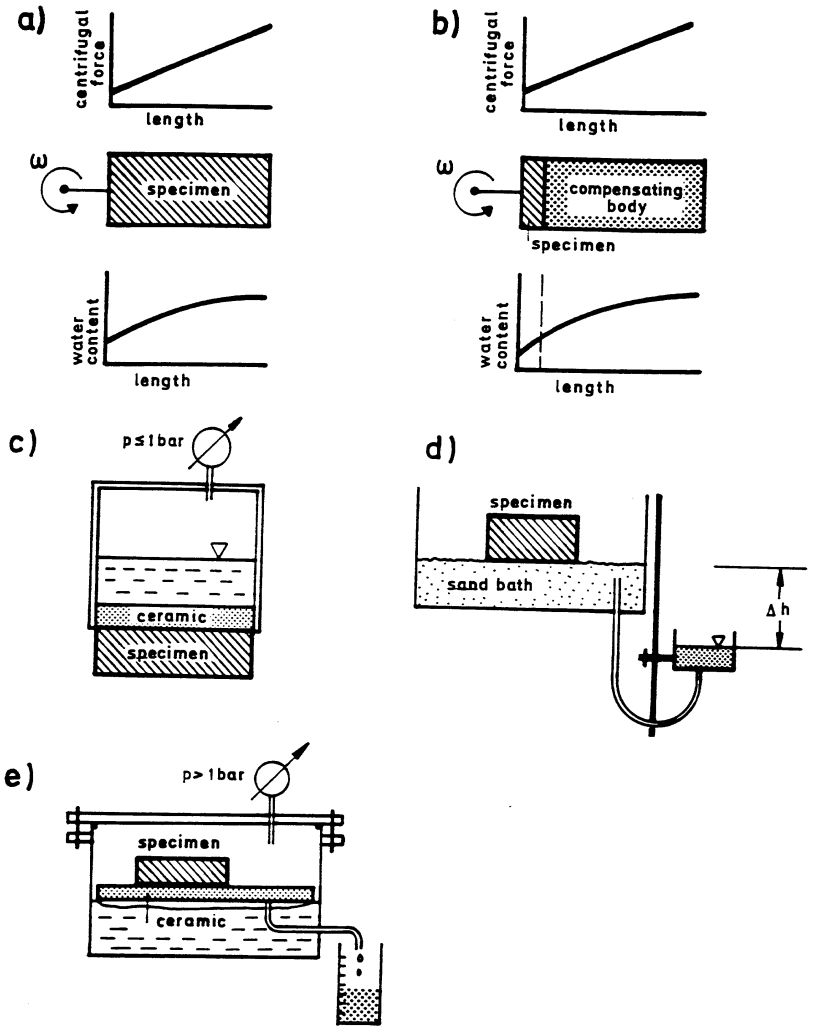

Fig. 14 Various methods of determining suction pressure.
a) centrifuge method: centrifugal forces are used to expel water from the specimen. A water content distribution corresponding to the centrifugal forces distribution is set up in the specimen.
b) centrifuging with compensating body: use of a very short specimen makes it possible to ignore the water content gradient in the specimen.
c) tensiometer: the specimen draws water from the sealed waterfilled container through the saturated ceramic until a suction pressure equilibrium develops from the resulting vacuum.
d) sand bath: lowering of the water level creates a hydrostatic underpressure
e) pressure plate apparatus: moisture is removed from the specimen by application of an overpressure.

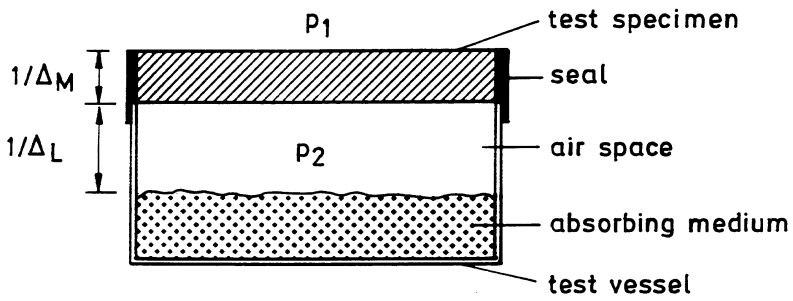

Fig. 15 Test set-up for measurement of water vapour permeability (schematic).

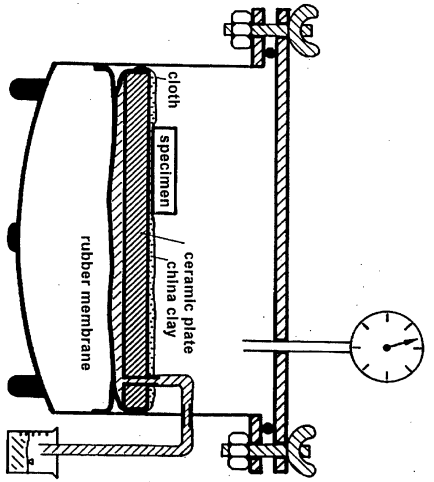

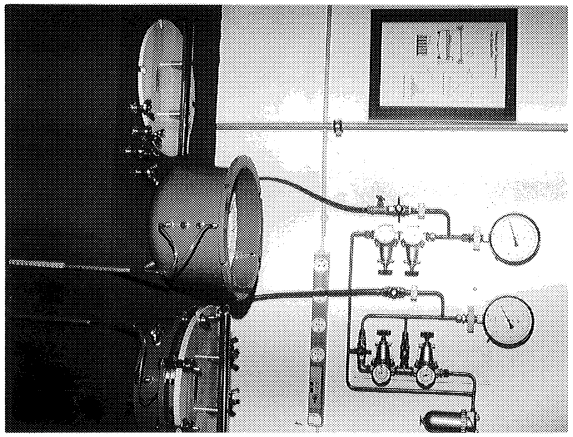

Fig. 16 Schematic layout of a pressure vessel in the suction pressure test unit (left) and a photographic view of the test equipment (right).

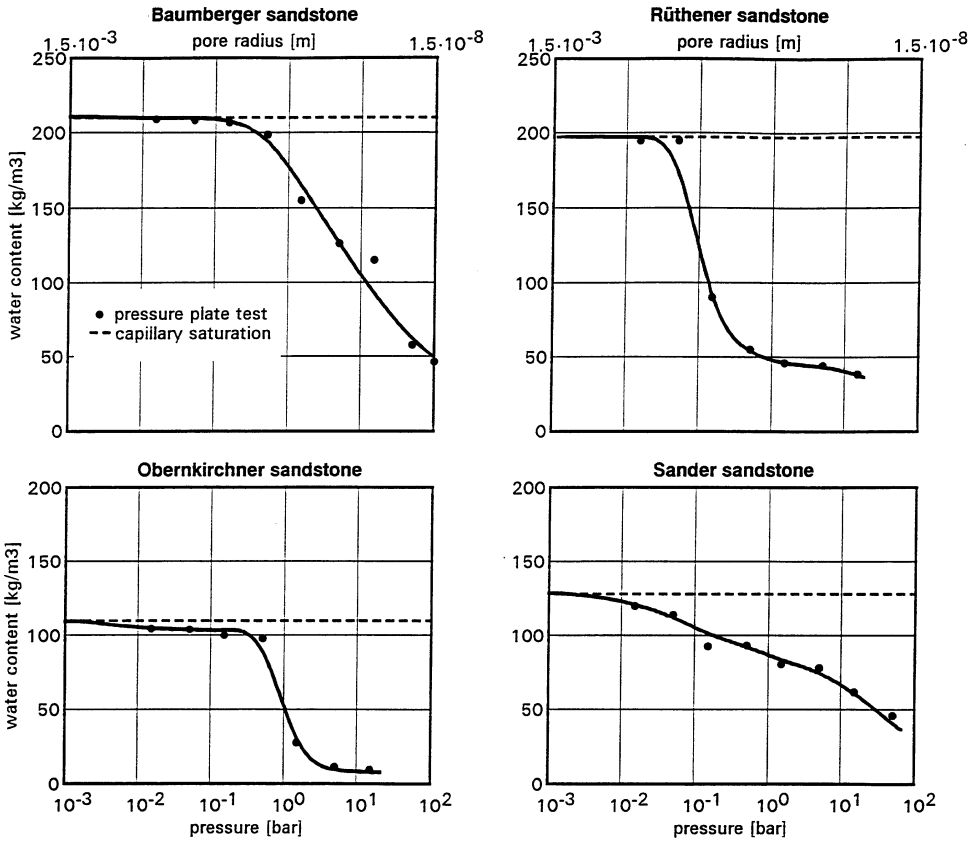

Fig. 17 Capillary pressure curve of Baumberger sandstone (top left) of Obernkirchner sandstone (bottom left), Rüthener sandstone (top right) and Sander sandstone (bottom right). Plotted as a second abscissa is the pore radius corresponding to the applied pressure.

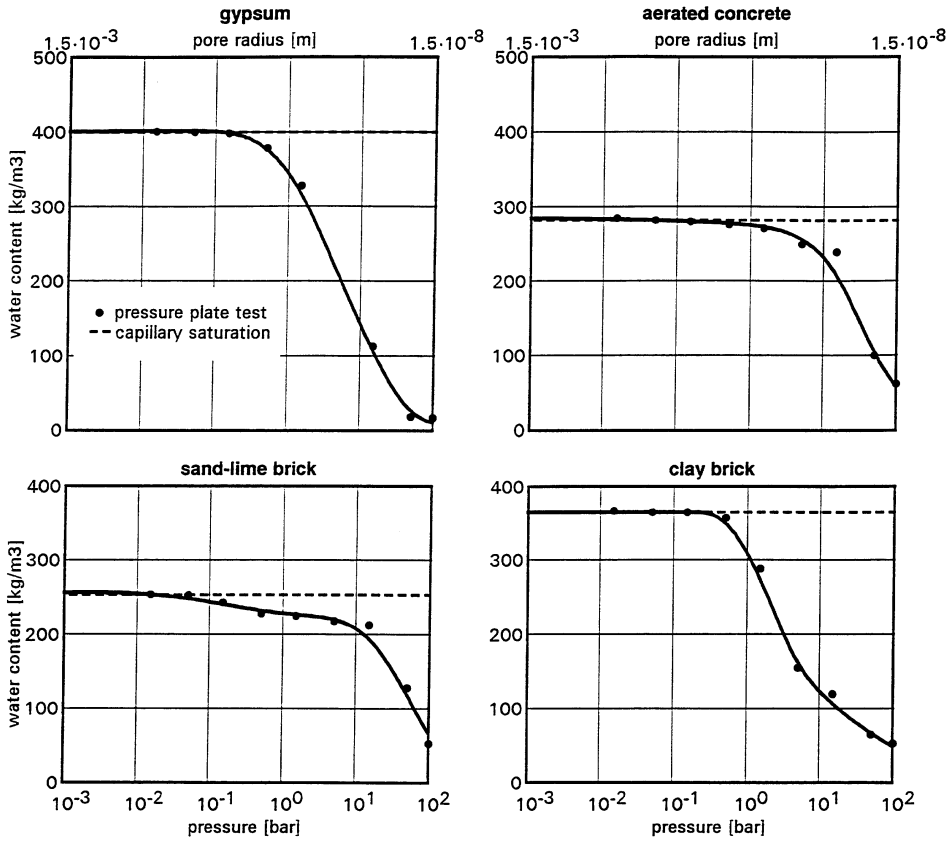

Fig. 18 Suction pressure curve for gypsum board (top left), sandlime brick (bottom left), aerated concrete (top right) and clay brick (bottom right). Plotted as a second abscissa is the pore radius corresponding to the applied pressure.

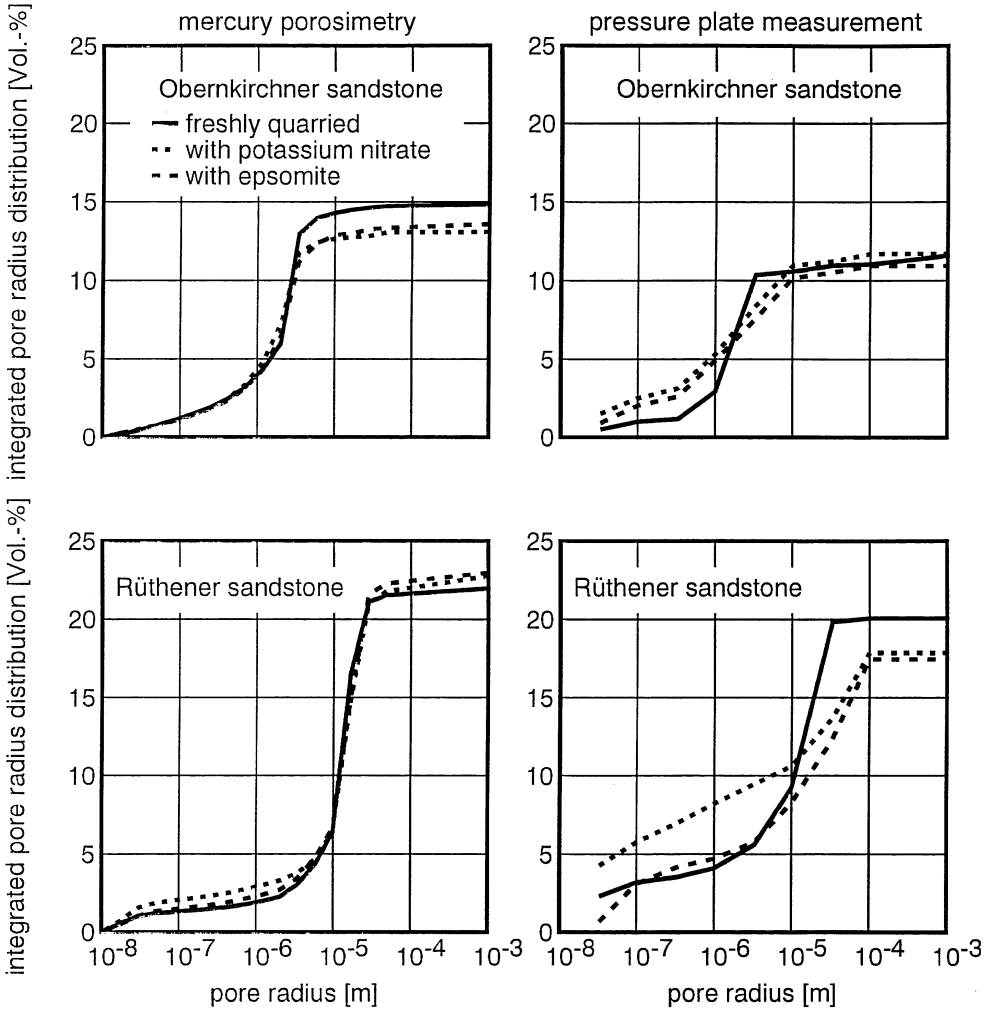

Fig. 19 Integrated pore radius distribution of freshly quarried and salt impregnated Obernkirchner and Rüthener sandstone measured using mercury porosimetry and the pressure plate equipment.

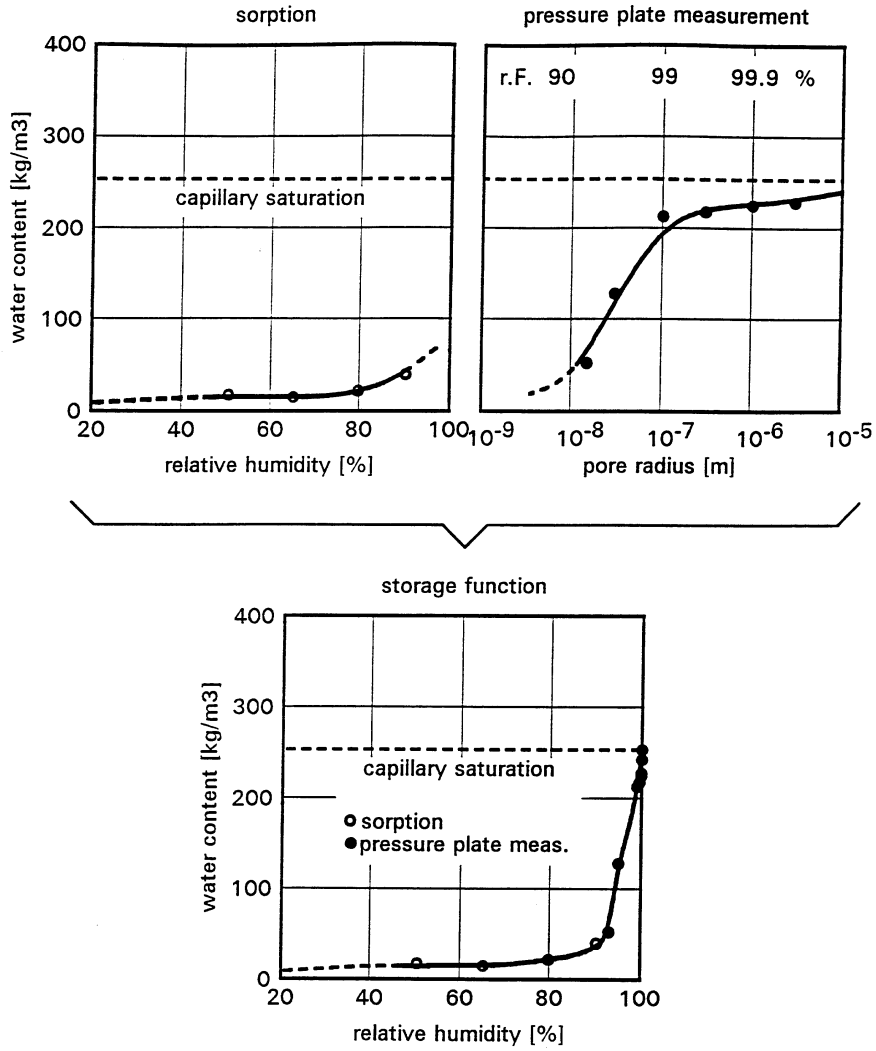

Fig. 20 Development of a storage function for the hygroscopic and superhygroscopic region from the sorption isotherm (top left) and the recorded suction pressure curve (top right) using sand-lime brick as an example.

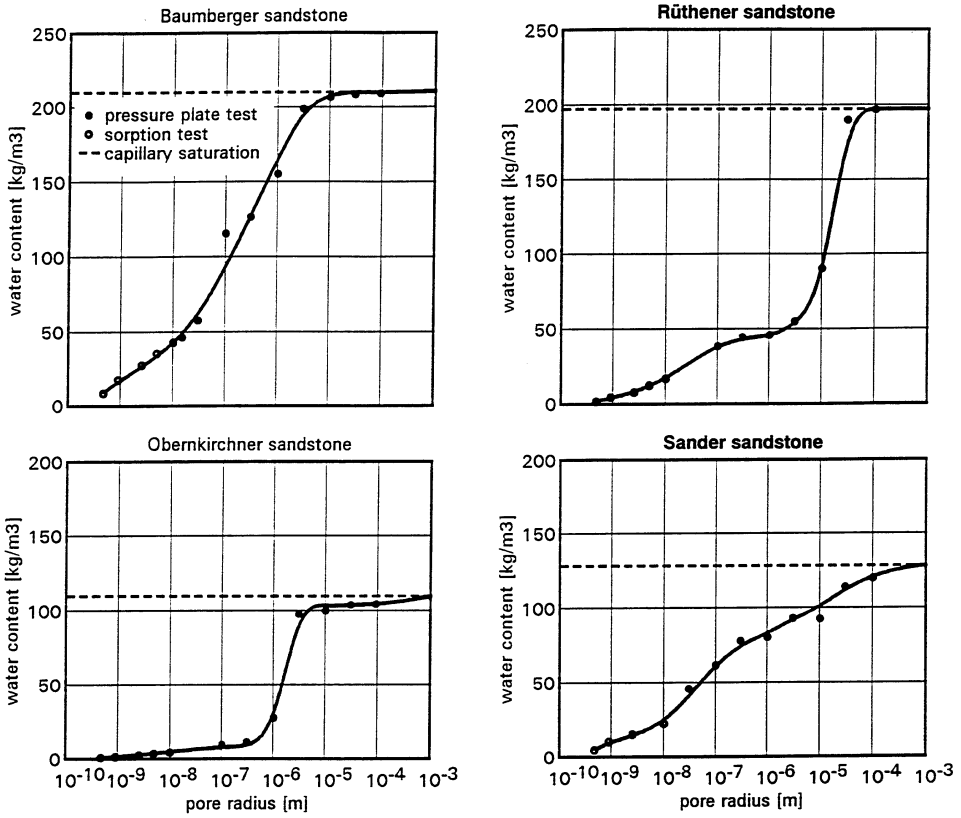

Fig. 21 Moisture storage function of Baumberger sandstone (top left), of Obernkirchner sandstone (bottom left), Rüthener sandstone (top right) and Sander sandstone (bottom right), developed from the sorption isotherm and the recorded suction pressure curve.

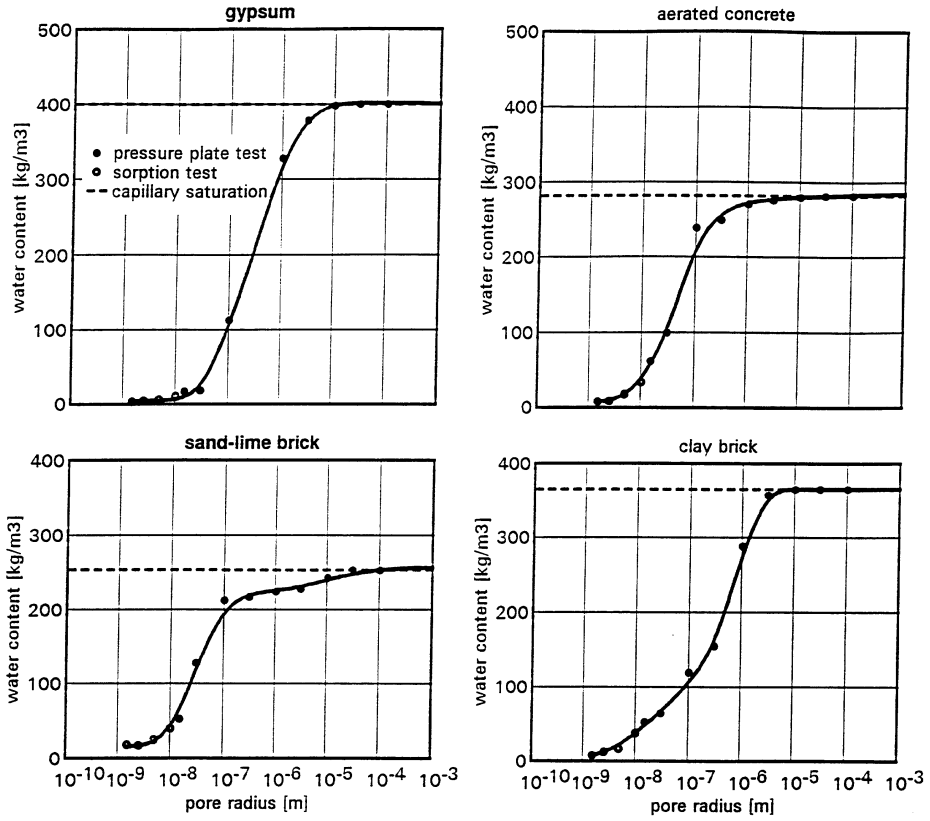

Fig. 22 Moisture storage function of gypsum wallboard (top left), sand-lime brick (bottom left), aerated concrete (top right) and clay brick (bottom right), developed from the sorption isotherm and the recorded suction pressure curve.

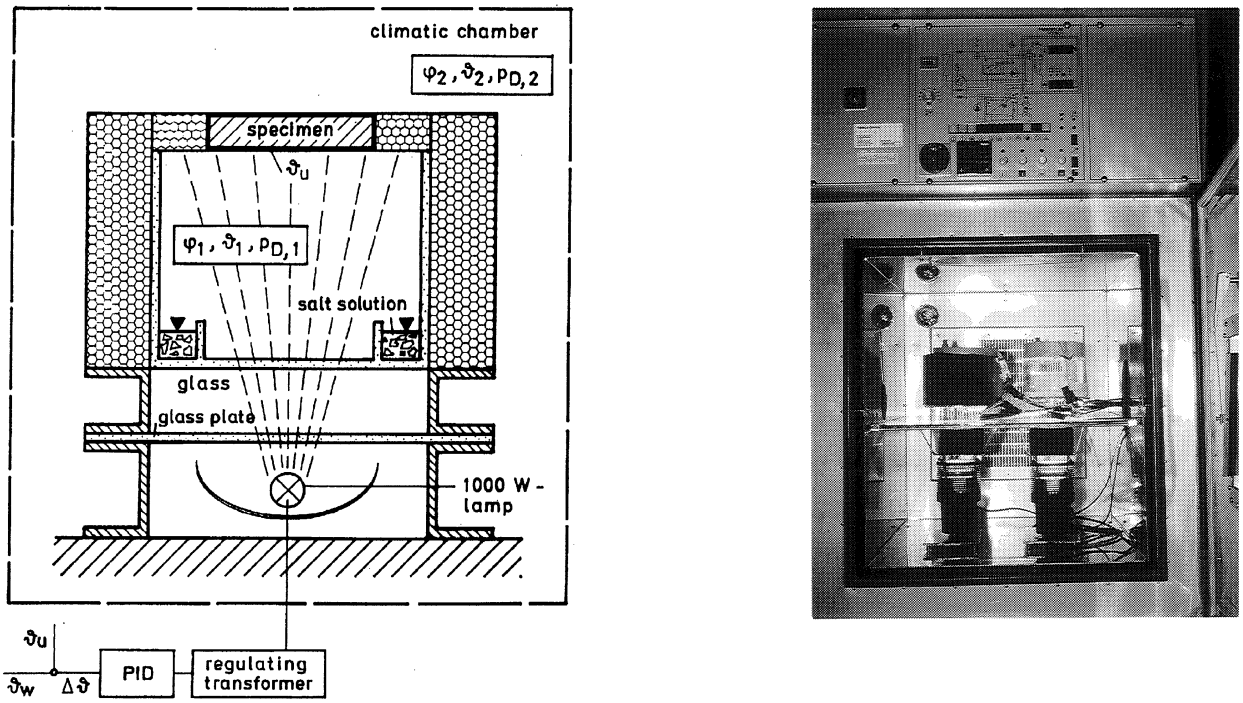

Fig. 23 Schematic layout of the test rig (left) and a photographic view of the system (right) for determining the vapour permeability of building materials under vapour pressure and temperature gradients. In the vessel on the right the insulation on the side has been removed

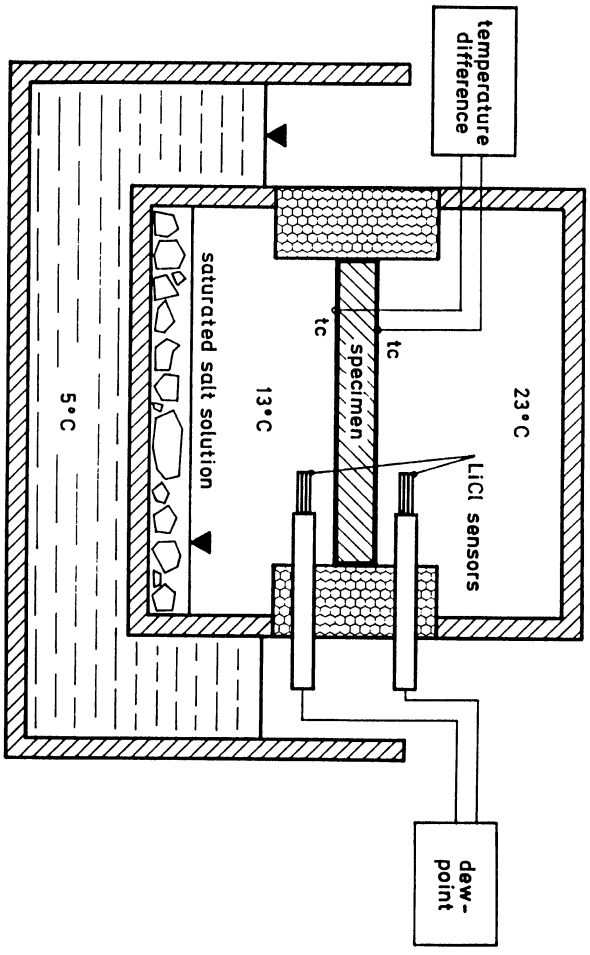

Fig. 24 Schematic layout of the test rig for determining the partial pressure equilibrium established when a temperature gradient develops between the upper side and the underside of the specimen.

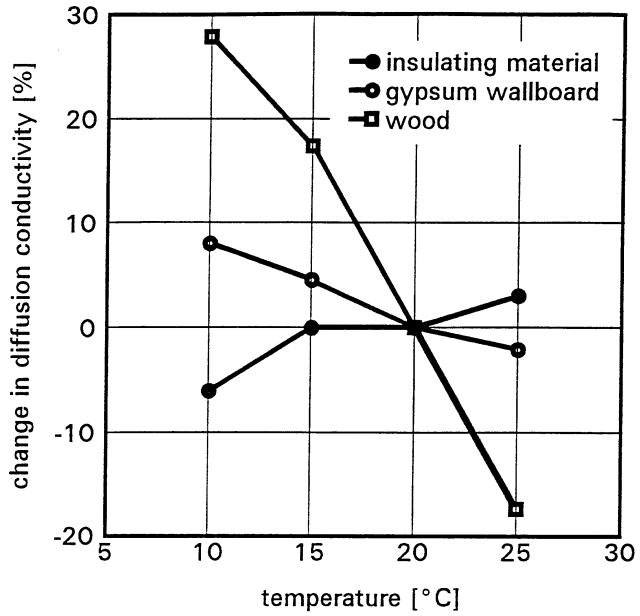

Fig. 25 Percentage change in the diffusion conductivity of various building materials as a function of measuring temperature (from [90]) relative to the test value at 20°C. When the measurements were taken there was an atmospheric humidity gradient from 60% to 93% RH over the specimen section.

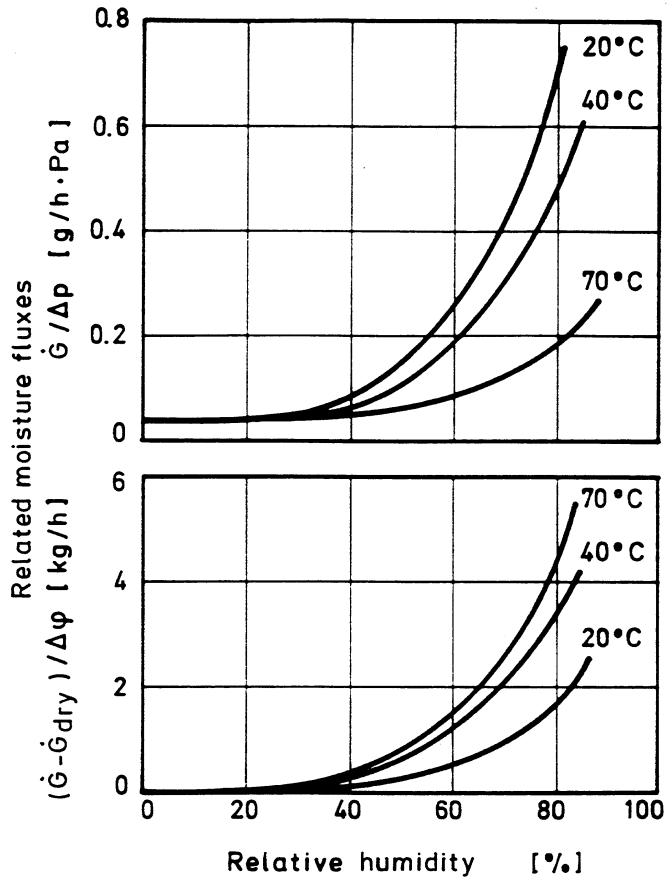

Fig. 26 Relative moisture flow M through a paper membrane [122] as a function of average relative humidity φ and ambient temperature.
If mass flow is related to vapour pressure difference Δp (top), it declines with increasing temperature contrary to the laws of gas diffusion. If the moisture-dependent increase in mass flows (moisture flow M minus moisture flow under dry conditions M_{dr}) is related to relative humidity (bottom), temperature-dependence is in conformity with the laws of physics.

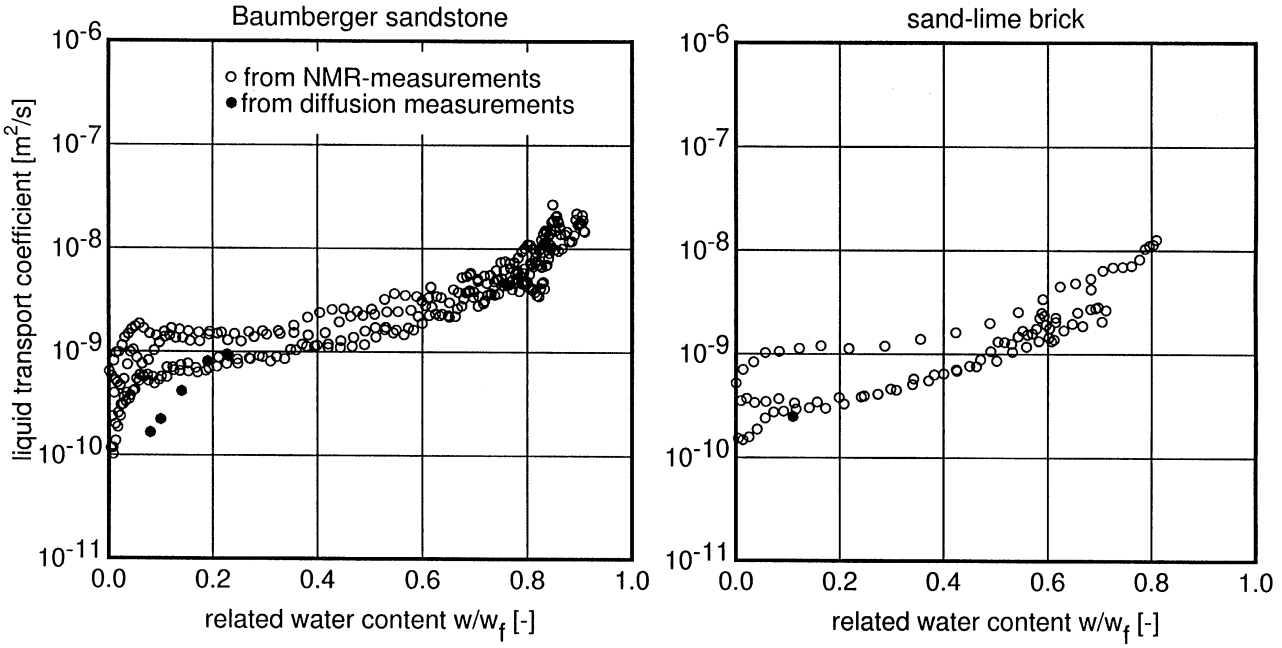

Fig. 28 Function of the transport coefficient for liquid water redistribution determined from moisture profile recordings using the NMR unit. Also shown are values for the coefficients in the hygroscopic moisture region calculated from moisture-dependent diffusion measurements.

Fig. 27 Annual profiles for dew-point temperatures of the air inside and outside an unheated church (St. Leonhardt, Moosberg) and a heated church (Marienstatt convent church)[82]. In the heated church dew-point temperature during the entire heating period is considerably above the dew-point temperature outside the church.

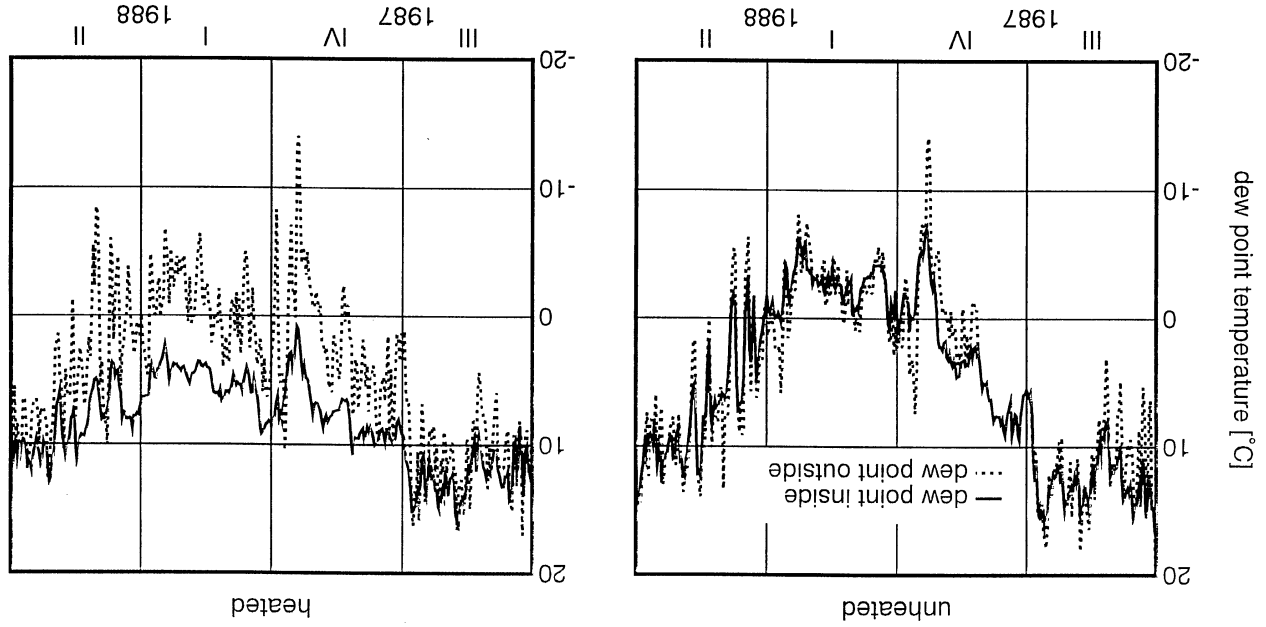

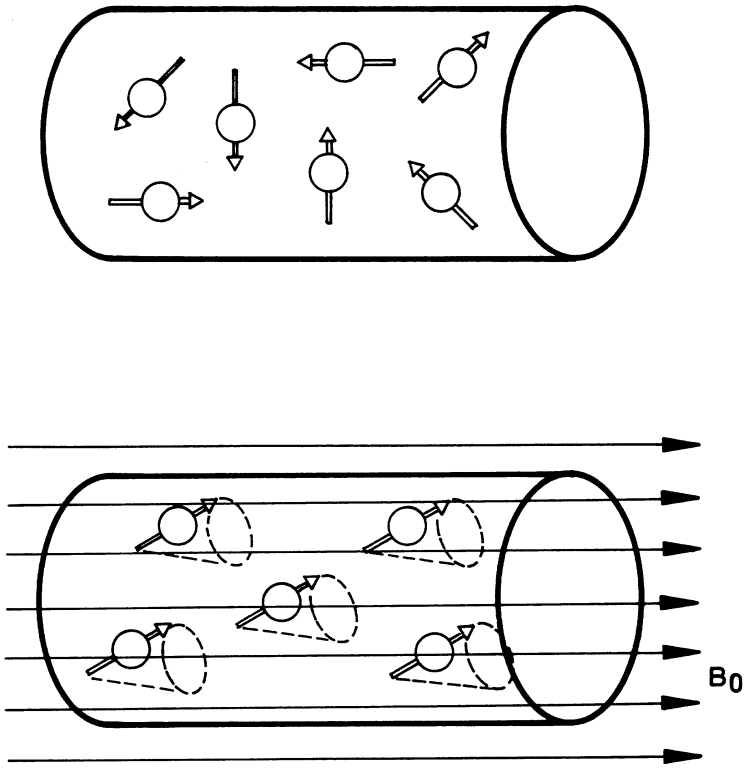

Fig. 29 Orientation of the magnetic dipole moments.

Top: In the absence of an external magnetic field the magnetic dipoles point in any given direction.
Bottom: When an external magnetic field B_0 is applied, the dipoles align themselves; they precess in a cone-shaped envelope about the B_0 fields lines.

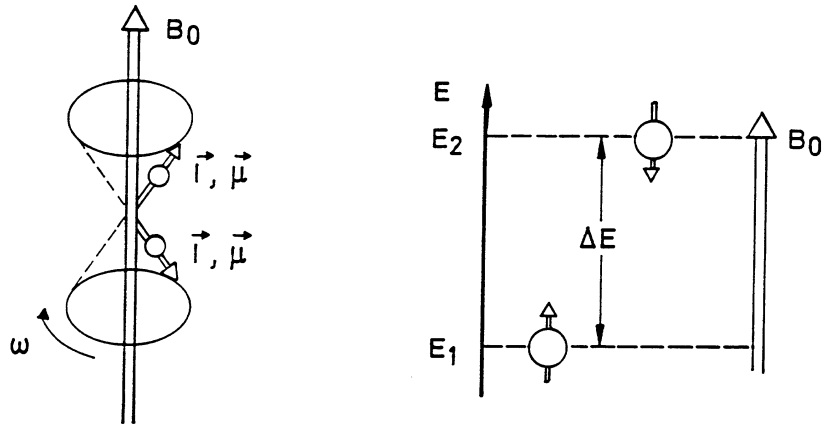

Fig. 30 Two possible orientations of a proton in a magnetic field.

Left: When the nucleii precess in a cone-shaped envelope about the magnetic B0 axis, orientations more parallel or more anti-parallel to the external field are possible.
Bottom: A nucleus dipole moment parallel to the field B_0 means a lower energy content relative to the dipole moment anti-parallel to the applied field. The energy difference ΔE is dependent on the strength of the magnetic field.

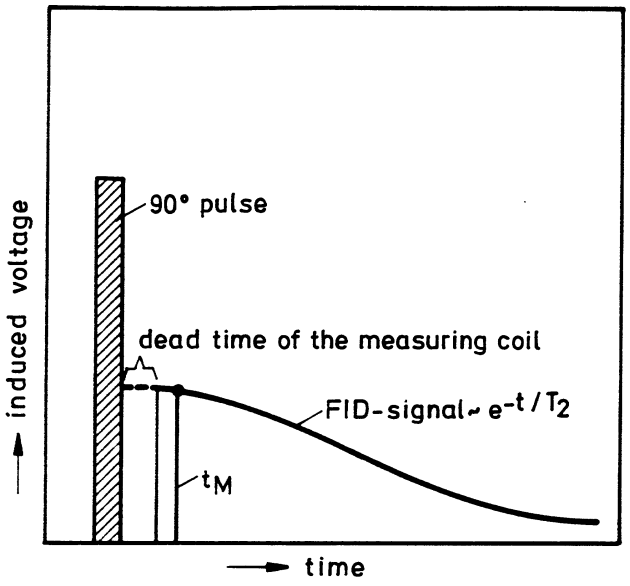

Fig. 31 Typical profile (schematic) of a parallel FID signal (Free induction Decay) following a 90^0 pulse.
T_2 transverse relaxation time
t_m time of signal scan

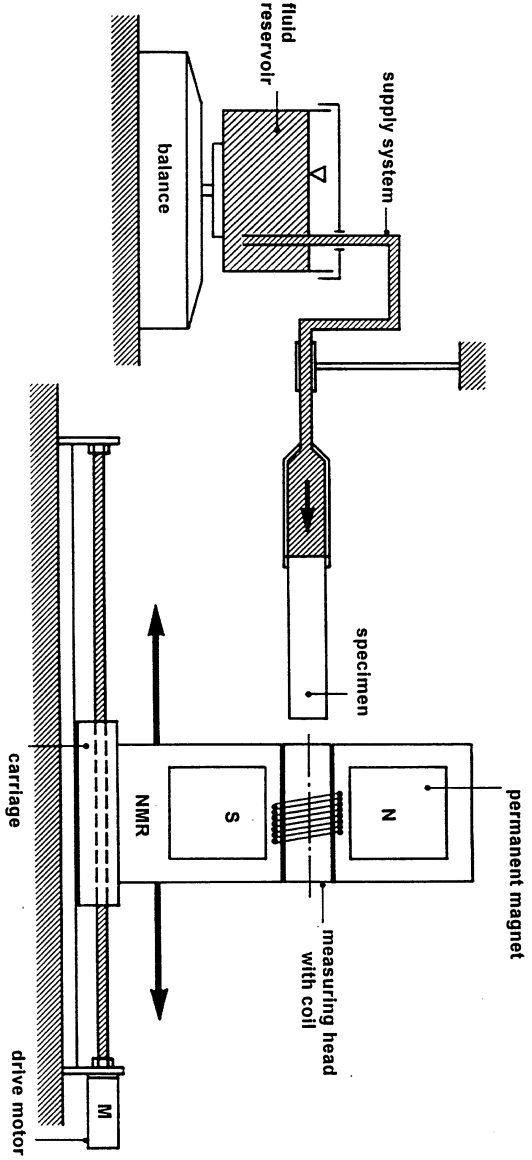

Fig. 32 Schematic layout of the NMR unit for determining liquid distributions in prismatic specimens during capillary liquid absorption

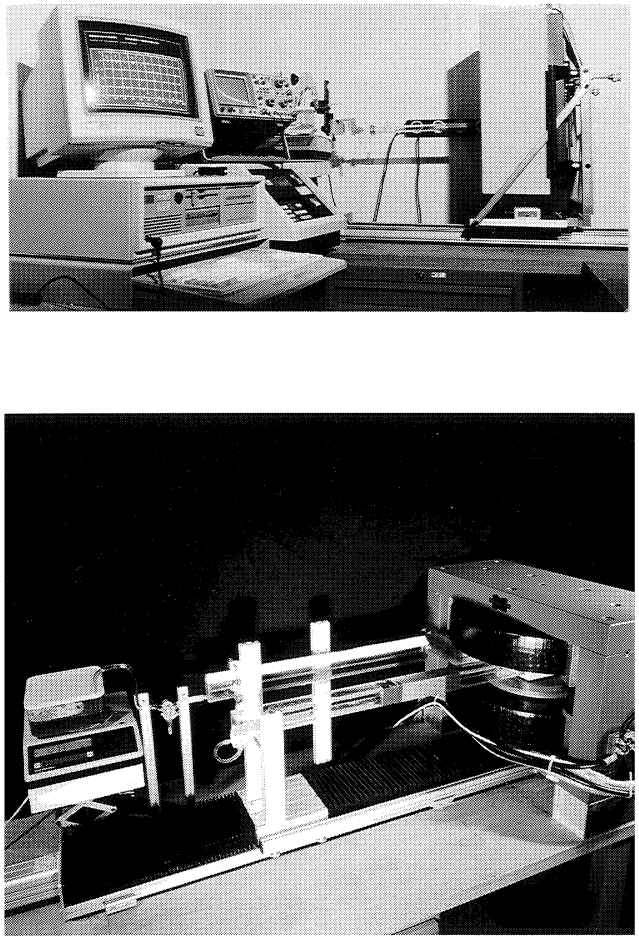

Fig. 33 Photographic view of the „little" NMR unit (above) and the „big" NMR unit (below). Using the two units measurements of liquid distributions can be made in specimens measuring up to 2x2 cm^2 or 5x5 cm^2 in sectional area respectively.

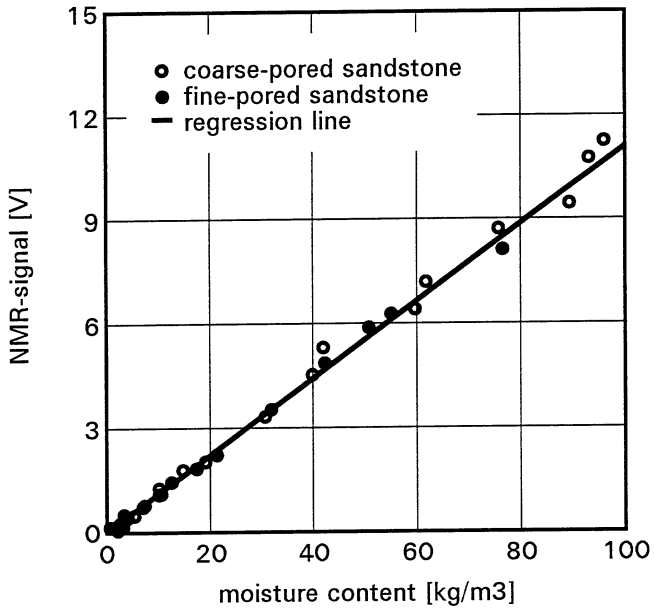

Fig. 34 Relationship between the NMR signal and moisture content. Because NMR ist a direct method of measuring moisture content, the same calibration curve may even be used for widley differing materials (in this case a coarse-pored, less absorbent sandstone and a fine-pored, more absorbent one).

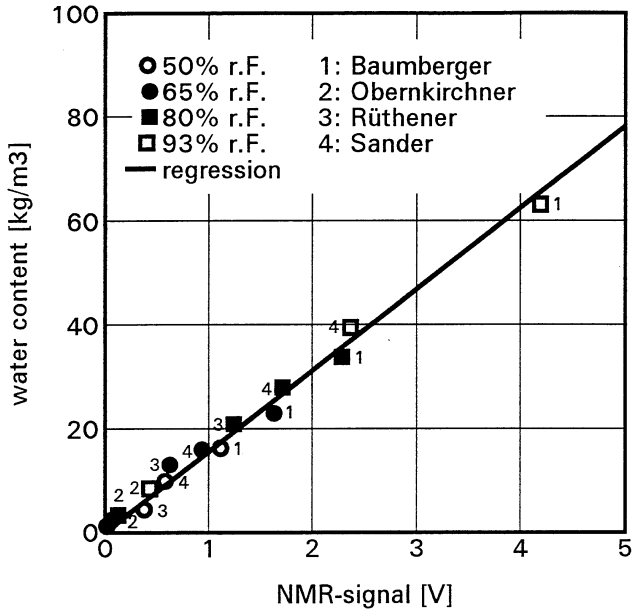

Fig. 35 Comparision of gravimetrically determined water contents and test signals recorded on the same specimens with the NMR unit for different varieties of sandstone in the hygroscopic moisture region. By increasing the number of individual measurements to average, the signal-to-noise ratio can be increased to the point that water content can be determined with an accuracy of better than 0.2% by volume.

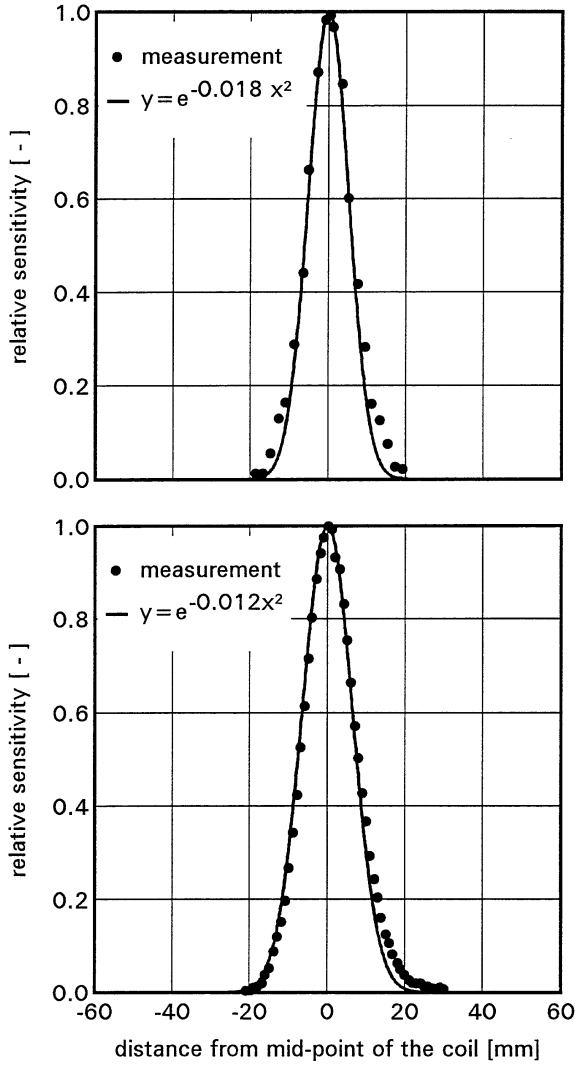

Fig. 36 Local sensivity of the measuring coils used in the NMR units. Local sensivity can be well described with the given Gauss distributions.
Top: „Little“ NMR
Bottom: „Big“ NMR

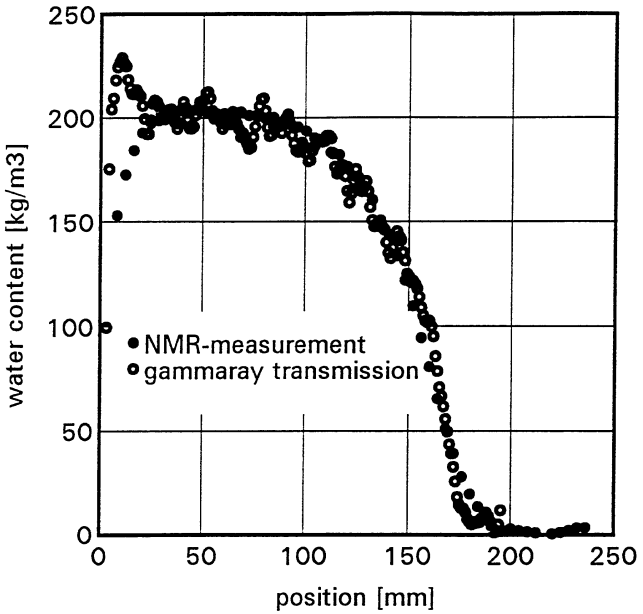

Fig. 37 Comparison of measuring water content distribution using gamma testing and magnetic nuclear resonance. The measurements were carried out on the same specimen after an absorption time of several hours, one immediately after the other. Although the gamma testing unit used achieves a significantly higher local resolution of only one millimeter, the two measuring methods reproduce the water content gradients approximately the same.

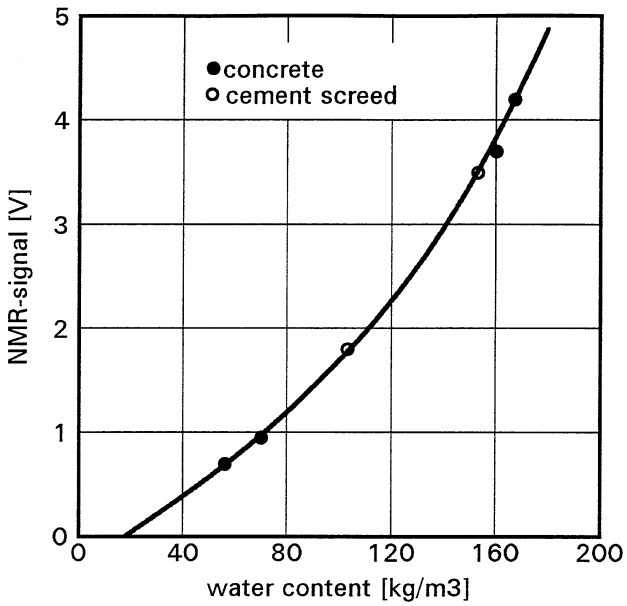

Fig. 38 Comparison of water contents determined gravimetrically and using the NMR test unit on specimens of concrete and cement screed. In the extremely small gel pores relaxation time is so low that it falls within the dead time of the measuring coil. As a result the water content of these gel pores ist not recorded or only recorded to some degree, which is why the calibration curve for materials of this kind does not pass through the starting point of the coordinate system.

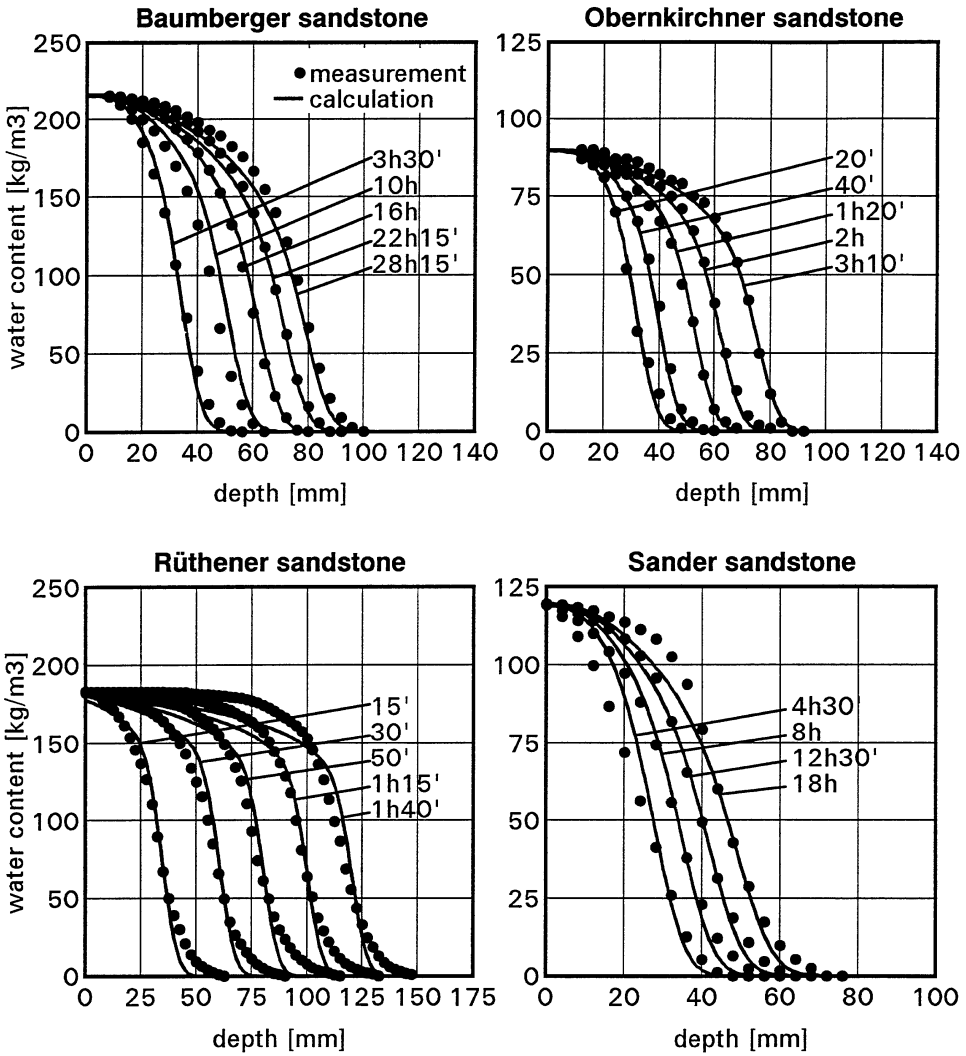

Fig. 39 Water content distributions over the depth of various natural stone specimens at different points in the time using NMR measurements resp. calculation results of the absorption process. The distributions depicted by a solid line were calculated using an exponential approximation.

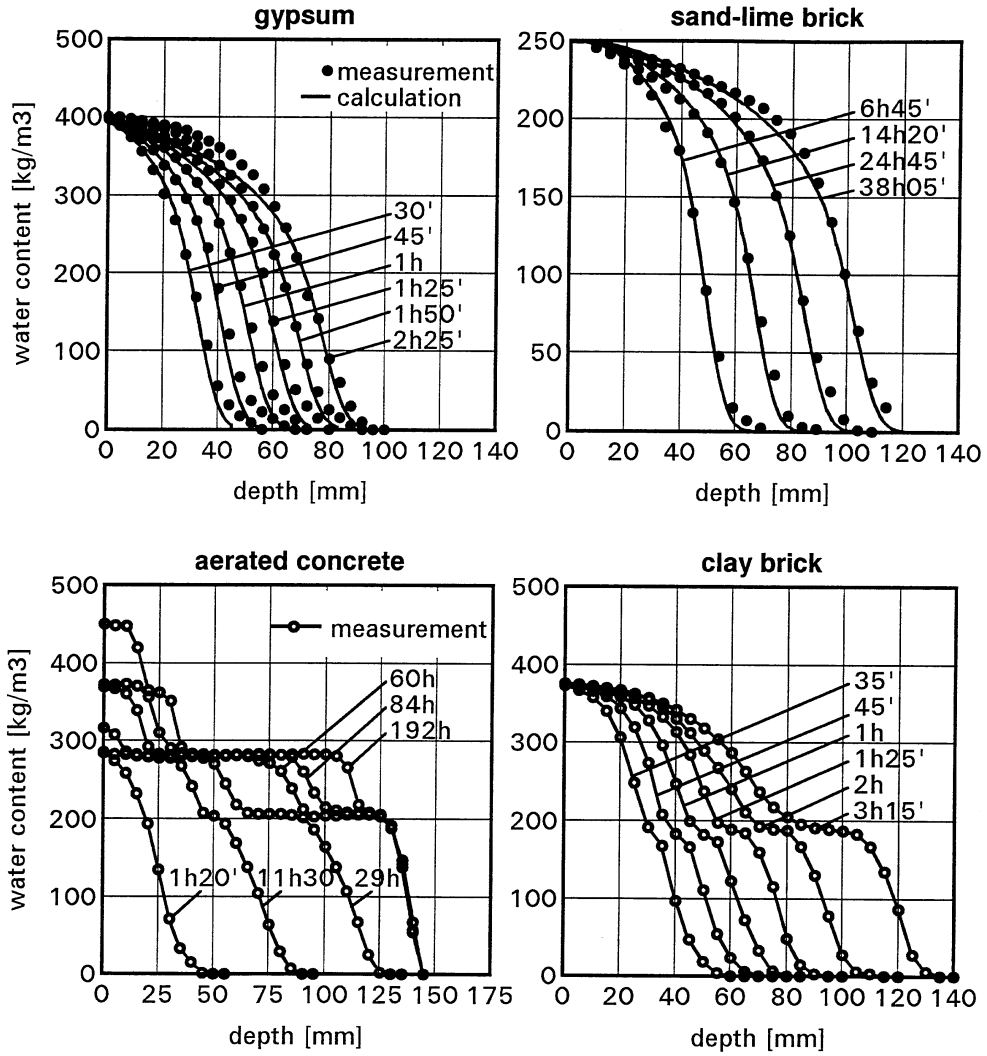

Fig. 40 Water content distribution over the depth of various building material specimens at different times using NMR measurements resp. calculation results of the absorption process. The distributions shown in the two upper diagrams as solid lines were calculated using an exponential approximation. To better see the profiles measured, the test points are connected by lines in the two lower diagrams.

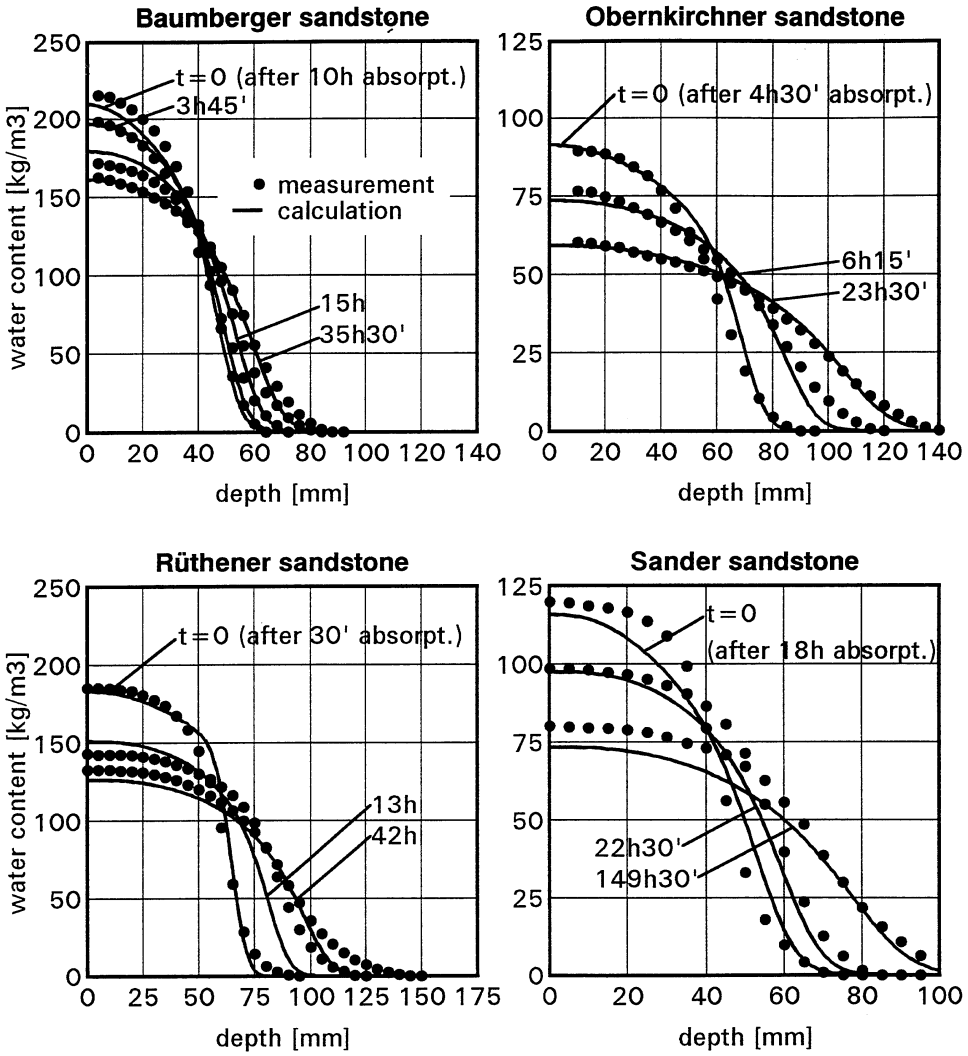

Fig. 41 Water content distributions over the depth of various natural stone specimens at different points in the time for liquid water redistribution using NMR measurements resp. calculation results. The distributions depicted by a solid line were calculated using an exponential approximation.

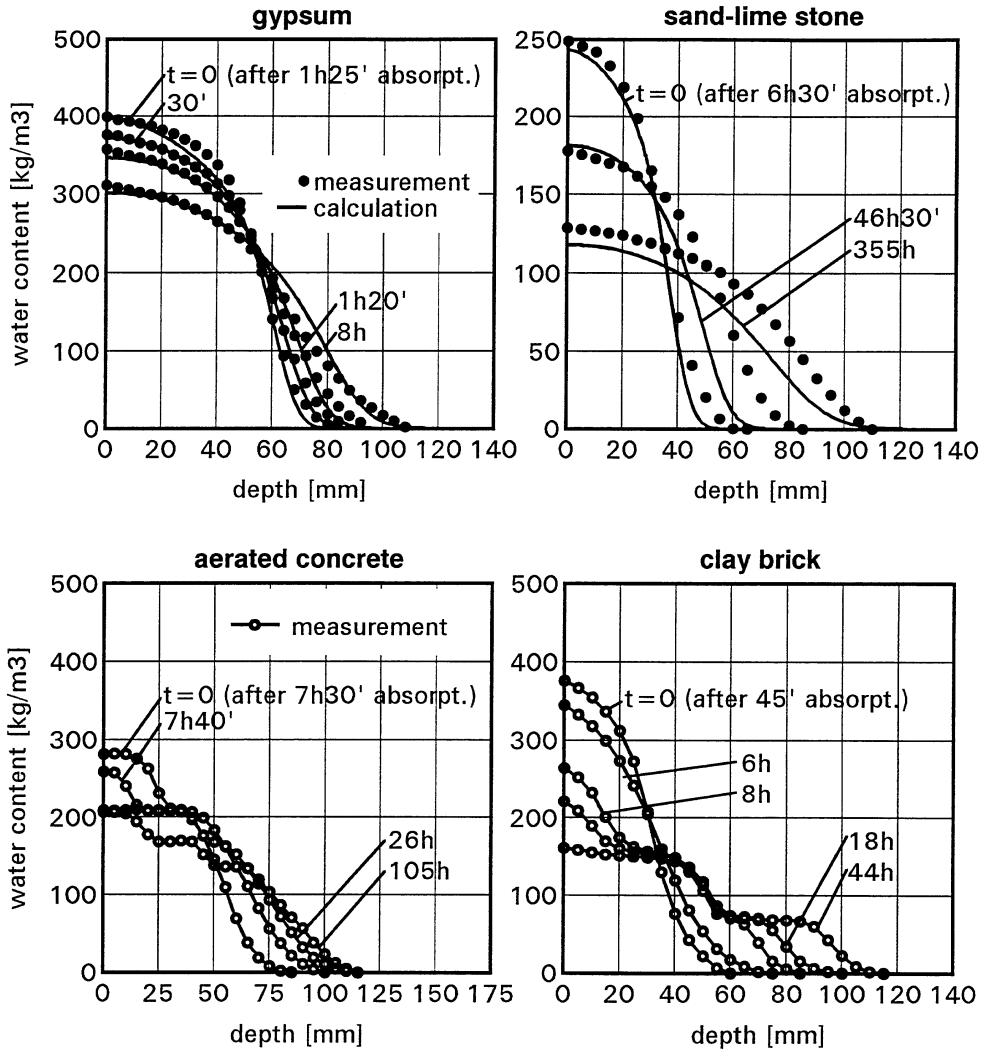

Fig. 42 Water content distribution over the depth of various building material specimens at different times for liquid water redistribution using NMR measurements resp. calculation results. The distributions shown in the two upper diagrams as solid lines were calculated using an exponential approximation. To better see the profiles measured, the test points are connected by lines in the two lower diagrams.

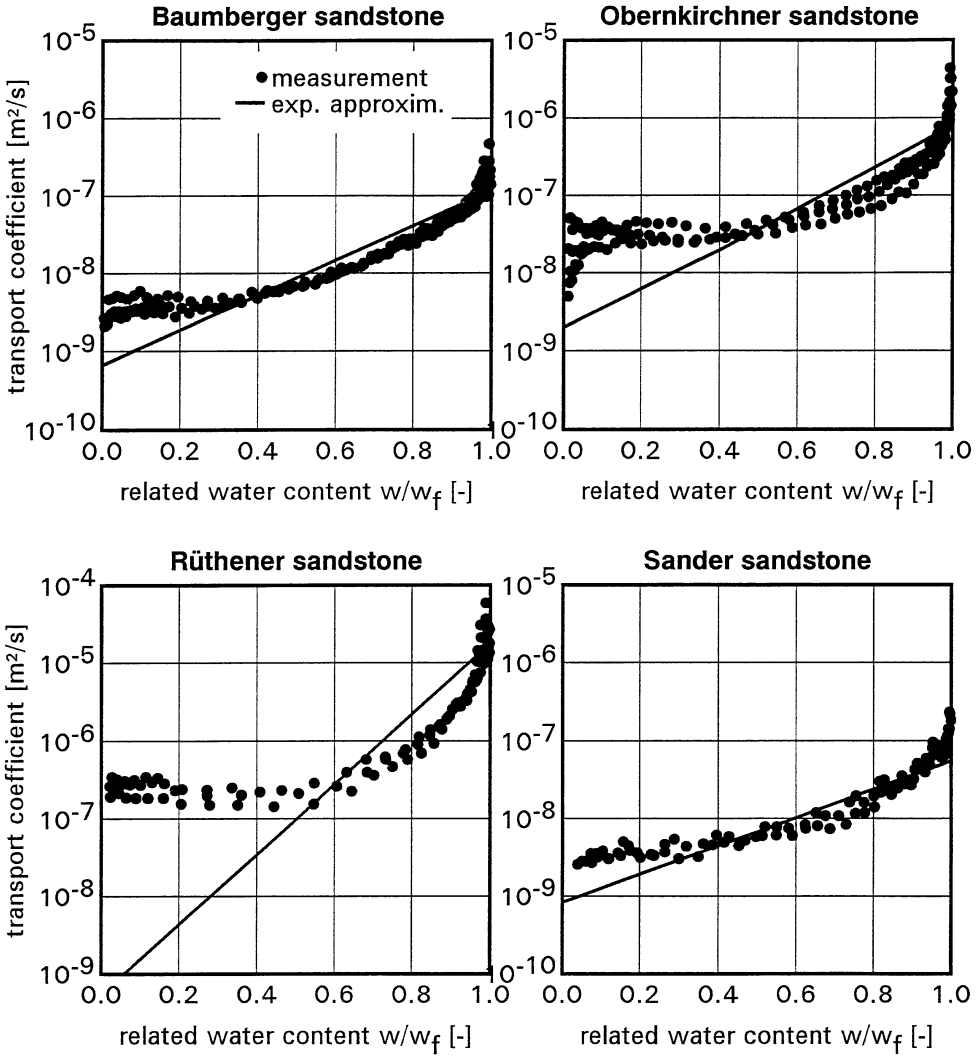

Fig. 43 Transport coefficients calculated from the measured water content distributions (Fig. 39) for capillary absorption as a function of relative water content. The solid lines represent exponential approximations for the transport coefficients.

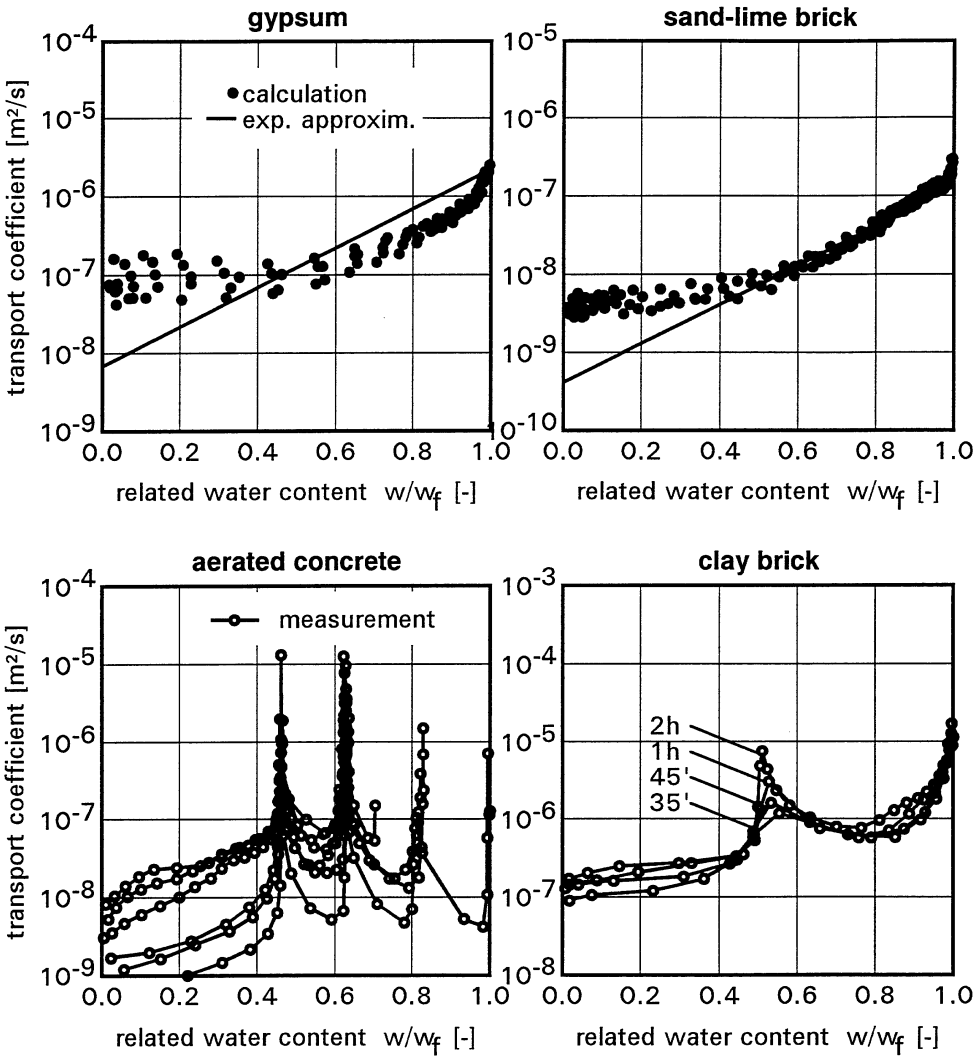

Fig. 44 Transport coefficients calculated from measured water content distributions (Fig. 40) for capillary absorption as a function of relative water content. The solid lines in the two top diagrams represent exponential approximations for the transport coefficients. To better see the profiles, the test points in the two lower diagrams are connected.

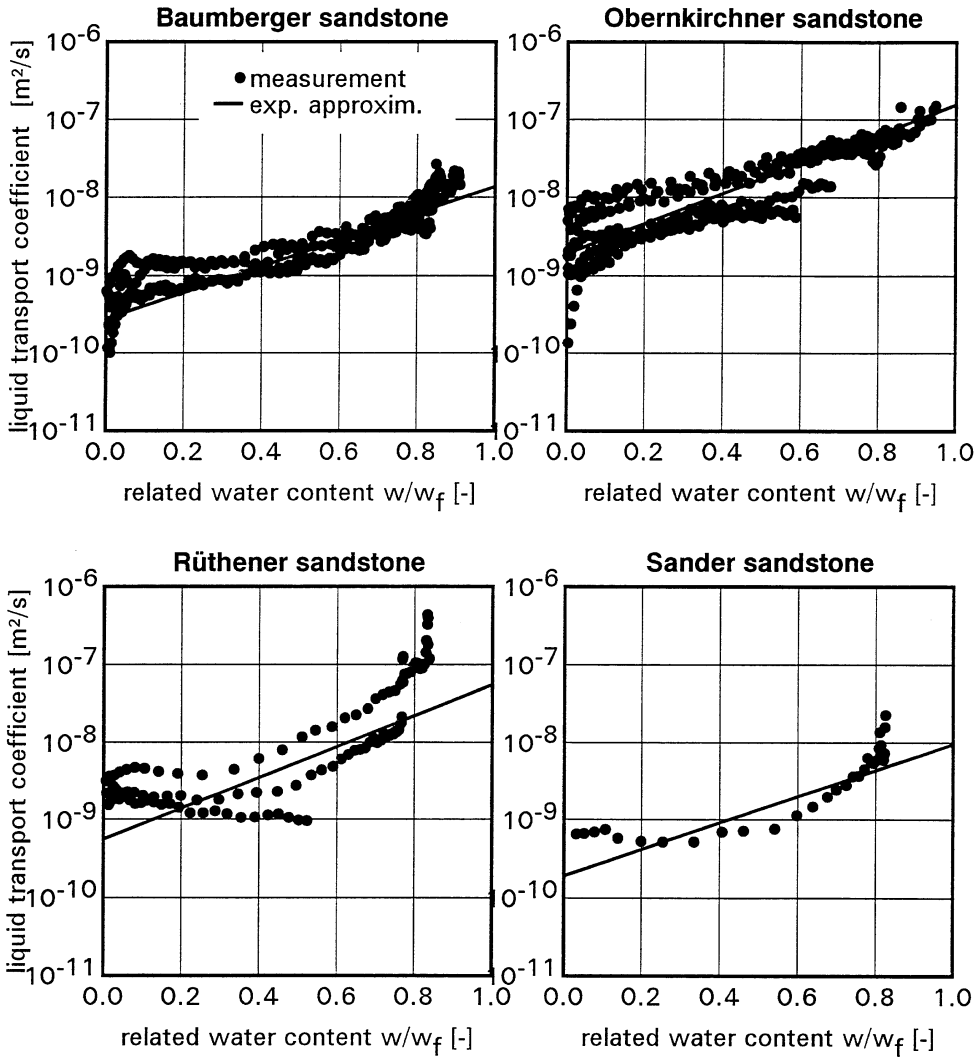

Fig. 45 Transport coefficients calculated from the measured water content distributions (Fig. 41) for liquid water redistribution as a function of relative water content. The solid lines represent exponential approximations for the transport coefficients.

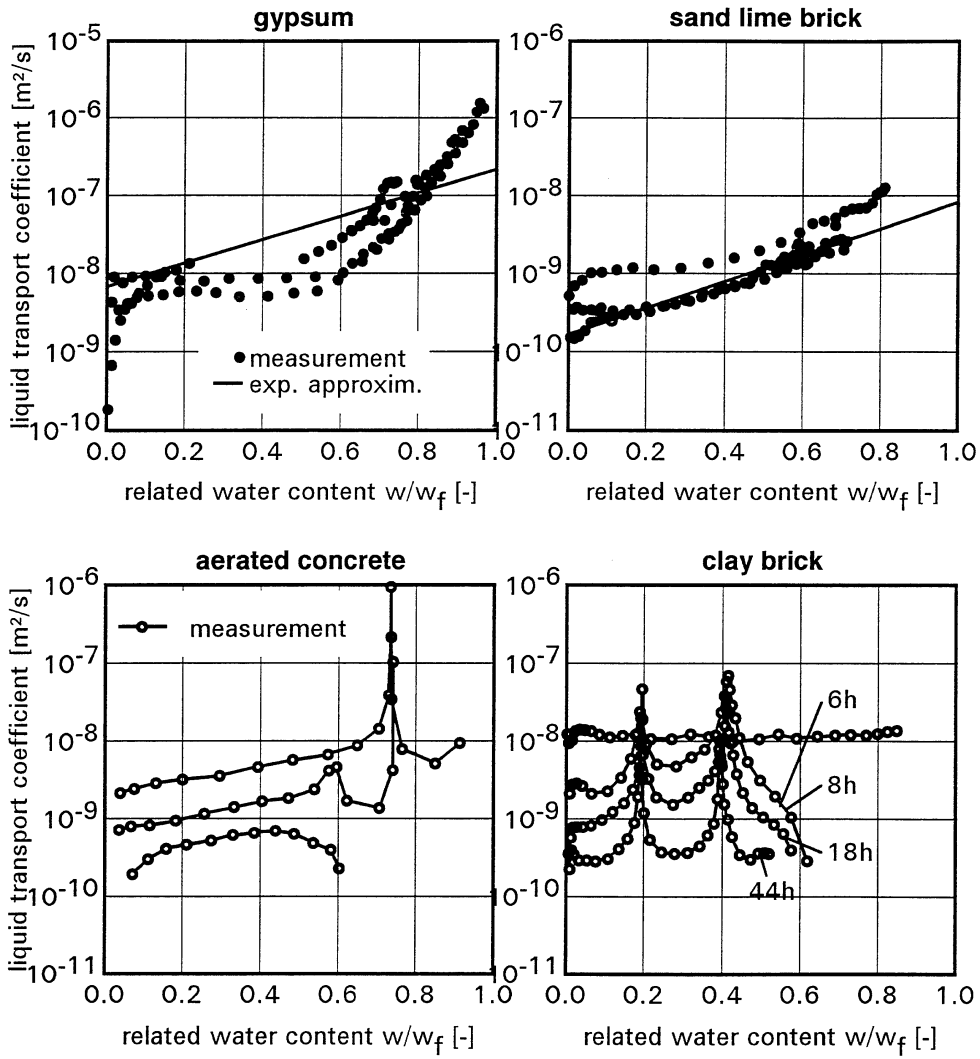

Fig. 46 Transport coefficients calculated from measured water content distributions (Fig. 42) for liquid water redistribution as a function of relative water content. The solid lines in the two top diagrams represent exponential approximations for the transport coefficients. To better see the profiles, the test points in the two lower diagrams are connected.

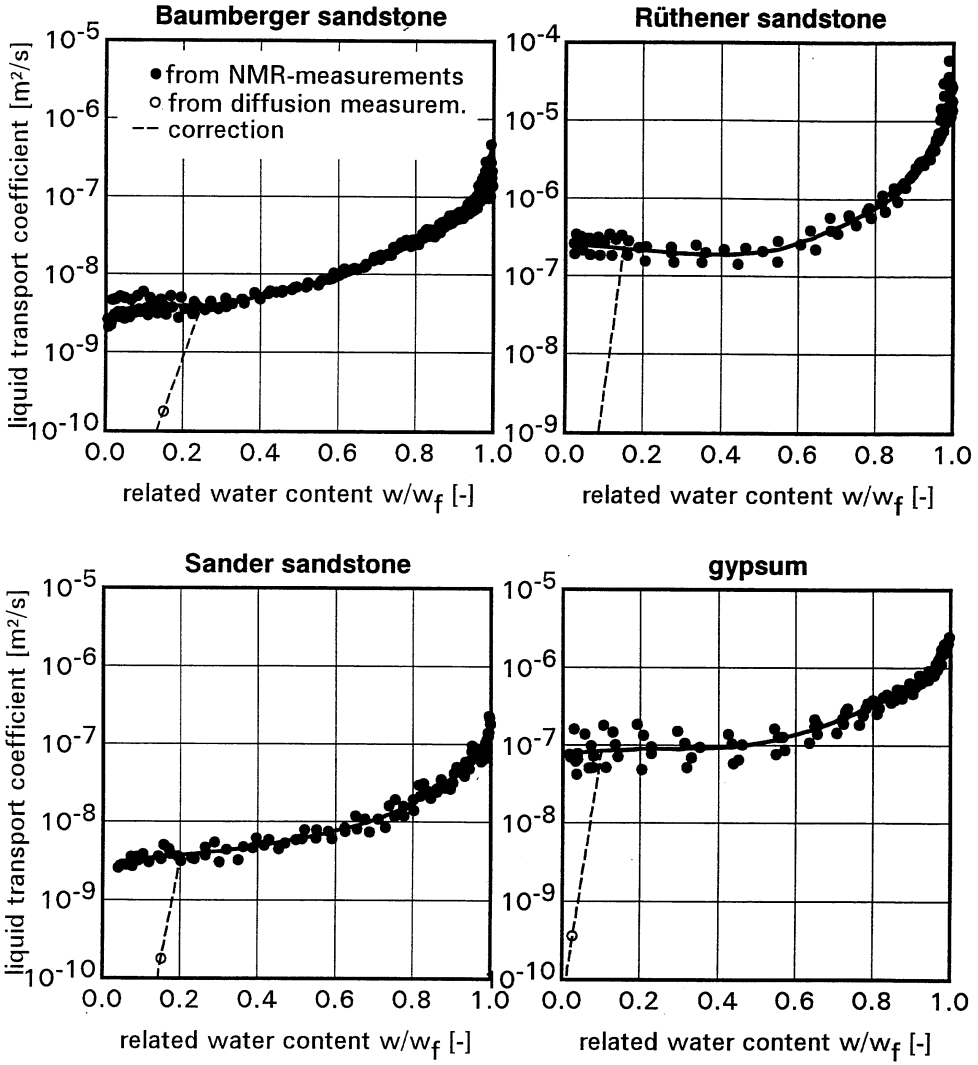

Fig. 47 Transport coefficients calculated from measured water content distributions (Fig. 39 and 40) for capillary absorption as a function of relative water content. Because the calculated transport coefficients in the hygroscopic moisture region are always too high owing to inaccuracies in computation, they have been corrected in this region (dashed line). The correction consists of a straight line passing through the transport coefficients calculated from dry and wet-cup measurements and merging into the NMR values at the sorption moisture of 95% RH.

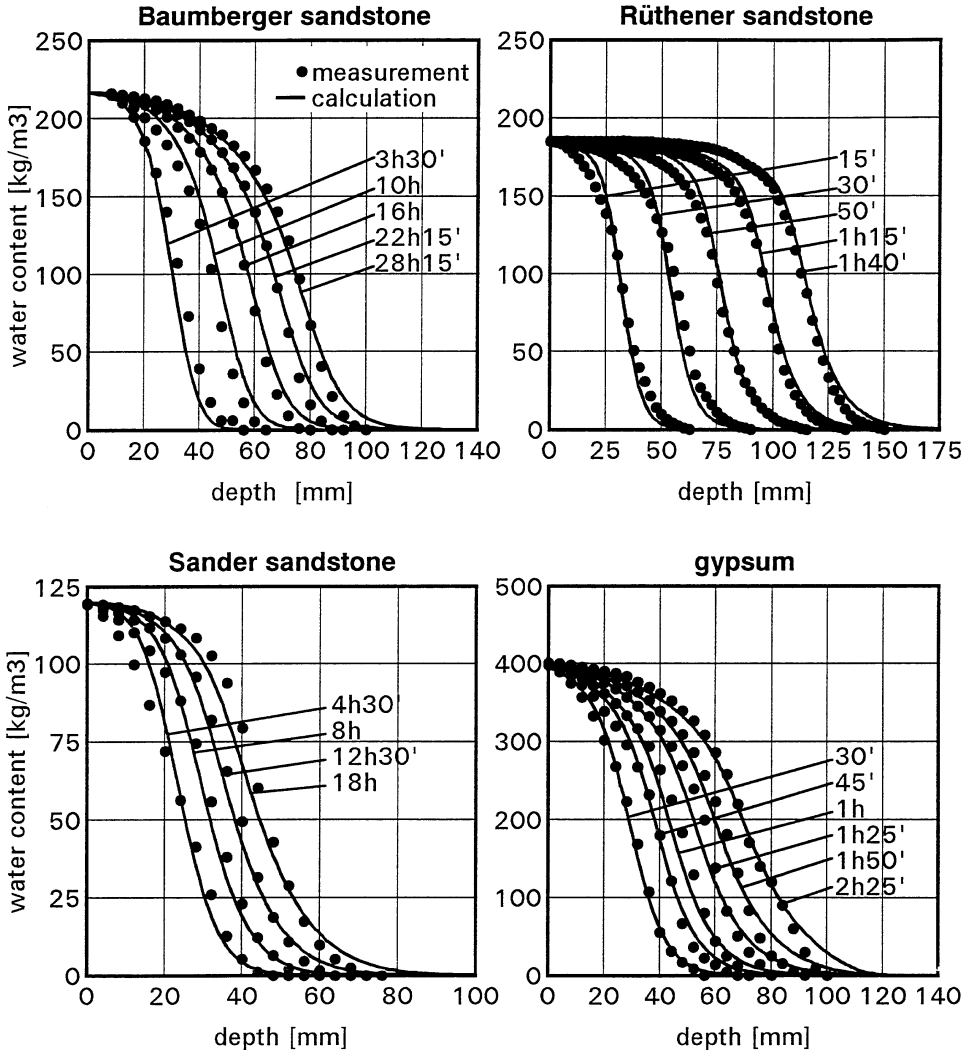

Fig. 48 Comparison of measured values and the water content distributions over specimen depth calculated using the transport coefficients determined from distributions (Fig. 47). Due to inaccuracies in computation, the calculated coefficients are too high in the low moisture region. This results in the discrepancies shown in the moisture region below about 20% of natural saturation.

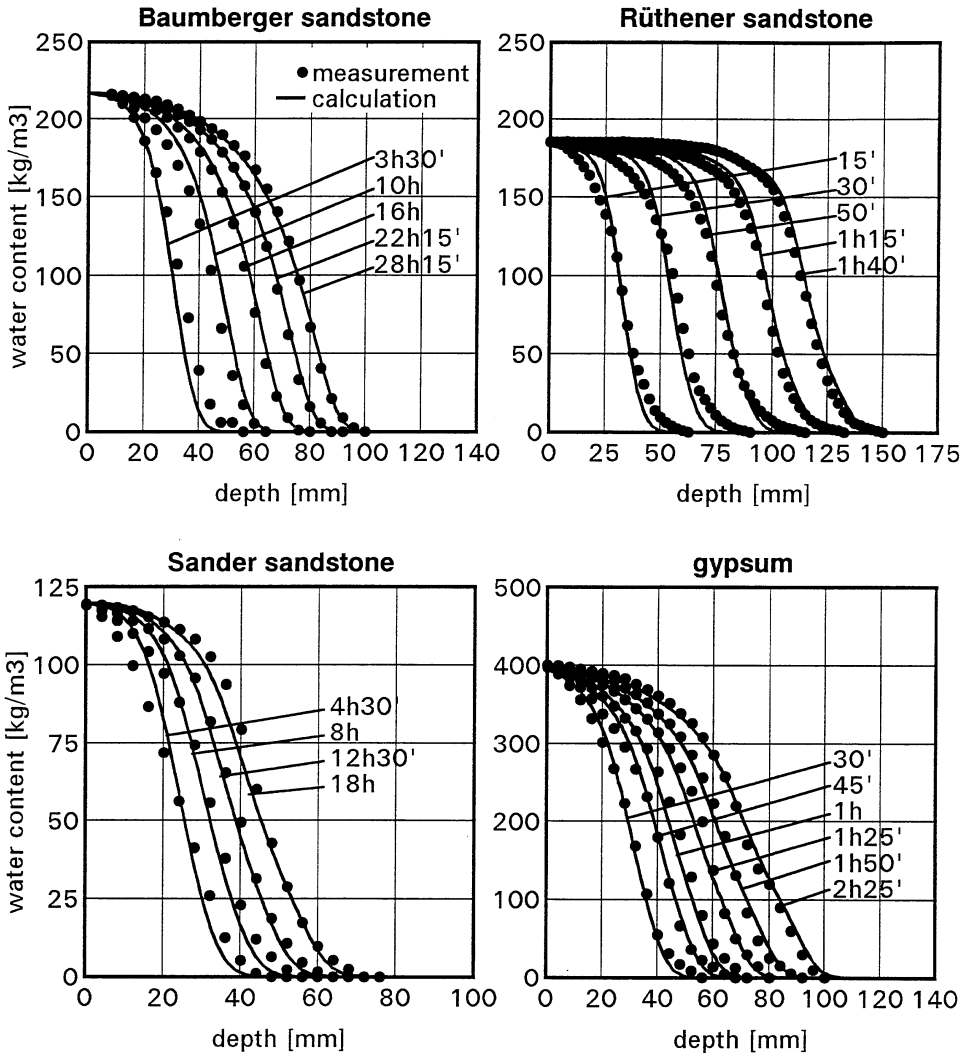

Fig. 49 Distributions of water content over the depth of specimens of building materials at various points in time.
The distributions shown with solid lines were calculated using the transport coefficients corrected in the hygroscopic moisture region per Fig. 47. In the low moisture region they show a much better correlation with the measurements distributions.

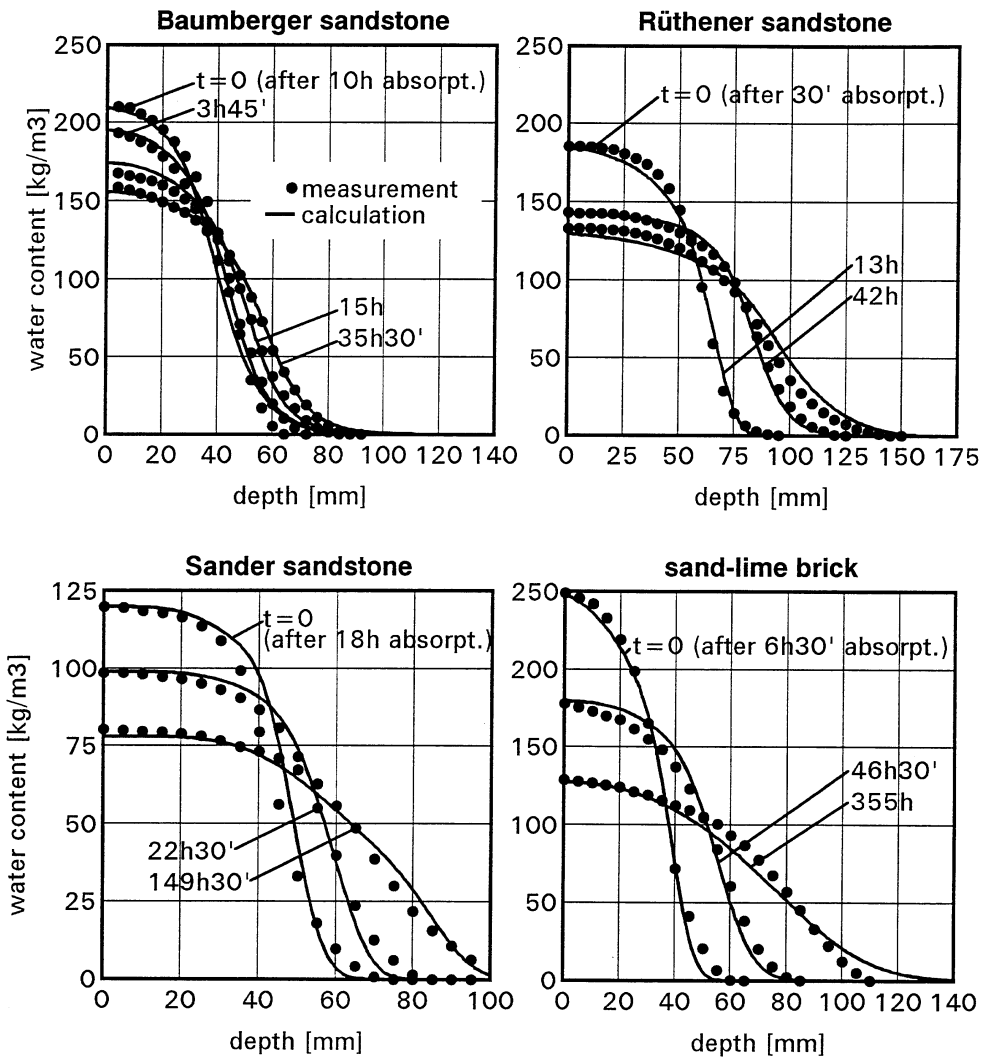

Fig. 50 Comparison of measured results and the water content distributions over specimen depth calculated using the transport coefficients determined from distributions (Fig. 45 and 46). These calculated profiles coincide better with the measured ones than those calculated using an exponential approximation (Fig. 41 and 42). Additional correction of the transport coefficients in the sorption region is not necessary here.

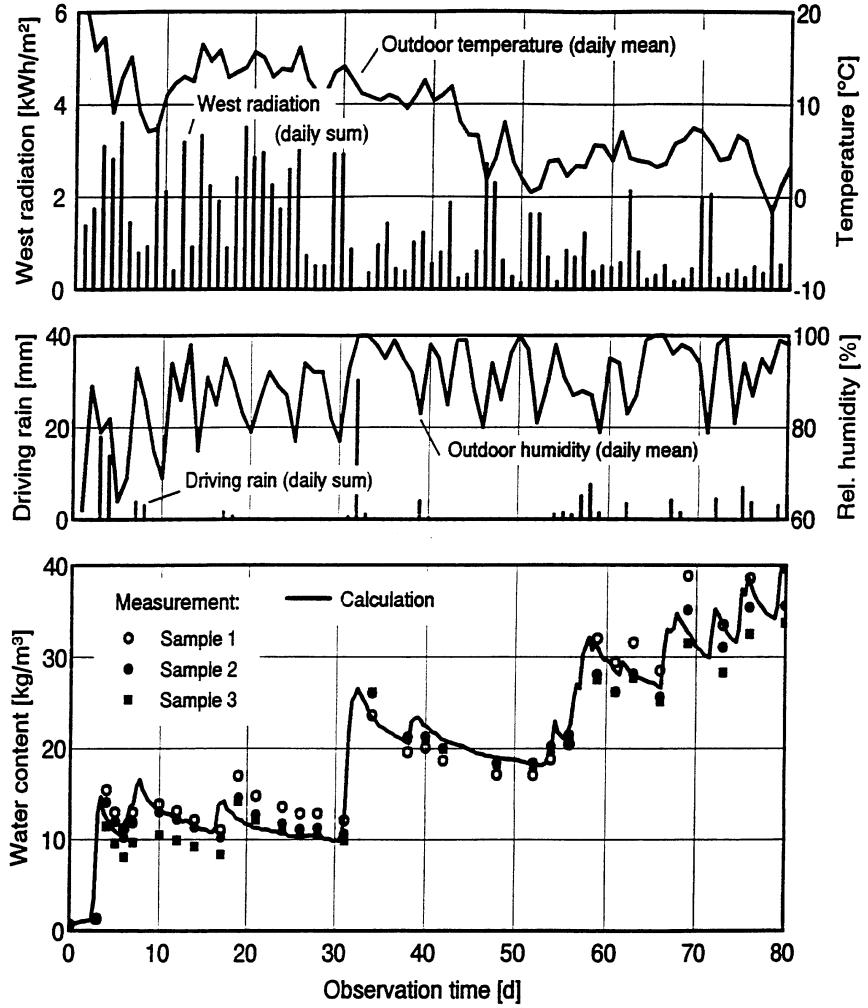

Fig. 51 Measured profile of outside air temperature and west sunlight (top) as well as relative humidity and rainfall (middle) for better depiction in the form of daily average values or totals over an 80 day period of observation [87]. The moisture profile calculated using these climatic parameters (in the form of hourly average values) of a wall of natural stone, 25 cm thick and initially dry is shown in comparison with measurements on 3 natural stone facade specimens (bottom).

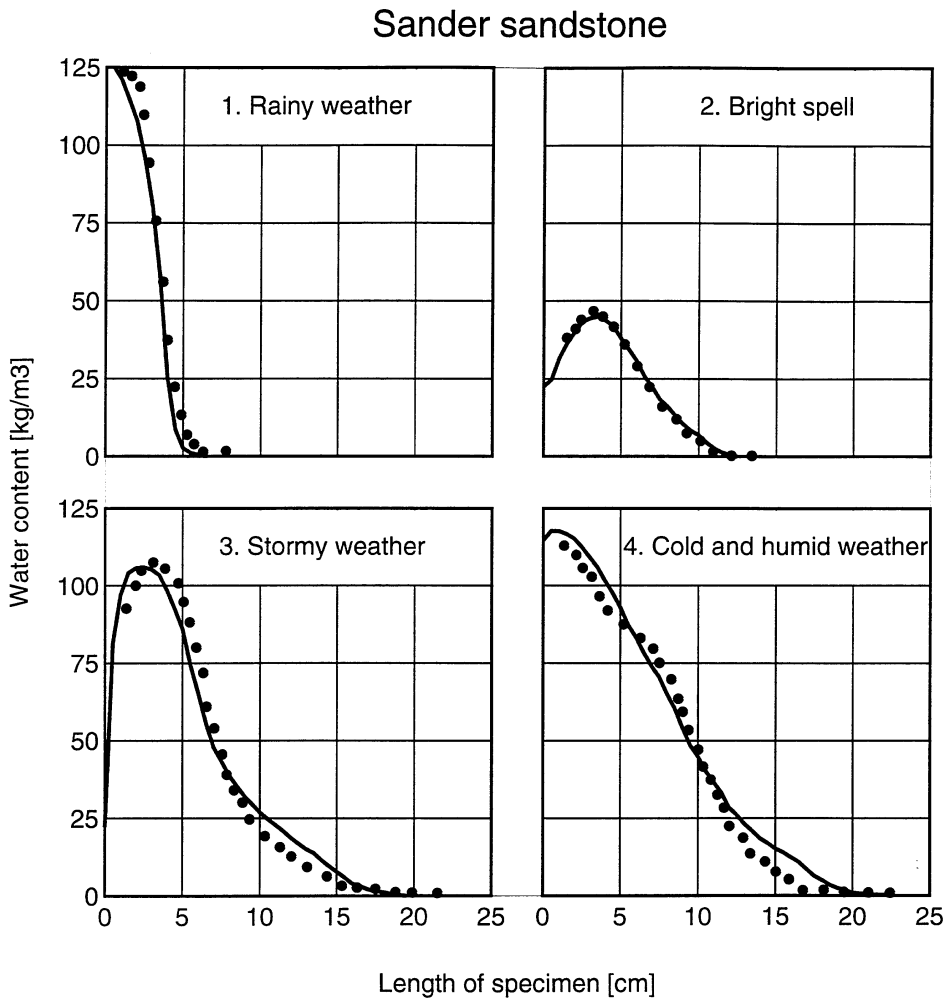

Fig. 52 Comparison of calculated and measured moisture profiles for Sander sandstone (Fig. 51, specimen 2) in four distinct weather periods: following the first major rain fall after start of the experiment, following a week-long period of fair weather, in dry blustery weather following rain and in a lengthy period of cold, wet weather at the end of the observation period (from [87]).

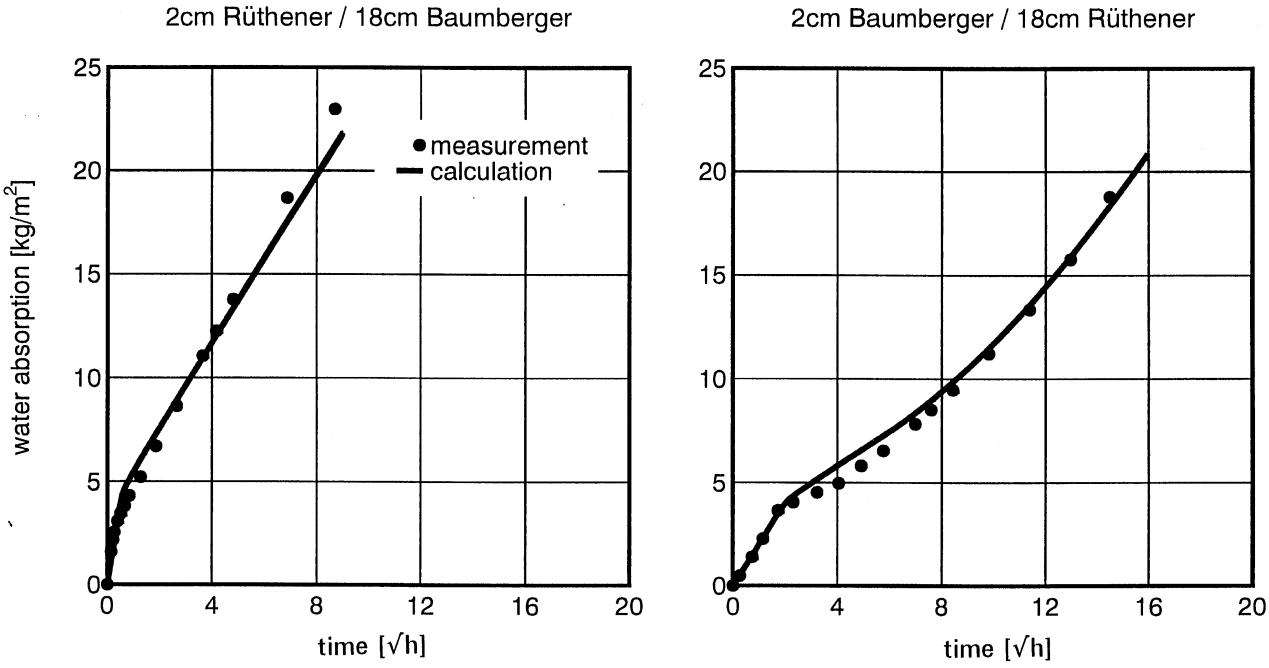

Fig. 54 Chronological course (root scale) of water absorption across the boundry layer of two specimens from Rüthener and Baumberger sandstone in hygric contact with one another. Whereas the course of the water absorption for the Baumberger sandstone is not influenced by the Rüthener sandstone (left), water absorption in the Rüthener sandstone is greatly retarded by the Baumberger sandstone (right).

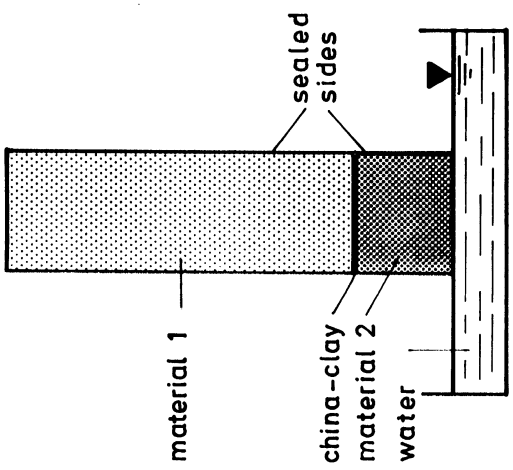

Fig. 53 Schematic representation of the test set-up for determining water absorption across the boundary layer of two different materials. The china clay provides a good hygric contact between the two specimens.

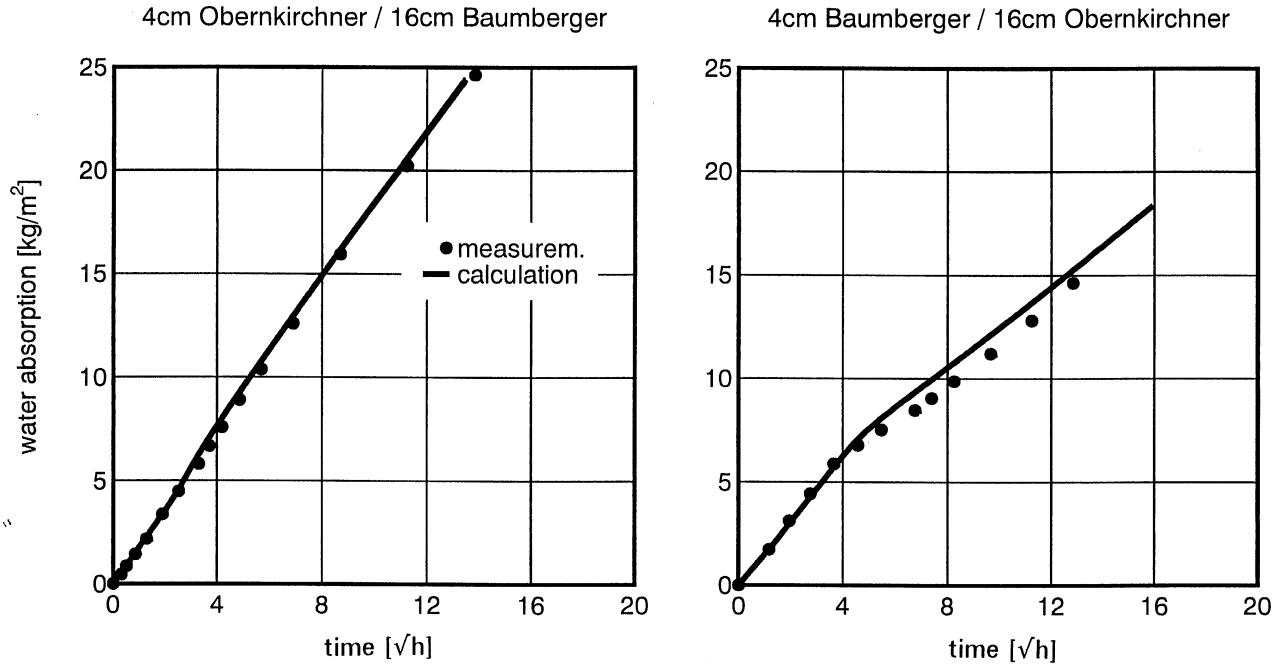

Fig. 55 Chronological course (root scale) of water absorption across the boundary layer of two specimens from Obernkirchner and Baumberger sandstone in hygric contact with one another. The two varieties of sandstone have the same water absorption coefficients, however the suction pressure of the Oberkirchner sandstone is markedly lower than that of the Baumberger sandstone (see Fig. 17). During suction from the Obernkirchner Sandstone by the Baumberger sandstones, behaviour is similar to that of a monolithic specimen (figure at left). During suction in the opposite direction (right) the influence of the differing suction pressure of the two specimens can be seen.